FEDERAL UNIVERSITY OF SANTA CATARINA
TECHNOLOGICAL CENTER (CTC)
POSTGRADUATE PROGRAM IN MATERIALS SCIENCE AND ENGINEERING

Maria Ester Cueto Alfaro

Accelerated Weathering Analysis and Determination of Shelf Life of Poly(Lactic Acid) Scaffolds Manufactured by 3D Printing

Florianópolis
2022

Maria Ester Cueto Alfaro

Accelerated Weathering Analysis and Determination of Shelf Life of Poly(Lactic Acid) Scaffolds Manufactured by 3D Printing

Dissertation submitted to the Postgraduate Program in Materials Science and Engineering at the Federal University of Santa Catarina in order to obtain the title of Master in Materials Engineering.

Advisors
Prof. Dr. Dachamir Hotza
Prof. Dr. Guilherme Barra

Florianópolis
2022

Ficha de identificação da obra elaborada pelo autor,
através do Programa de Geração Automática da Biblioteca Universitária da UFSC.

Alfaro, Maria Ester Cueto
Accelerated Weathering Analysis and Determination of Shelf Life of Poly (Lactic Acid) Scaffolds Manufactured by 3D Printing / Maria Ester Cueto Alfaro ; orientador, Dachamir Hotza, coorientador, Guilherme Mariz de Oliveira Barra, 2022.
129 p.

Dissertação (mestrado) - Universidade Federal de Santa Catarina, Centro Tecnológico, Programa de Pós-Graduação em Ciência e Engenharia de Materiais, Florianópolis, 2022.

Inclui referências.

1. Ciência e Engenharia de Materiais. 2. Accelerated Weathering. 3. Shelf Life. 4. PLA Scaffold. 5. 3D Printing. I. Hotza, Dachamir. II. Barra, Guilherme Mariz de Oliveira. III. Universidade Federal de Santa Catarina. Programa de Pós-Graduação em Ciência e Engenharia de Materiais. IV. Título.

Maria Ester Cueto Alfaro

Accelerated Weathering Analysis and Determination of Shelf Life of Poly(Lactic Acid) Scaffolds Manufactured by 3D Printing

The present work at the Master level was evaluated and approved by an examining board composed of the following members:

Prof. Dachamir Hotza, Dr.
Federal University of Santa Catarina (UFSC)

Steferson Luiz Stares, Dr.
Federal University of Santa Catarina (UFSC)

Prof. Caio Gomide Otoni, Dr.
Federal University of São Carlos (UFSCar)

We certify that this is the original and final version of the final dissertation, which was deemed appropriate to obtain the title of master in Materials Science and Engineering.

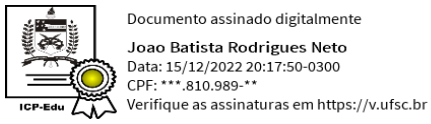

Prof. Dr. João Batista Rodrigues Neto
Program Coordinator

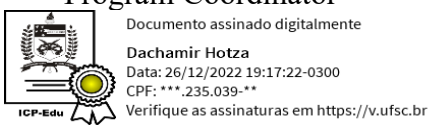

Prof. Dr. Dachamir Hotza
Advisor
Federal University of Santa Catarina

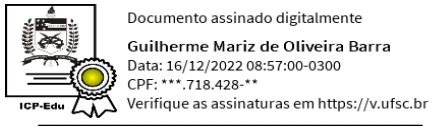

Prof. Dr. Guilherme Barra
Advisor
Federal University of Santa Catarina

Florianópolis, 2022

AKNOWLEDGMENT

I would like to thank the Federal University of Santa Catarina (UFSC) and the entire faculty of the Materials Science and Engineering course.

I would also like to thank Prof. Dachamir Hotza and Prof. Guilherme Barra, for all their dedication and solicitude, both as professors and as advisors, in this and other academic research projects I have participated.

Thanks to the post-doctoral and co-supervisor Steferson Luiz Stares and the course colleague Thiago Boimer, from the Interdisciplinary Laboratory for Nanostructure Development (LINDEN), UFSC – who were directly involved in the activities of this work – for all the guidance and willingness to help.

To FAPESC (Research and Innovation Support Foundation of Santa Catarina State), for the financial support provided for this work.

To the other colleagues from LINDEN – Emanoelle, Aline, and Jeyse – for all the kindness and help to perform the activities related to this work.

To my friends, for all the support, the good company, and the fun moments we shared.

To the colleagues and people in charge of the other laboratories in which the tests and analyses discussed in this work were performed: Central Laboratory of the Chemical and Food Engineering Department, Laboratory of Control and Polymerization Processes (LCP), Laboratory of Ceramic Processing (ProCer), Central Laboratory of Electronic Microscopy (LCME), Polymers and Composites Laboratory (POLICOM), Materials Laboratory (LabMat) – from UFSC – as well as the SENAI Institute of Materials Technology – from Criciúma.

To my family – my parents, my sister, and my brother – for being part of my life and for all the effort invested in my education.

To my life partner Juliano Fin, for being always by my side, and for all the love, support, and encouragement given every day.

To all those who, in some way, were involved in the journey that brought me here.

“Nothing in life is to be feared, it is only to be understood”.

– Marie Skłodowska-Curie

RESUMO

Este trabalho visa analisar os efeitos de envelhecimento acelerado nas propriedades físico-químicas de matrizes extracelulares (*scaffolds*) de poli (ácido láctico) (PLA) produzidas por impressão 3D. Visou-se também a determinação do tempo de vida útil da peça, por meio de equações que correlacionem o tempo de exposição sob envelhecimento acelerado com o envelhecimento natural. Foram adotadas duas metodologias: sob controle isolado de temperatura (35 e 45 °C) – com base na ABNT NBR 16469 (2020) – e sob ciclos com controle de temperatura, umidade e radiação ultravioleta (UV) – com base na ASTM G154 (2016). As amostras submetidas a envelhecimento acelerado foram caracterizadas por meio de calorimetria exploratória diferencial (DSC), difração de raios-X (DRX), espectroscopia no infravermelho por transformada de Fourier (FTIR), viscosimetria e microscopia eletrônica de varredura (MEV), além de ensaios de resistência ao torque por inserção de parafuso. Para os envelhecimentos sob 35 °C e sob temperatura, umidade e radiação (T-U-R) controladas, foi observado um comportamento crescente da temperatura de transição vítrea e do grau de cristalinidade (com efeito mais expressivo para o ensaio T-U-R), indicando que a degradação atuou predominantemente sobre regiões amorfas do polímero. Para o envelhecimento a 45 °C, ambas as propriedades apresentaram, inicialmente, um comportamento crescente – indicando que a degradação sobre regiões amorfas foi predominante – seguido de um comportamento decrescente – indicando que a degradação passou a atuar também sobre regiões cristalinas. Os ensaios de envelhecimento provocaram mudanças nos espectros de FTIR, indicando a intensificação da quebra de cadeias por fotólise e hidrólise, com efeitos mais expressivos para o ensaio T-U-R, seguido do ensaio sob 45 °C e, finalmente, sob 35 °C. A taxa de degradação também mostrou uma correlação positiva com a intensidade das variáveis de envelhecimento aplicadas, de modo que foi potencializada seguindo a ordem de criticidade dos ensaios (35 °C < 45 °C < T-H-R). As micrografias mostraram o surgimento de defeitos superficiais notáveis somente nas amostras do ensaio T-U-R após 336 h de exposição. A partir dos ensaios de resistência mecânica, estabeleceu-se a falha funcional das amostras. Para o ensaio da ABNT NBR 16469 (2020), determinou-se 456 h como o tempo para a falha (sob 45 °C), correspondendo a 171 dias em condição real. Para o ensaio da ASTM G154 (2016), determinou-se a falha em 168 h, correspondendo a 38 dias em condição real. De acordo com a análise estatística (ANOVA e Tukey), houve diferença significativa entre os resultados de resistência mecânica do ensaio T-U-R, em relação àqueles de ensaios com controle isolado de temperatura, para 240 e 336 h de exposição. Além disso, houve variação significativa – em relação à resistência mecânica inicial – a partir de 336 h (p-valor = 0,0419) sob 35 °C, a partir de 240 h (p-valor = 0,0198) sob 45 °C e a partir de 168 h (p-valor = 0,0173) sob T-U-R. Definiu-se um tempo de vida útil da peça de 150 dias (5 meses) – devendo-se, obrigatoriamente, armazená-la e transportá-la ao abrigo da luz solar, sob temperatura e umidade relativa de até 25 °C e 70%, respectivamente.

Palavras-chave: envelhecimento acelerado, tempo de vida útil, *scaffold*, PLA, impressão 3D.

RESUMO EXPANDIDO

Introdução

A engenharia de tecidos consiste no desenvolvimento de estruturas sintéticas porosas chamadas de *scaffolds* (ou matrizes extracelulares) que atuam como suporte para a regeneração tecidual, estimulando o crescimento de células próprias do paciente (GUPTA; REVAGADE; HILBORN, 2007). O uso de *scaffolds* poliméricos é bem documentado na literatura (CAMINERO et al., 2019; LI et al., 2014; VISSCHER et al., 2016; XU et al., 2010; YANG et al., 2005), mostrando-se promissora a utilização de polímeros biodegradáveis; pois proporciona-se, assim, uma estrutura temporária, com a formação guiada de um novo tecido funcional, o qual permanece ativo após a completa absorção do *scaffold* pelo corpo (KIM; MOONEY, 1998; O'BRIEN, 2011).

O poli (ácido láctico) (PLA) apresenta alta biocompatibilidade e biodegradabilidade, sendo, por conta disso, uma importante matéria-prima para a produção de *scaffolds* (GUPTA; REVAGADE; HILBORN, 2007; SAVIOLI LOPES; JARDINI; MACIEL FILHO, 2012; SINGHVI; ZINJARDE; GOKHALE, 2019). Uma das aplicações possíveis para *scaffolds* consiste na reconstrução oral e maxilofacial (MELEK, 2015). A eficácia do PLA e de seus compósitos como biomateriais de uso odontológico vem sendo demonstrada por estudos que avaliaram sua capacidade, sob a forma de *scaffolds*, de promover a reconstrução de tecidos ósseos alveolares (CHANDRAHASA; MURRAY; NAMEROW, 2011; GEBHARDT et al., 2009; GENDVILIENE et al., 2021; MOHANDESNEZHAD et al., 2020; WANG et al., 2010).

A manufatura aditiva permite que matrizes extracelulares sejam produzidas de maneira customizada – em termos de estruturas externa e interna – e uma das principais técnicas utilizadas para esse fim, a partir de matérias-primas poliméricas, é a Fabricação por Filamento Fundido (FFF), que consiste em fundir um filamento de polímero termoplástico e extrudá-lo através de um bico (FARRÉ-GUASCH et al., 2015; WANG et al., 2017).

Junto ao desenvolvimento tecnológico de *scaffolds*, surge a demanda por se definir o tempo de vida útil desses implantes, quando expostos a condições ambientais, bem como requisitos de armazenamento para que sejam preservados seus requisitos funcionais. Diferentes métodos normativos de envelhecimento acelerado podem ser empregados para obter o tempo de serviço de produtos poliméricos, de maneira controlada e aceitável em termos de tempo para validação de uma tecnologia (por meio da posterior correlação com o envelhecimento natural); permitindo, ainda, a reprodutibilidade e a comparação de resultados (CHÁVEZ-MONTES et al., 2015; SAWPAN et al., 2019; WHITE; TURNBULL, 1994).

Objetivos

O objetivo geral deste trabalho é analisar os efeitos do envelhecimento artificial acelerado – conduzido sob diferentes configurações de variáveis ambientais aplicadas – nas propriedades de *scaffolds* de poli (ácido láctico) (PLA), produzidas por manufatura aditiva, utilizando os resultados para definição e comparação de tempos de vida útil obtidos de acordo com variáveis atuantes.

Os objetivos específicos são:

• Definir fatores de aceleração para correlacionar resultados de diferentes ensaios normativos de envelhecimento acelerado – sob controle de temperatura e sob controle de temperatura, umidade e radiação ultravioleta (UV) combinadas – ao envelhecimento natural dos *scaffolds* de PLA;

• Medir e comparar as variações de propriedades e da microestrutura das amostras submetidas a diferentes ensaios normativos de envelhecimento acelerado realizados – relacionando os efeitos aos mecanismos de degradação do PLA;

• Determinar os tempos para falha funcional, em temos de resistência mecânica, referentes aos ensaios de envelhecimento acelerado sob exposição à maior temperatura empregada e sob exposição a temperatura, umidade e radiação UV combinadas;

• Calcular os tempos de vida útil dos *scaffolds* para os diferentes métodos de envelhecimento acelerado, por meio das respectivas equações de correlação com o envelhecimento natural e, assim, determinar as melhores condições de armazenamento das estruturas.

Metodologia

Os *scaffolds* foram fabricados por meio da técnica de FFF, utilizando-se monofilamento incolor de PLA Ingeo^{TM} 3D850 (NatureWorks, Blair, Estados Unidos) para imprimir estruturas quase cilíndricas com uma região interna sólida (destinada à acomodação do parafuso) e uma região externa porosa (destinada a promover a osseointegração).

Os ensaios de envelhecimento sob controle de temperatura (ensaios T) – ABNT NBR 16469 (2020) – foram realizados em estufa de bancada, sob 25, 35 e 45 °C – com tempos de exposição de 24 a 336 h, para 25 e 35 °C; e de 24 a 528 h, para 45 °C. Os ensaios sob controle de temperatura, umidade e radiação (ensaios T-U-R) – Ciclo 1 da ASTM G154 (2016) – foram realizados em câmara de intemperismo, com tempos de exposição de 24 a 336 h.

As amostras foram caracterizadas, antes e após envelhecimento, por meio de análises de DSC, para medições de grau de cristalinidade (χc) e temperatura de transição vítrea (T_g); DRX, para confirmar qualitativamente os efeitos sobre a cristalinidade; FTIR, para detectar mudanças de estrutura química associadas a mecanismos de degradação; viscosimetria, para medições de peso molecular viscosimétrico médio; e MEV, para avaliar os efeitos sobre a superfície das amostras. Além disso, realizaram-se ensaios de resistência ao torque por inserção de parafuso (já que se trata de um carregamento pertinente à aplicação, presente durante a acomodação do implante dentário no *scaffold*) – cujos resultados passaram por uma análise estatística.

A determinação do tempo de vida útil por meio das diferentes metodologias de envelhecimento acelerado foi baseada em um critério de aceitação para a resistência ao torque dos *scaffolds* e em equações de correlação com o envelhecimento natural das estruturas. Os fatores de aceleração serão definidos com base em literatura científica, bem como nas normas técnicas ABNT NBR 16469 (2020) e ASTM G154 (2016).

Resultados e Discussão

Somente o ensaio T-U-R tornou as amostras foscas, com perceptível amarelamento/embranquecimento, a partir de 168 h de exposição, o que pode ser explicado pelos

grupos cromóforos (carbonilas) do PLA, já que absorvem radiação UV e desencadeiam a fotodegradação; levando, assim, ao aumento de grupos carbonilas no polímero.

Sob 35 °C, interpretou-se que a degradação atuou somente sobre regiões amorfas dos *scaffolds* de PLA, com aumento gradual do χc e da T_g. Já sob 45 °C, houve uma etapa de degradação também em regiões cristalinas, com fases de crescimento e de decaimento do χc e da T_g, corroborado também pelo desaparecimento do pico de planos cristalinos em DRX. Os resultados para o envelhecimento T-U-R condizem com a maior criticidade associada ao ensaio. Não se identificou o pico da T_g e houve um aumento acelerado do χc (indicando a degradação intensa sobre regiões amorfas), corroborado por resultados de DRX, em que houve evidenciação de picos de planos cristalinos e o desaparecimento da banda amorfa.

O envelhecimento sob 25 °C não provocou mudanças significativas da resistência máxima ao torque. O envelhecimento sob 35 °C provocou variação significativa em 336 h; sob 45 °C, a queda de resistência foi significativa a partir de 240 h; e sob T-U-R, a partir de 168 h de exposição. Houve diferença significativa apenas entre o ensaio T-U-R e sob 25 °C – para 168 h; e entre T-U-R e todos os ensaios T – para 240 e 336 h. Não se verificou mudança significativa, para nenhum tempo de exposição, entre os resultados dos ensaios T.

A taxa de degradação (em termos de variação de peso molecular), bem como a redução na intensidade de picos característicos de FTIR (associada à intensificação da quebra de cadeias), mostraram uma correlação positiva com a intensidade das variáveis de envelhecimento, sendo acentuadas de acordo com a ordem de criticidade dos ensaios (35 °C < 45 °C < T-U-R). Os resultados estão de acordo com os níveis de redução de resistência mecânica, uma vez que a taxa de quebra de cadeias está associada à taxa de decaimento de propriedades mecânicas.

As análises de microestrutura por MEV indicaram que somente o ensaio T-U-R introduziu defeitos consideráveis (principalmente microporos) na superfície dos *scaffolds* de PLA, devido à degradação do polímero em monômeros voláteis de ácido láctico. O tempo para falha funcional determinado pelo ensaio T foi de 456 h, o que, empregando-se a equação para correlacionar ao envelhecimento natural, corresponde a 171 dias de tempo de vida útil. Já para o ensaio T-U-R, o tempo para falha funcional foi de 168 h, o que corresponde a 38 dias de tempo de vida útil.

Considerações Finais

Verificou-se, assim, o efeito expressivo que condições críticas de umidade relativa e radiação UV – quando combinadas com temperatura – provocam sobre propriedades de produtos poliméricos como os *scaffolds* de PLA aqui avaliados, de maneira que sua funcionalidade – em termos, neste caso, de resistência ao torque por inserção de parafuso – pode ser consideravelmente prejudicada em um tempo de exposição relativamente curto. O tempo de vida útil obtido pelo ensaio T-U-R foi cerca de 4,5 vezes menor que o determinado pelo ensaio T sob 45 °C.

Sendo aceitável o tempo de vida útil obtido pelo ensaio T, definiu-se que os *scaffolds* de PLA devem ser, obrigatoriamente, armazenadas e transportadas ao abrigo da luz solar, além de se manter valores de temperatura e umidade comumente recomendadas para produtos de uso médico: 25 °C e até 70%, respectivamente. Mantidas essas condições, define-se um tempo de vida útil de 150 dias para o produto – estabelecendo-se, assim, uma margem de segurança quanto ao período durante o qual o produto pode ser utilizado, após sua fabricação.

Palavras-chave: envelhecimento acelerado, tempo de vida útil, *scaffold*, PLA, impressão 3D.

ABSTRACT

This work aims to analyze the effects of accelerated weathering on physicochemical properties of poly(lactic acid) (PLA) scaffolds fabricated by 3D printing. It was also intended to predict the scaffolds' shelf life, by using equations that correlate the exposure time under accelerated weathering to natural weathering. Two methodologies were followed: by temperature control alone (35 and 45 °C) – based on ABNT NBR 16469 (2020) – and by controlled cycles of temperature, humidity, and ultraviolet (UV) radiation – based on ASTM G154 (2016). The weathered specimens were characterized through differential scanning calorimetry (DSC), X-ray diffraction (XRD), Fourier transform infrared spectroscopy (FTIR), viscosimetry, and scanning electron microscopy (SEM), in addition to torque strength by screw insertion tests. For the weathering tests at 35 °C and under controlled temperature, humidity, and radiation (T-H-R), there was an increasing behavior of the glass transition temperature and the degree of crystallinity (the effect for the T-H-R test was more pronounced), due to degradation acting predominantly on the polymer amorphous parts. For 45 °C weathering, both properties initially showed an increasing behavior – suggesting that degradation over amorphous parts was predominant – followed by a decreasing behavior – indicating that degradation started to act also over crystalline parts. The accelerated weathering tests produced changes in the FTIR spectra, indicating intensified chain scissions by photolysis and hydrolysis, with more pronounced effects for the T-R-H test, followed by the tests under 45 °C and 35 °C. The degradation rate also had a positive correlation with the intensity of the weathering variables applied, so it was potentialized following the order of criticality of the tests (35 °C < 45 °C < T-H-R). Micrographs showed the appearance of noticeable surface defects only on the weathered specimens of the T-H-R test after 336 h exposure. The functional failure of the specimens was established from the mechanical strength tests. For the ABNT NBR 16469 (2020) test, the failure occurred at 456 h (at 45 °C), corresponding to 171 days in real conditions. For the ASTM G154 (2016) test, the failure occurred at 168 h, corresponding to one 38 days in real conditions. According to the statistical analysis (ANOVA and Tukey) of the mechanical strength results, there was a significant difference between the T-H-R test results compared to the ones of temperature control alone, after 240 and 336 h exposure. Furthermore, there was a significant change – compared to the initial mechanical strength – starting at 336 h (p-value = 0.0419) at 35 °C, starting at 240 h (p-value = 0.0198) at 45 °C, and starting at 168 h (p-value = 0.0173) under T-H-R. A shelf life of 150 days (five months) was defined for the scaffolds – which must be stored and transported away from sunlight, at a temperature and relative humidity of up to 25 °C and 70%, respectively.

Keywords: accelerated weathering, shelf life, scaffold, PLA, 3D printing.

LIST OF FIGURES

LIST OF TABLES

LIST OF ABBREVIATIONS AND ACRONYMS

3D	Three-dimensional
AH	Absolute humidity
AM	Additive manufacturing
BSE	Backscattered electrons
CMF	Cranio-maxillo-facial
DLP	Digital light processing
DMLS	Direct metal laser sintering
DPSC	Dental pulp stem cells
DSC	Differential scanning calorimetry
EBM	Electron beam fusion
ECM	Extracellular matrix
FFF	Fused filament fabrication
LA	Lactic acid
LOM	Laminated object manufacturing
PCL	Poly(caprolactone)
PDLA	Poly(D-lactic acid)
PDLLA	Poly(D,L-lactic acid)
PEEK	Poly(ether-ether-ketone)
PGA	Poly(glycolic acid)
PLA	Poly(lactic acid)
PLGA	Poly(lactic acid-co-glycolic acid)
PLLA	Poly(L-lactic acid)
PP	Polypropylene
RH	Relative humidity
SE	Secondary electrons
SEM	Scanning electron microscopy
SLA	Stereolithography
SLM	Selective laser melting
SLS	Selective laser sintering
UV	Ultraviolet
XRD	X-ray diffraction

LIST OF SYMBOLS

A	Constant related to the reaction entropy
E	Elastic modulus
E_a	Activation energy
F_a	Acceleration factor between natural weathering and accelerated weathering
I	Irradiance
k	Reaction rate
M_v	Viscosity-average molecular weight
mw	Molecular weight
O	Oxygen pressure
p	Coefficient of *Schwarzchild*'s Reciprocity Law
$Q10$	Reaction rate coefficient
R	Universal gas constant
T_{aw}	Temperature used in accelerated weathering
t_{aw}	Time for failure in accelerated weathering
T_g	Glass transition temperature
T_m	Melting temperature
t_{nw}	Time for failure in natural weathering
T_r	Room temperature
α	Exponent of the relationship between irradiance and degradation rate
β	Exponent of the relationship between oxygen pressure and degradation rate
γ	Exponent of the relationship between relative humidity and degradation rate
ΔH_m^*	Melting enthalpy corresponding to the polymer in its 100% crystalline condition
ΔH_{cc}	Cold crystallization enthalpy obtained in the polymer analysis
ΔH_m	Melting enthalpy obtained in the polymer analysis
ε_t	Total energy absorbed by a specimen exposed to a radiation source
[η]	Intrinsic viscosity
η_{inh}	Inherent viscosity
η_{rel}	Relative viscosity
λ	Wavelength
χc	Degree of crystallinity

SUMMARY

1 INTRODUCTION

Poly(lactic acid) (PLA) is a thermoplastic polymer that presents high biocompatibility and biodegradability, being produced from renewable and non-toxic sources. For these reasons, PLA has acquired great relevance as a polymeric material for biomedical use, for example. Some of the applications in this specific area are surgical sutures, orthopedic implants, drug delivery systems, and tissue engineering structures, such as scaffolds for tissue engineering (GUPTA; REVAGADE; HILBORN, 2007; SAVIOLI LOPES; JARDINI; MACIEL FILHO, 2012; SINGHVI; ZINJARDE; GOKHALE, 2019).

Tissue engineering consists of the study and development of porous synthetic structures – from polymeric and/or ceramic materials, for example – that are implanted after having cells cultured in their porous interior, acting as a support for tissue regeneration, by stimulating the patient's cells to grow in the body region under treatment (GUPTA; REVAGADE; HILBORN, 2007). The use of polymeric scaffolds for cell regeneration purposes is well documented in the literature (CAMINERO et al., 2019; LI et al., 2014; VISSCHER et al., 2016; XU et al., 2010; YANG et al., 2005), and the use of biodegradable polymers as raw materials is a promising technique since they provide a temporary porous structure, in which cells will adhere and multiply, leading to a guided formation of a new fully functional tissue, which remains active after the complete absorption of the scaffold by the body (KIM; MOONEY, 1998; O'BRIEN, 2011).

One possible application for scaffolds is oral and maxillofacial reconstruction, in which these structures act as osteoconductors after surgical procedures; being important especially when the patient has some bone deficiency (MELEK, 2015). It is possible, for example, to use scaffolds in combination with bone grafts for dental implants, as an adjunct to the subsequent osseointegration of the device into the patient's gingival cavity (JEONG et al., 2020).

Among the existing techniques to produce scaffolds, there is additive manufacturing, popularly known as 3D (three-dimensional) printing, which uses a computational model to create customized parts that meet the specific needs of the patient and the application site (REN et al., 2005; SHARIF et al., 2019). PLA and its composites are some of the main raw materials that have been used in studies about additive manufactured scaffolds (CAMINERO et al., 2019; XU et al., 2010).

Along with the technological development of scaffolds, there is a demand to define the shelf life of these implants when exposed to environmental conditions, as well as to define storage requirements to preserve adequate functional characteristics. When it comes to medical

devices, the determination of their shelf life is essential to ensure their safety and efficiency and, thus, mitigate implant failure and risks to the patient's health.

ANVISA (Brazilian Health Regulatory Agency), through the Collegiate Directory Resolution n° 56 (ANVISA, 2001), establishes that: "The characteristics and performance of health products must not change to such an extent that they compromise the clinical condition and safety of patients or consumers or, where applicable, other persons, for as long as the shelf life specified by the manufacturer and under normal conditions of use". The U.S. Food and Drug Administration (FDA) also provides orientation in the Shelf Life of Medical Devices Guidance Document (FDA, 1991): " To determine if a particular device requires a shelf life and assign an expiration date, there are a number of different parameters that must be considered. The device must be analyzed to determine if it is susceptible to degradation that would lead to functional failure and the level of risk that the failure would present".

The exposure of polymeric devices to conditions such as temperature, humidity, and ultraviolet (UV) radiation causes significant changes in physicochemical properties over time, which has been demonstrated by several studies that subjected these materials to weathering (natural and accelerated) (KAYNAK; SARI, 2016; PICKETT, 2020; SANTOS et al., 2013; SAWPAN et al., 2019; VARSAVAS; KAYNAK, 2017; WEIR et al., 2004; WHITE; TURNBULL, 1994; YANG; DING, 2006; YEW et al., 2009). Each type of degradation – thermal, hydrolytic, oxidative, photolytic, etc. – is driven by different mechanisms, with different effects on the properties' variation over exposure time (PICKETT, 2020; SAWPAN et al., 2019; WHITE; TURNBULL, 1994).

Ideally, the determination of the durability of a product would be conducted by exposing it to natural atmospheric conditions, since they best match practical experience. However, the exposure times required to observe significant changes in physicochemical properties may reach several months or even years; which makes it impractical from a commercial point of view and in terms of technology validation for use. In addition, it is difficult to reproduce such studies, because there is no control of variables, so the system is susceptible to drastic fluctuations in environmental conditions (LV et al., 2015; PICKETT, 2020; POSPÍŠIL et al., 2006).

In order to overcome such impediments, normative methods of accelerated artificial weathering are commonly employed to characterize the durability, and thus the shelf life, of polymeric materials; applying controlled intensities of temperature, radiation, humidity, etc., in a more rigorous way than conditions that would occur during, for example, storage and transportation. Therefore, such experiments can be conducted for relatively short periods and

used to establish a correlation with weathering under natural conditions to predict the shelf life, after which significant structural and functional changes would occur, leading the product to lose its intended performance. In addition, the reproducibility and the comparison of weathering tests become possible, due to the controlled environmental parameters (constant or cyclic) (CHÁVEZ-MONTES et al., 2015; SAWPAN et al., 2019; WHITE; TURNBULL, 1994).

This work was carried out as an extension of studies already held at the Interdisciplinary Laboratory for Nanostructures Development (LINDEN), Federal University of Santa Catarina, concerning the design of PLA scaffolds, intended for oral and maxillofacial reconstruction. Initially, the project involved the selection of different printing infill configurations for porous structures computationally modeled and subsequent mechanical tests of torsion strength through metallic screw insertion, as well as biological activity tests. For the present work, the computational model of the scaffolds printed and evaluated under accelerated weathering was the one associated with the highest mechanical strength and promising biological activity results.

It is aimed to evaluate the degradation, i.e. the variation of physicochemical properties of scaffolds designed for bone reconstruction – manufactured in PLA, by additive manufacturing – as a function of the exposure time to conditions that lead to the accelerated weathering of polymeric materials. Standardized methodologies will be used to evaluate the influence of temperature alone – according to guidelines of ASTM F1980 (2016) and ABNT NBR 16469 (2020) – as well as temperature combined with humidity and ultraviolet radiation – according to ASTM G154 (2016) specifications.

In addition, it is intended to establish the relationship between accelerated weathering, conducted under two different techniques, and the weathering that would occur under natural conditions, in order to determine the shelf life that could be assigned to the product, i.e., the period within which it could be used in surgical procedures without considerable risk of structural and/or functional failure.

The relevance of this research also lies in helping to understand the degradation behavior of polymeric devices in terms of functional properties, and the methods used for accelerated weathering and correlation with natural weathering may be used as a basis for many other polymeric products that require similar characterization.

In the scientific literature concerning accelerated weathering of polymeric parts, usually, studies report the effects of the tests on physicochemical properties, but there are only a few also focused on estimating a shelf life based on accelerated weathering tests and an established acceleration factor – especially for PLA structures and the combined influence of

temperature, humidity, and radiation (CHÁVEZ-MONTES et al., 2015; HUKINS; MAHOMED; KUKUREKA, 2008; LV et al., 2018, 2015; PICKETT; COYLE, 2013). Moreover, the mechanical characterization of PLA weathered devices is normally based on tests that require modified structures (tensile, flexural, or impact test), rather than the final application shape, frequently without a faithful representation of the loading imposed during the product use (ISADOUNENE et al., 2018; ISLAM; PICKERING; FOREMAN, 2010; KAYNAK; SARI, 2016; LIN; XIE; QIU, 2019; LIZÁRRAGA-LABORÍN et al., 2018; LV et al., 2017, 2018; MARTÍN DEL CAMPO et al., 2020; SAWPAN et al., 2019; VARSAVAS; KAYNAK, 2017; YATIGALA; BAJWA; BAJWA, 2018).

Another gap from previous literature consists of the sparse data on accelerated weathering specifically on 3D-printed PLA parts (ALDEEN; OWAID, 2020; GRASSI; SPAGNOLO; PAOLETTI, 2019; LIN; XIE; QIU, 2019). In addition, the failure of weathered devices is usually established when one of its properties reaches 50% of its initial value, without defining a value as an acceptance criterion more pertinent to the final application (COPINET et al., 2004; HULME; COOPER, 2012; KOCKOTT, 1989; YEW et al., 2009; ZAIDI et al., 2010).

Measurements of properties suitable to evaluate the degradation behavior of the scaffolds were performed. Considering they are polymeric structures, the analyses included differential scanning calorimetry (DSC), for quantitative measurements of crystallinity degree (χc) and glass transition temperature (T_g); X-ray diffractometry (XRD), to qualitatively confirm the effects on the degree of crystallinity; Fourier transform infrared spectroscopy (FTIR), to detect chemical structure changes associated with degradation mechanisms; viscosimetry, for measurements of viscosity-average molecular weight, and scanning electron microscopy (SEM), to evaluate the effects of accelerated weathering on the surface of the specimens. Furthermore, since the scaffolds are intended for dental application, tests of torque strength under the insertion of a metallic screw were performed to evaluate the influence of the imposed conditions on the specimens' mechanical strength – a key factor to the implantation procedure and the functions of implant support and stability during the osseointegration process.

2 OBJECTIVES

2.1 GENERAL OBJECTIVE

The general objective of this work is to analyze the effects of accelerated artificial weathering – conducted under different combinations of applied environmental variables – on the properties of poly(lactic acid) (PLA) scaffolds produced by additive manufacturing, as well as to use the results to define and compare shelf life results obtained according to the acting variables.

2.2 SPECIFIC OBJECTIVES

The specific objectives are:

- To define acceleration factors that correlate results from different normative accelerated weathering tests – under temperature control and under combined temperature, humidity, and ultraviolet (UV) radiation control – to natural weathering of the PLA scaffolds;
- To measure and compare variations in physicochemical properties and microstructure of specimens subjected to different normative accelerated weathering tests – linking the effects to PLA degradation mechanisms;
- To determine the times for functional failure, in terms of mechanical strength, for the accelerated weathering tests under exposure to the highest temperature employed and under exposure to combined temperature, humidity, and UV radiation;
- To calculate the scaffolds' shelf life for the different accelerated weathering methods through the respective equations of correlation with natural weathering and, thus, determine the best storage conditions for the structures.

3 BIBLIOGRAPHIC REVIEW

3.1 TISSUE ENGINEERING

3.1.1 General

Tissue engineering consists of an interdisciplinary field that applies engineering and natural sciences principles to the development of biological substitutes to restore, maintain, and improve the activity of human body tissues in cases of trauma, tumors, or congenital deficiencies (LANGER; VACANTI, 1993; LEVI et al., 2012). One of the most common practices within this area of research involves synthesizing three-dimensional (3D) porous structures, called scaffolds, which are used to generate new natural tissues from isolated cells. By collecting some cells from the patient, specifically from the intended tissue of application, they can be multiplied *in vitro* and then cultivated in a scaffold made of a biocompatible and biodegradable material. Then, the structure can be implanted in the patient and, over time, a new tissue is formed as the scaffold completely degrades and is absorbed by the body (Figure 1) (KIM; MOONEY, 1998; PUTNAM; MOONEY, 1996).

Figure 1 - Schematic representation of the tissue regeneration stages employing synthetic scaffolds: cells are isolated from a biopsy and multiplied (*in vitro*), then they are deposited in the scaffold and the assembly is later transplanted to the patient.

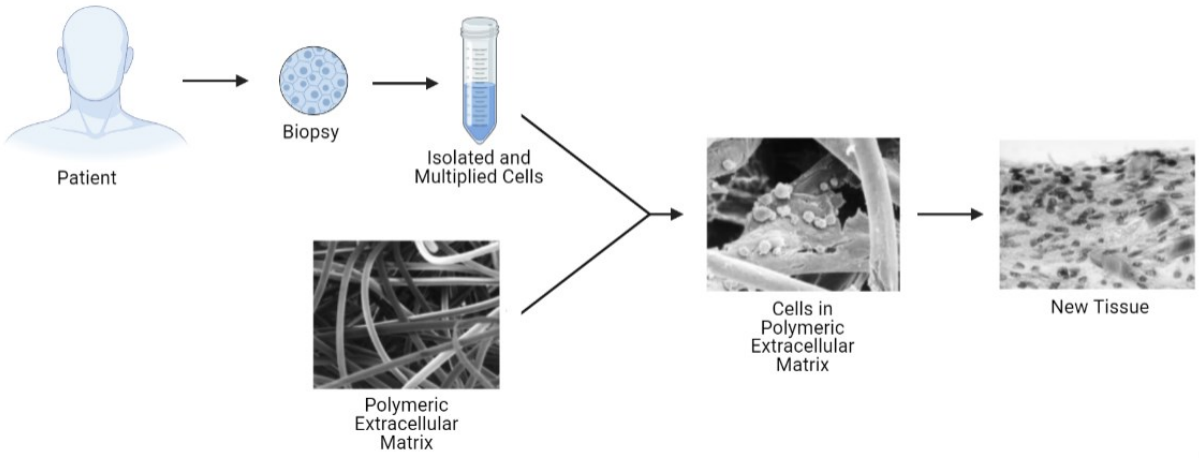

Source: Adapted from Kim and Mooney (1998).

In general, the materials used to produce scaffolds can be classified as organic or inorganic. Organic materials are obtained from natural precursors such as collagen, chitosan, and fibrinogen, or synthetic polymers such as poly(lactic acid) (PLA), poly(glycolic acid)

(PGA), and poly(caprolactone) (PCL). Common inorganic materials are metals and mineral compounds – such as calcium, sodium, aluminum, carbonates, and phosphates (LANGER; VACANTI, 1993; SALGADO; COUTINHO; REIS, 2004).

Regardless of the application site, there are some essential requirements that a synthetic scaffold must meet to be suitable for tissue engineering: 1) it should be made of biocompatible and biodegradable materials, so that they stimulate adhesion, migration, and proliferation of cells through the scaffold structure; and that, over time, it degrades and is completely replaced by the patient's own cells. In addition, the compounds generated by the degradation must be non-toxic to the human body; 2) it should present sufficient mechanical strength to fulfill the support function in the treated region while a new tissue is formed; 3) it should present adequate geometry, that is, a porous structure that allows the transit of cells, of nutrients necessary for tissue regeneration and of residues formed during the scaffold degradation (thus, it is important the porosity to be sufficient for biological activity, but not so high as to compromise the mechanical requirement); 4) it should be manufactured from a commercially scalable process, and the costs involved in the production, storage and final use of the scaffold should be taken into account (O'BRIEN, 2011).

3.1.2 Dental Application

An application that has been widely studied for scaffolds is their use as a graft for dental implants, in cases where, due to some bone deficiency, it becomes complicated to insert the device and maintain its stability after implantation (JAZAYERI et al., 2020). Problems with the bone structure of patients who need dental implants are quite common, and it is often necessary to use bone grafts (autogenous, allogeneic, xenogeneic, or synthetic) during this type of procedure (CHA et al., 2016).

One possible technique consists in filling a synthetic scaffold with osteoconductive compounds and combining it with a dental implant, so that this system can be subsequently inserted into the gingival cavity, reinforcing the alveolar bone layer. This way, tissue engineering represents an alternative to traditional, prolonged and expensive procedures – in which the gingiva is filled with bone graft only, the region is sutured, and after months the site is reopened to insert the dental implant (JEONG et al., 2020). The main raw materials used in the production of scaffolds for dental use consist of natural polymers – such as collagen, fibrin, chitosan, hyaluronic acid, alginate, and peptide-based hydrogels – and synthetic polymers – such as PGA and PLA (JAZAYERI et al., 2020).

The effectiveness of PLA as a biomaterial for dental use has been demonstrated by many studies that used it as a raw material for scaffolds intended for alveolar bone tissue reconstruction. Besides the use in its pure state, several PLA-based composites have also been developed aiming to optimize its performance, in terms of biological and mechanical properties (CHANDRAHASA; MURRAY; NAMEROW, 2011; GEBHARDT et al., 2009; GENDVILIENE et al., 2021; MOHANDESNEZHAD et al., 2020; WANG et al., 2010).

Chandrahasa, Murray, and Namerow (2011) conducted *in vitro* tests to measure the biological activity of mature human dental pulp tissue in scaffolds fabricated in three different materials: PLA, bovine collagen, and calcium phosphate. The authors were able to conclude that the cell proliferation rate depends on the chemical composition of the scaffold and that this rate was higher for structures made of PLA than for the other raw materials. Furthermore, *in vitro* and *in vivo* tests demonstrated that PLA can induce differentiation of human dental pulp-derived stem cells (DPSCs) into mature odontoblasts, as well as form soft and hard tissues that resemble the dentin histoarchitecture (WANG et al., 2010).

In vitro studies were conducted by Mohandesnezhad et al. (2020) in DPSC cultures, with PCL and PLA 3D-printed scaffolds and nano-hydroxyapatite and zeolites bone grafts. Good adhesion and cell proliferation were observed, indicating that the structures had the potential capacity to promote bone regeneration in dental procedures. Gendviliene et al. (2021) performed *in vivo* experiments, in animals, with PLA and hydroxyapatite 3D-printed scaffolds and observed a successful formation of new bone tissues, with or without a culture of DPSC inside the scaffolds before implantation.

3.2 ADDITIVE MANUFACTURING

3.2.1 General

Additive manufacturing (AM), also known as 3D printing, encompasses different technologies whose common principle is based on fabricating parts layer-by-layer from a computationally designed three-dimensional model. Some AM techniques include liquid-based processes such as stereolithography (SLA), digital light processing (DLP), and electrospinning; powder-based processes such as selective laser sintering (SLS), direct metal laser sintering (DMLS), electron beam melting (EBM), and selective laser melting (SLM); and solid-based processes such as fused filament fabrication (FFF) and laminated object manufacturing (LOM). Specifically for bone tissue engineering, the most relevant AM techniques to produce synthetic

scaffolds consist of SLS, SLM, FFF, EBM, SLA, and electrospinning (FARRÉ-GUASCH et al., 2015; YANG et al., 2019).

One of the great advantages of additive manufacturing, compared to more traditional polymer processing techniques – such as molding and extrusion – consists of the possibility of obtaining complex and varied geometries. In addition, the technology is associated with considerably less or even zero waste, being more cost-effective (NGO et al., 2018).

Additive manufacturing allows scaffolds to be produced in a customized manner, not only in their outer shape but also in their inner porous structure, both of which are very important factors for proper tissue regeneration. It is possible to use computerized tomography or MRI data from a patient, for example, to create a 3D model of a synthetic scaffold (FARRÉ-GUASCH et al., 2015; WANG et al., 2017). Different AM techniques have been successfully employed to treat bone deficiencies, e.g. in the craniomaxillofacial (CMF) region (LI et al., 2011; MUELLER et al., 2011; SAIJO et al., 2009; SÁNDOR et al., 2013; XU et al., 2010).

3.2.2 Fused Filament Fabrication (FFF)

Fused filament fabrication (FFF) technology, which is within the scope of this work, consists of heating a thermoplastic polymer filament until it melts so it can be extruded through a nozzle. The extruded material is then deposited on a surface and layers are progressively formed (Figure 2), according to the movement of the extruder nozzle and other computationally defined printing parameters. The dimensional accuracy between the printed structure and the 3D model strongly depends on the nozzle that is used (CHOI et al., 2020; YANG et al., 2019).

Figure 2 - Schematic representation of a FFF 3D printer.

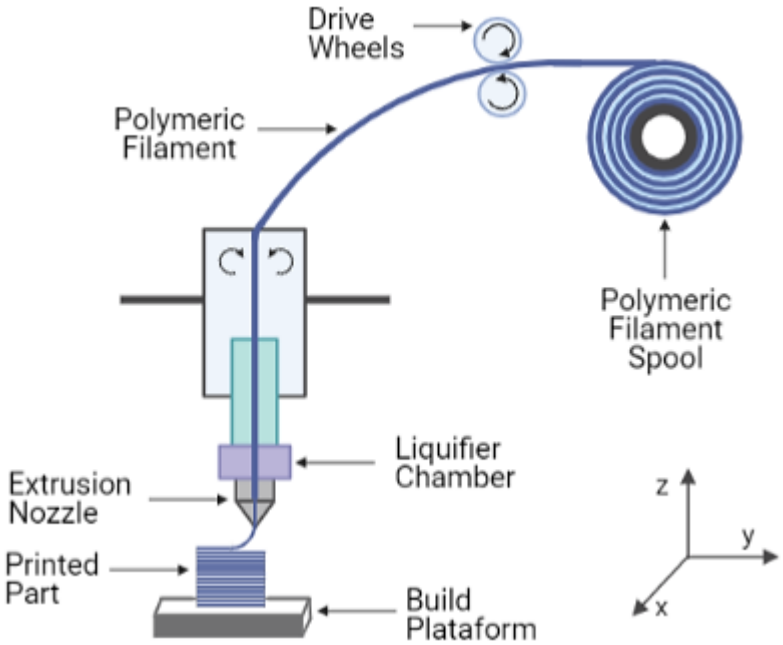

Source: Author.

Some important parameters for 3D printing, besides the nozzle diameter, consist of the extrusion multiplier (which determines the extruded material flow rate, through the filament puller), as well as the extrusion height and width (depending on the distance between the nozzle and the surface, the nozzle movement speed, and the extrusion multiplier). In addition, there are the fill pattern (type of geometry produced on the outside or inside of the piece, such as rectilinear, triangular, concentric, etc.), fill percentage (i.e. the percentage of each layer filled by extruded material), and contour overlap (i.e. the percentage of an extruded filament that overlaps an already extruded adjacent filament, which determines the level of adhesion between nearby filaments).

Some examples of polymers employed to produce scaffolds, both in their pure state and as composites, through FFF, are PLA (CHOI et al., 2020) and poly(caprolactone) PCL (HUTMACHER et al., 2001), poly(ether-ether-ketone) (PEEK) (VAEZI; YANG, 2015), and poly(lactic acid-co-glycolic acid) (PLGA) (YEN et al., 2009) – which are suitable for 3D printing technique because of their low melting points and short solidification times (CAMINERO et al., 2019; YEN et al., 2009). 3D printing represents a major advance in the tissue engineering area, as previous technologies are not equally able to reproduce the internal structure of human tissues, with good control of pore size and distribution (WANG et al., 2017).

3.3 POLY(LACTIC ACID)

Poly(lactic acid) (PLA) is obtained from the lactic acid (LA) monomer, $C_3H_6O_3$, whose official nomenclature is "2-hydroxypropionic acid"[1]. Lactic acid is a chiral molecule that presents two enantiomers: L-lactic acid and D-lactic acid, which differ in their effect on polarized light (LUNT, 1998).

PLA is an aliphatic (open-chain) (Figure 3), $[(C_3H_4O_2)_n]$ polyester, with biodegradability and biocompatibility. It can be synthesized from renewable sources such as corn, sugarcane, potato, and other biomasses. The polymer has two stereoisomers: poly(L-lactic acid) (PLLA) and poly(D-lactic acid) (PDLA), their racemic mixture generates poly(D, L-lactic acid) (PDLLA), and there is also the meso-poly(lactic acid). PLLA and PDLLA are the most relevant and studied forms of PLA for biomedical applications (GUPTA; REVAGADE; HILBORN, 2007; SAVIOLI LOPES; JARDINI; MACIEL FILHO, 2012; ULERY; NAIR; LAURENCIN, 2011).

Figure 3 - Chemical structure of poly(lactic acid).

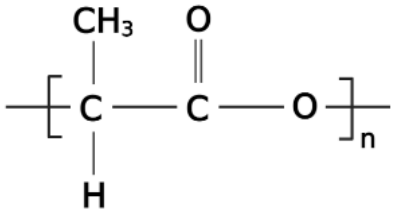

Source: Author.

PLA presents a glass transition temperature (T_g) that varies between 50 and 64 °C and a melting temperature (T_m) between 145 and 186 °C. The crystallinity (χc) varies with the type of PLA isomer: PDLA is classified as semi-crystalline, PDLLA as amorphous and PLLA presents χc between 0 and 37% (LU; MIKOS, 1999).

Other characteristics that make PLA suitable for surgical procedures are its hydrolytic degradability, its bioabsorbability, and that it does not produce toxic compounds during degradation. When implanted in the body, hydrolysis of PLA generates lactic acid molecules, which are incorporated into the citric acid cycle, resulting in products such as carbon dioxide and water (SHARMA; MUDHOO, 2011).

[1] According to the nomenclature rules of the International Union of Pure and Applied Chemistry (IUPAC).

Due to its eco-friendly, biocompatibility, and biodegradability properties, in addition to its good mechanical properties, PLA has been standing out as an advantageous material for biomedical use. Examples of applications are orthopedic devices, drug delivery systems, and porous scaffolds for use in regenerative medicine, among others (PAWAR et al., 2014).

Three-dimensional porous scaffolds, presenting PLA as raw material, have already been developed and widely used in tissue engineering. Some applications are in cell regeneration of bones (CAI et al., 2012; CARLETTI et al., 2011; CHEN et al., 2019; SAHMANI et al., 2020; SCHOFER et al., 2008; SHIM et al., 2010), cartilages (FARSI; ASEFNEJAD; BAHARIFAR, 2022; JU et al., 2007; ROSENZWEIG et al., 2015), tendons (GOTTARDI et al., 2021; INUI et al., 2010; JIANG et al., 2020), and vascular tissues (HU et al., 2011; KARBASIAN et al., 2021; LIU et al., 2020). The scaffolds developed in the studies show promising results, in terms of stimulating cell adhesion, differentiation, and growth – when subjected to *in vitro* tests, with cell cultures, and/or *in vivo* tests, through implantation in animals.

3.4 NATURAL WEATHERING

The weathering of polymers, in general, is the area of science dedicated to studying the variation of their properties when exposed to natural conditions or artificial conditions applied in a controlled manner. Natural weathering results from the combination of several environmental variables that trigger different degradation mechanisms, and the main factors acting on the weathering of polymeric materials are light (radiation), temperature, and humidity (JACQUES, 2000).

When it is intended to evaluate a material for its associated degradation phenomena and rates, clearly natural weathering tests more faithfully represent the conditions to which a product will be subjected in practice, with environmental variables applied at natural rates. Therefore, natural weathering could be understood as the most appropriate technique to determine the durability of a product in situations prior to use: storage and transportation, for example (PICKETT, 2020).

However, the times required, in this type of experiment, to identify significant physicochemical changes, i.e., that would lead to the functional failure of the product, are considerably long, in addition to the high costs associated. Due to these factors, natural weathering studies are often unfeasible – both for developers and consumers of a particular technology, especially in the current competitive market (JACQUES, 2000; LV et al., 2015). Another obstacle in determining the shelf life of a material by natural weathering tests is the

inherent variability of nature: climatic conditions can be extremely irregular – even for the same location and time of year – which makes it difficult to reproduce the experiments, and degradation profiles can considerably vary from one region to another (JACQUES, 2000; POSPÍŠIL et al., 2006).

There are also several configurations in which a polymeric material can be exposed to natural weathering conditions, which may favor one or more degradation mechanisms. According to the technical standards ASTM D1435 (2020) and ASTM G90 (2017), which elucidate natural weathering testing procedures, the variables include, for example, angle of exposure, use of a support or not, direct exposure or under glass, and use of equipment in a fixed position or with sunlight tracking. The standard ASTM G7 (2013) provides guidance on natural weathering tests with non-metallic materials under direct exposure to the natural atmosphere and solar radiation, while ASTM G24 (2013) defines the methodology for natural weathering testing in which sunlight is filtered by glass, simulating the presence of a window.

One of the strategies adopted for natural weathering tests was to define certain sites, with severe climatic conditions, as reference sites to conduct these tests – based on the idea that since it is not possible to determine a product's shelf life for several different climates, it is important to, at least, obtain information about its degradation behavior in critical environments (KOCKOTT, 1989). Thus, there are natural weathering test stations in these reference sites, such as Florida (United States), approximately 26°N latitude – with subtropical, hot, and humid climate – and Arizona (United States), approximately 34°N latitude – with desert, hot and dry climate (ASTM D5272 (2008); KOCKOTT, 1989; PICKETT, 2020).

Yew et al. (2009) analyzed the natural weathering of PLA – pure and as composites with rice starch and epoxidized natural rubber – and they have observed, for pure PLA, a decrease of approximately 50% in the percentage of strain to failure (%) after eight weeks. Zaidi et al. (2010) also conducted natural weathering tests – with PLA and PLA/Cloisite clay composites – verifying a reduction of about 50% in the molecular weight ($g \cdot mol^{-1}$) of the pure PLA structures after sixty days (about eight weeks as well).

3.5 ACCELERATED ARTIFICIAL WEATHERING

3.5.1 General

Given the difficulties involved with performing natural weathering tests, as well as the commercial demand for quick answers regarding the performance of developing polymer

products – in terms of durability – accelerated weathering tests have become necessary. This has promoted the development and improvement of artificial weathering methodologies in recent decades, although even today it is difficult that the results obtained and interpreted from these analyses accurately reflect reality – due to the inherent variability of nature (PICKETT, 2018).

It is possible to apply artificial conditions, more critical than those naturally observed, in order to accelerate the process of physical-chemical degradation of a polymeric material and subsequently – by establishing a correlation with natural weathering factors – predict the product's shelf life within a shorter and more acceptable time. Shelf life is the period after which a property essential to the function of the manufactured product reaches or exceeds a minimum acceptable value (HULME; COOPER, 2012; WHITE; TURNBULL, 1994).

The exposure variables must be consistent with the conditions that act upon the product post-manufacturing and that may affect its physical-chemical stability. The main natural factors that contribute to the degradation of polymeric materials and thus affect their functional properties are sunlight – particularly the ultraviolet radiation portion – heat – which accelerates thermally activated reactions and leads to thermodegradation – and moisture – which causes degradation by hydrolysis, also leading to chain scission (JACQUES, 2000; WHITE; TURNBULL, 1994).

3.5.2 Related Technical Standards

There are several technical standards that define methodologies for accelerated weathering tests, which mainly differ by the light sources used and, consequently, by the wavelength range that acts on the material – which determines how photochemical reactions occur, since the shorter the wavelength, the higher the photon energy intensity (JEON; KIM, 2013; WHITE; TURNBULL, 1994). ISO 4892-1 (2016) and ASTM G151 (2019), for example, provide general information and guidance regarding different methods for exposing polymeric materials to laboratory radiation sources (UV, visible, infrared, and others) for accelerated artificial weathering tests.

The standards ASTM G152 (2013) and ASTM G153 (2013) define methodologies for accelerated weathering tests with open and closed carbon arc lamps, respectively – which emit wavelengths shorter than 260 nm. The standard ASTM G155 (2013) establishes the method using xenon arc lamps, which emit wavelengths bigger than 270 nm. Finally, ASTM G154 (2016) standard refers to the method that employs ultraviolet (UVA and UVB) lamps, with

three main radiation types: by UVA-340 lamp, with an emission peak of 343 nm; the UVA-351 lamp, with an emission peak of 351 nm; and the UVB-313 lamp, with an emission peak of 313 nm.

Any artificial weathering technique can be employed to draw conclusions about the degradation of a polymeric material, if there is an understanding of the results and associated limitations. Pickett (2018) presents a detailed analysis of the different radiation sources used in accelerated weathering tests, giving attention to the techniques that present certain problematics for correlating laboratory tests and natural environment conditions and should, therefore, be avoided, as there are more suitable methodologies to perform shelf life predictions of polymers. These problems arise from the fact that some light sources are significantly distant from the wavelength range emitted by the Sun – from 295 nm to 400 nm – and from the spectral distribution of solar radiation (PICKETT, 2018).

The standardized techniques Pickett (2018) advises against are those using 1) carbon arc lamps, 2) xenon arc lamps, and 3) UVB-313 fluorescent lamps. All the light sources mentioned excessively emit wavelengths below the sunlight cutoff value of 295nm, which ends up accelerating degradation in a way that is not consistent with real-world conditions; moreover, 1) and 3) have spectral radiation distributions that considerably differ from that presented by the Sun.

Among the techniques given as recommendable for accelerated weathering studies there are xenon arc lamps associated with ceramic UV radiation filters – which cuts off much of the excess UV shorter than 295 nm on the material – and temperature and humidity controllers. In addition, the use of UVA-340 fluorescent lamps is recommended, as also advised by ASTM G154 (2016), since they do not have irradiance below the sunlight wavelength cutoff. The UVA-340 lamps' emission range is between 295 nm and 365 nm, while UVB-313 lamps have an emission range of 270 nm to 313 nm (PICKETT, 2018). Figure 4 compares the spectral radiation distributions (irradiance as a function of wavelength) of the sun – based on the technical standard ASTM G177 (2020) – of a UVA-340 lamp and a UVB-313 lamp.

Figure 4 - Spectral radiation distributions of UVB-13 lamp, UVA-340 lamp, and sunlight.

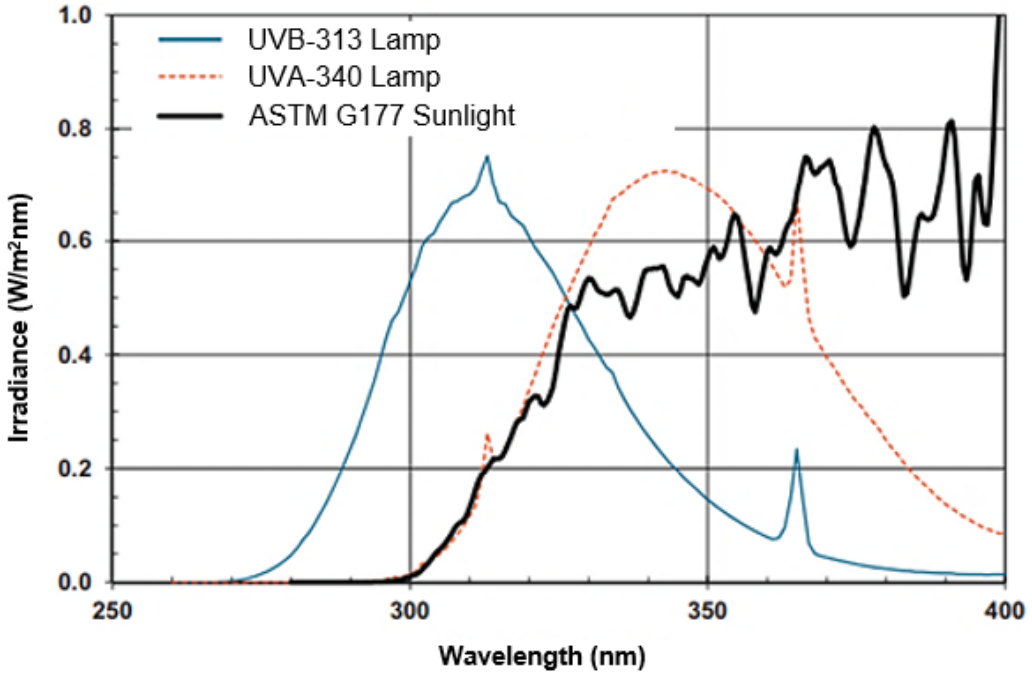

Source: Adapted from Pickett (2018).

The ASTM G154 (2016) methodology, specific for accelerated weathering tests with non-metallic materials, basically consists of subjecting the material, inside a chamber, to cycles of exposure to ultraviolet light, humidity, and temperature, in a controlled manner. There are eight possible cycle configurations, which are differentiated by the type of lamp (UVA or UVB, and emission peak), the irradiance of the lamp, the type of humidity applied (condensation or water spray), the periods with and without applied radiation, as well as the humidity and temperature intensities during each exposure condition (Table 1). The UVA-340 lamp is recommended for simulating direct exposure to sunlight, while the UVA-351 lamp is recommended for simulating exposure to sunlight through a glass window. Furthermore, it is stated that the UVB-313 lamp can give faster results by accelerating the degradation process; and yet it often leads to degradation by mechanisms that would not occur in a real situation under sunlight exposure.

Table 1 - Cycles of UV radiation, temperature, and humidity of ASTM G154 (2016).

Cycle	Lamp	Typical Irradiance [W/(m^2) · nm]	Approximate Wavelength [nm]	Exhibition Cycle
1	UVA-340	0.89	340	8 h of UV application at 60(±3) °C and 4 h of condensation at 50(±3) °C.
2	UVB-313	0.71	310	4 h of UV application at 60(±3) °C and 4 h of condensation at 50(±3) °C.
3	UVB-313	0.49	310	8 h of UV application at 70(±3) °C and 4 h of condensation at 50(±3) °C.
4	UVA-340	1.55	340	8 h of UV application at 70(±3) °C and 4 h of condensation at 50(±3) °C.
5	UVB-313	0.62	310	20 h of UV application at 80(±3) °C and 4 h condensation at 50(±3) °C.
6	UVA-340	1.55	340	8 h of UV application at 60(±3) °C and 4 h condensation at 50(±3) °C.
7	UVA-340	1.55	340	8 h of UV application at 60(±3) °C, 0,25 h of water *spray* (no light), uncontrolled temperature, and 3.75 h of condensation at 50(±3) °C
8	UVB-313	28	270 a 700	8 h of UV application at 70(±3) °C and 4 h condensation at 50(±3) °C.

Source: data extracted from the technical standard ASTM G154 (2016).

PLA has assumed technological importance in areas such as biomedical, textile, and packing (FARAH; ANDERSON; LANGER, 2016). Therefore, the research field related to its degradation process shows great relevance. There are many accelerated weathering studies with PLA conducted according to ASTM G154 (2016) guidelines, for example. In these studies, the types of exposure cycles selected vary; using, most often, UVA radiation sources (BOLIO-LOPEZ et al., 2013; GONZÁLEZ-LÓPEZ et al., 2020; ISADOUNENE et al., 2018; ISLAM; PICKERING; FOREMAN, 2010; LIN; XIE; QIU, 2019; LV et al., 2017, 2018; MARTÍN DEL CAMPO et al., 2020; SAWPAN et al., 2019; SIAKENG et al., 2020; YATIGALA; BAJWA; BAJWA, 2018) – given the advantages previously presented – however, some use UVB lamps (KAYNAK; SARI, 2016; VARSAVAS; KAYNAK, 2017).

In the mentioned studies, the evaluation of the accelerated degradation of PLA over exposure time is done, for example, through chemical analysis: identification of crystalline phases, measurement and distribution of molecular weight, identification of functional groups and chemical bonds, measurement of chromaticity, measurement of thermal stability, determination of glass transition and melting temperatures, as well as enthalpies of

crystallization and melting, and degree of crystallinity. Macroscopic physical analyses (such as mass variation, level of water absorption, dimensional stability, surface roughness, and visual analysis of color, cracks, etc.) and microscopic physical analyses (such as optical and scanning electron microscopy), as well as mechanical tests (such as tensile test, bending test, impact test, and fracture toughness test), are also employed.

3.5.3 Exposure Variables

3.5.3.1 Ultraviolet Radiation

The shortest wavelengths of UV radiation emitted by the Sun can reach up to 120 nm, but oxygen and ozone of the atmosphere absorb those below 295 nm, preventing them from reaching Earth's surface. The resulting UV radiation corresponds to only 6%, approximately, of all incident solar radiation on Earth; but it still produces the most significant photochemical degradation phenomena on polymeric materials – since it has short wavelengths and, consequently, high photon energy intensity (ASTM E490 (2019); KOCKOTT, 1989; PICKETT, 2020; WHITE; TURNBULL, 1994).

The total radiation acting on a specimen, that is, the total energy (ε_t) absorbed when exposed to a radiation source (in $\mathrm{J} \cdot \mathrm{m}^{-2}$), can be obtained by multiplying the irradiance (I) of the source, i.e. the radiant energy flux incident per unit area of the specimen (in $\mathrm{W} \cdot \mathrm{m}^{-2}$), and the exposure time (t) of exposure (in hours), multiplied by 3600, because $\mathrm{W} = \mathrm{J/s}$, as indicated by Equation (1) (KOCKOTT, 1989).

$$\varepsilon_t = I \cdot t \cdot 3600 \tag{1}$$

For cyclic accelerated weathering tests using UV radiation, for example, the ε_t during exposure will consist of the sum of the energy ε absorbed during the exposure time (t_{exp}) of each UV cycle, considering the average, or typical, irradiance ($\bar{I}$), of the lamp. Thus this situation can be illustrated by a graph of I as a function of t, where ε_t is the area under the curves corresponding to the periods when UV is used (Figure 5), that is, it will be given by the integral of Equation (2).

Figure 5 - Representative graph of the energy absorbed during testing with UV radiation application.

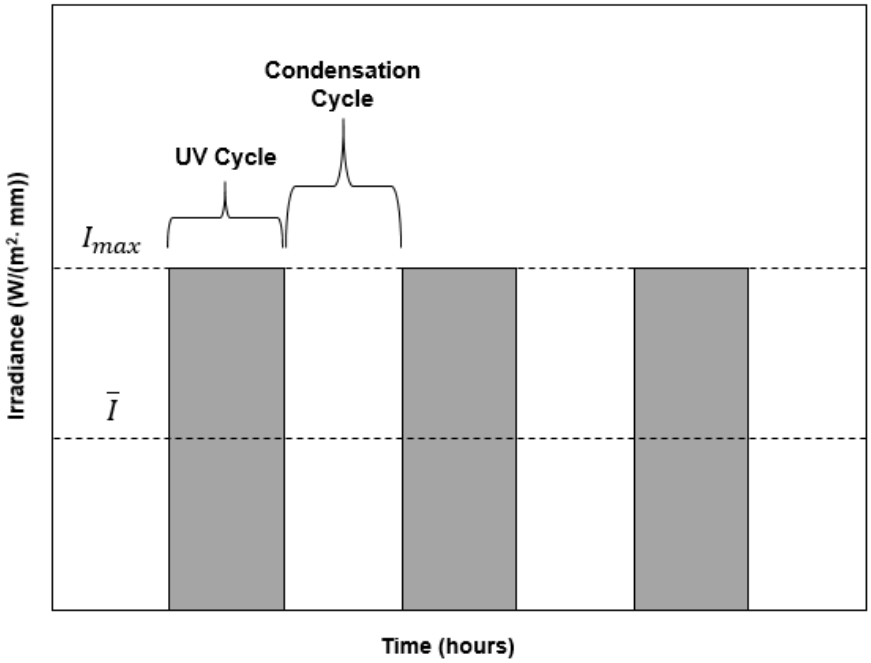

Source: Adapted from González-López et al. (2020).

$$\varepsilon_t = \int_0^{t_{exp}} \bar{I}\, dt = \bar{I} \cdot t_{exp} \qquad (2)$$

There are two main sources of UV radiation for artificial polymer weathering tests: xenon arc lamps and UV fluorescent lamps. Both are capable of reproducing solar specifications reasonably faithfully and have largely become substitutes for older light sources like carbon arc lamps and mercury vapor lamps (WHITE; TURNBULL, 1994).

As explained above, xenon arc lamps need filters to block wavelengths below the cutoff of solar radiation. In addition, humidity controllers must be used, and the high-intensity infrared radiation emitted by these lamps must be filtered to prevent overheating of specimens. The main disadvantage associated with the use of these lamps is the rapid deterioration of the xenon burners and filters, so their performance has to be checked regularly, making the technique expensive to run (KOCKOTT, 1989; WHITE; TURNBULL, 1994).

UV fluorescent lamps, on the other hand, allow considerably cheaper test operation for a longer service time, and produce no significant heat, with low emission of visible light and zero emission of infrared radiation. Therefore, a separate heat source is required, which is not a disadvantage, as independent lighting and heating control systems are desirable in test

equipment. Nevertheless, it is still necessary to periodically check if the spectral output meets the specifications for the type of lamp being used (WHITE; TURNBULL, 1994).

3.5.3.2 Temperature

The temperature has a great influence on the weathering of polymeric materials and the heating of a specimen will depend on the environmental temperature, the absorbed radiation, the heat transfer between the specimen and the air, and the thermal conduction within the material. Temperature cycles used in accelerated weathering tests, which aim to reproduce heating and cooling phenomena, cause dilations and contractions of the specimen, which may generate residual stresses that lead to the appearance of cracks or fissures, for example (ISLAM; PICKERING; FOREMAN, 2010; LILA et al., 2019; SAWPAN et al., 2019; WEIR et al., 2004).

By increasing temperature, the rate at which chemical reactions occur usually increases. This phenomenon is commonly estimated by Arrhenius Law, given by Equation (3), where k is the reaction rate, A is the constant related to the reaction entropy, E_a is the activation energy (given in $\mathrm{J \cdot mol^{-1}}$) – which is material-specific and varies from 0 to 60 $\mathrm{J \cdot mol^{-1}}$ for polymer thermodegradation – R is the universal gas constant (8.13 $\mathrm{J \cdot mol^{-1}K^{-1}}$), and T is the absolute temperature (given in K) (PICKETT, 2018, 2020).

$$k = A \cdot e^{\left(\frac{-E_a}{R \cdot T}\right)} \tag{3}$$

An empirically-based rule often called the Arrhenius 10 °C Rule states that the reaction rate of degradation processes doubles with a 10 °C increase in temperature, which means a reaction rate coefficient ($Q10$) equal to 2. This relationship is often employed in accelerated weathering studies, under elevated temperatures, conducted with biomaterials and polymeric medical devices (HUKINS; MAHOMED; KUKUREKA, 2008).

Even though the Arrhenius 10 °C Rule, with $Q10 = 2$, is of great relevance for the research field that aims to determine the shelf life of polymeric products, $Q10$ can, in fact, present a little or great variation from this value, depending on the material. Pickett (2018) has proposed that more accurate values of $Q10$ can be estimated from the range of values in which the material E_a is. However, it is recommended, whenever possible, to consult the specific literature in search of a more appropriate coefficient for the studied polymer, i.e., that more

faithfully characterizes the temperature influence over its rate of weathering reactions (ABNT NBR 16469 (2020)).

3.5.3.3 Humidity

Water is one of the most abundant substances in the environment, either in the form of atmospheric moisture, rain, or dew. The use of moisture cycles in accelerated weathering tests allows simulating situations in which the polymeric product could come into contact with water under the mentioned forms – which, normally, is intended to avoid using packing, although there is still the possibility of a poor sealing allowing the formation of droplets inside this packing, for example – and also simulating situations of alternate cooling and heating – as, for example, in cases of transport without adequate temperature control.

Absolute humidity basically consists of the water content in the air, usually given in kg steam/m^3 air. Relative humidity, on the other hand, is the absolute humidity normalized to the water content of saturated air at a certain temperature, given in %. As the temperature increases, the water content of the saturated air increases (i.e. the air's maximum capacity to absorb water also increases). Thus, if the air temperature increases and no water is added to the system, the relative humidity will decrease as the absolute humidity remains constant.

Water can be used in accelerated weathering tests through chamber air humidification, condensation (saturated air humidity), water spray, or immersion. Water immersion represents an extreme situation that mainly promotes hydrolysis (i.e., degradation of hydrolytic components) of the material; whereas humidification, condensation, and the use of spray are more related to the intensification of photodegradation (GONZÁLEZ-LÓPEZ et al., 2020).

The susceptibility of polymers to degradation, reduction in mechanical properties, cracking or crazing, and fading is enhanced by the presence of moisture (COPINET et al., 2004; HO; POMETTO; HINZ, 1999; MICHEL; BILLINGTON, 2012). Copinet et al. (2004) have observed that PLA hydrolysis is intensified by both temperature and relative humidity.

3.6 PLA DEGRADATION MECHANISMS

PLA degradation can occur through different mechanisms, triggered by different external stimuli, such as those discussed in section 3.5.3. Regarding photolytic mechanisms, there are two main types described in the literature: Norrish I and Norrish II. In the first one, a carbonyl group in the middle of the chain breaks down forming free radicals and leading to the

chain scission, which causes a reduction in molecular weight. However, in the case of PLA, the second mechanism is predominant (IKADA, 1997). Norrish II (Figure 6) consists of the absorption of a photon (with $h\nu$ energy) by the polymer chain and the subsequent breaking of C-O bonds, so the formation of hydroperoxides leads to degradation by generating carboxylic acid and diacetone terminal groups. In addition, photolysis of diacetones results in homolytic[2] cleavage of the C-C bond between the two carbonyl groups. The presence of carbonyl groups (C=O) in the structure of PLA favors its photodegradation, as they absorb UV radiation (GONZÁLEZ-LÓPEZ et al., 2020; JANORKAR; METTERS; HIRT, 2007; YEW et al., 2009).

Figure 6 - Norrish II mechanism of PLA photolytic degradation.

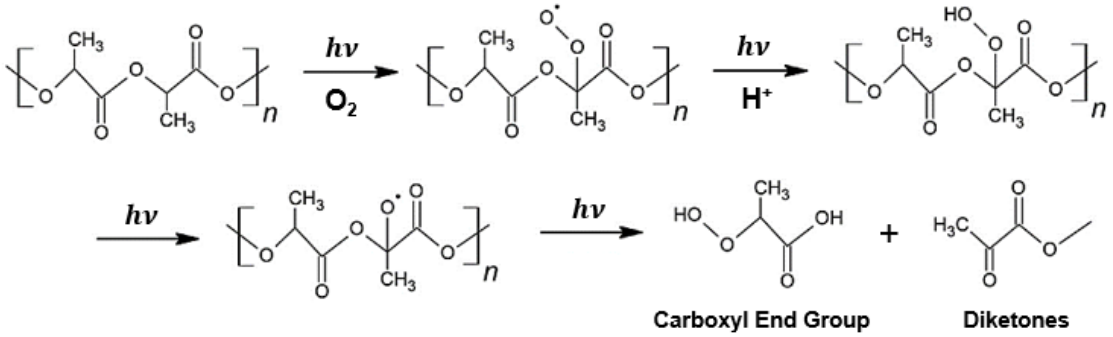

Source: Adapted from González-López et al. (2020).

The hydrolytic degradation of PLA (Figure 7) occurs by chain scission preferentially in the amorphous regions of the material, in which the segments of the macromolecules are more flexible and susceptible to react with water, and it is a phenomenon intensified by temperature action. The hydrolysis rate depends on the amount of absorbed water and occurs mainly due to the presence of carbonyl groups, which makes the molecule susceptible to hydrolysis by scission of ester bonds (COPINET et al., 2004; DE JONG et al., 2001; ELSAWY et al., 2017; YUAN; MAK; YAO, 2002).

The degradation of chain segments in amorphous regions of PLA reduces the molecular entanglements, characteristic of these regions, and increases the mobility of the chains, which can reorganize and slowly become crystalline – leading to an increase in the material's degree of crystallinity. After the preferential attack on amorphous regions, degradation starts in the material's crystalline regions, which are less susceptible to degradation due to their ordered structure (YATIGALA; BAJWA; BAJWA, 2018; YUAN; MAK; YAO, 2002).

[2] A covalent bond scission in which each of the segments receives one of the shared electrons.

Figure 7 - PLA hydrolysis mechanism.

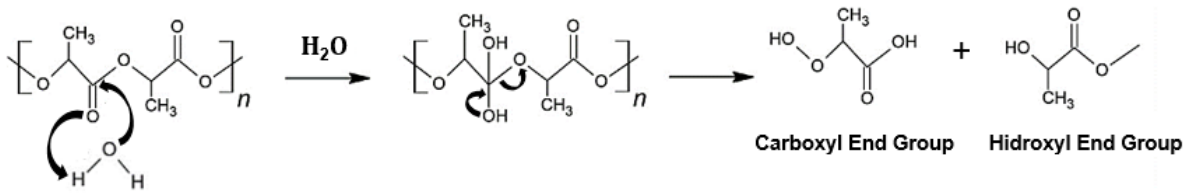

Source: Adapted from Al-Itry, Lamnawar, and Maazouz (2012).

Temperature is also responsible for triggering degradation reactions, and there are differences between those that occur below and above the melting point of a given polymer (AOYAGI; YAMASHITA; DOI, 2002; KOPINKE et al., 1996; RASSELET et al., 2014; WACHSEN; PLATKOWSKI; REICHERT, 1997). In the present work, the PLA thermodegradation process that occurs at temperatures below the melting point is more relevant, since it is aimed to evaluate its durability in post-processing conditions and prior to end-use.

Rasselet et al. (2014) investigated the possible mechanisms of PLA thermooxidative degradation under temperatures below its melting point and concluded that it is a closed-loop mechanism (in which the reaction produces its own starting compound to trigger the reaction again), that occurs according to the scheme shown in Figure 8. The tertiary C-H bond is considered to have the lowest dissociation energy and hydroperoxides (R-OOH) are the main contributors to initiating the thermooxidative process – being, therefore, the reaction initiators (AUDOUIN et al., 1995; RASSELET et al., 2014).

Figure 8 – PLA thermo-oxidation mechanism.

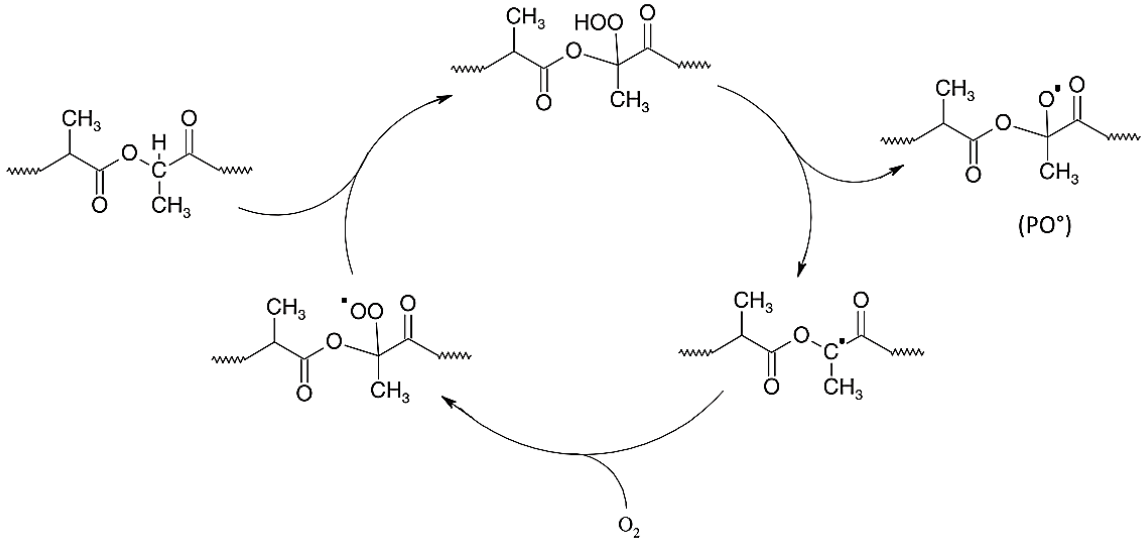

Source: Rasselet et al. (2014).

3.7 CORRELATION BETWEEN ACCELERATED ARTIFICIAL WEATHERING AND NATURAL WEATHERING

As stated in previous sections, laboratory accelerated weathering tests performed with polymers aim to verify, in an acceptable time (not excessively long), the stability of a material under critical conditions of temperature, humidity, and/or radiation, etc. By establishing a relationship between the variables artificially employed and those present in a real situation, the shelf life of the polymeric material can be predicted. The correlation between accelerated weathering and natural weathering is done by means of an acceleration factor (F_a), which should be calculated taking into account the differences between the chosen artificial variables and those observed in real conditions, so that it is possible to estimate how many hours of natural weathering are simulated in an accelerated weathering test.

A F_a is calculated specifically for a given polymer and given artificial weathering conditions. Therefore, for tests that simulate the effects of more than one climatic variable, mathematic models are defined by considering the influence of the different parameters of interest – such as temperature, humidity, radiation, oxygen pressure, among others – so that the long-term degradation behavior of the polymeric material can be determined (GORDON et al., 2018; LV et al., 2018, 2015; MAN et al., 2012; PICKETT; COYLE, 2013; SANTONJA-BLASCO; RIBES-GREUS; ALAMO, 2013; TSUJI; KIDOKORO; MOCHIZUKI, 2007).

The degradation of a polymeric material in natural and accelerated weathering tests is analyzed by means of measurements of physicochemical properties established as relevant to the functionality of the product under evaluation. The stopping criterion for such tests, i.e., when the material failure is detected, is often defined as the point at which an essential property reaches 50% of its initial value (COPINET et al., 2004; HULME; COOPER, 2012; KOCKOTT, 1989; YEW et al., 2009; ZAIDI et al., 2010).

3.7.1 Temperature Control

One of the strategies used to accelerate the degradation process and thus assess the durability of biomaterials and polymeric medical devices is to use high temperatures, which, according to Arrhenius Law (Equation (3)), increases the rate of reactions related to the weathering process (HEMMERICH, 1998; HUKINS; MAHOMED; KUKUREKA, 2008). ABNT NBR 16469 (2020) and ASTM F1980 (2016) – on which ABNT NBR 16469 (2020) is based – provide guidance on shelf life determination for polymeric materials of implant industry

– through accelerated weathering tests at elevated temperatures – where the acceleration factor is defined based on the Arrhenius 10 °C Rule and is given by the Equation (4).

The mentioned technical standards are primarily directed to tests with polymeric packing for medical devices. However, the same methodology for testing and determining shelf life is employed for medical devices themselves when manufactured in polymeric raw materials (HEMMERICH, 1998; HUKINS; MAHOMED; KUKUREKA, 2008).

$$F_{a(T)} = Q10^{\left(\frac{T_{aw}-T_r}{10}\right)} \quad (4)$$

where:

$F_{a(T)}$ is the acceleration factor between natural weathering and accelerated weathering under temperature control;

$Q10$ is the reaction rate coefficient;

T_{aw} is the temperature used in accelerated weathering (given in °C);

T_r is the room temperature (given in °C), usually between 20 and 25 °C.

As exposed in section 3.5.3.2, conservatively, the acceleration factor (F_a) is defined using a reaction rate coefficient ($Q10$) equal to 2. However, ABNT NBR 16469 (2020) recommends using a value that best represents the effect of temperature increase on the material's reaction rate, when it is well characterized in the literature.

Copinet et al. (2004) and Ho, Pometto, and Hinz (1999) studied the degradation behavior of PLA under temperatures above room temperature, also controlling the relative humidity during thermal exposure. Copinet et al. (2004) employed temperatures of 30, 45, and 60 °C, under relative humidity (RH) values of 50 and 100%; while Ho, Pometto, and Hinz (1999) used temperatures of 25, 40, and 55 °C, under RH of 10, 50 and 100%, employing PLA with three different molecular weights (mw).

In order to determine an appropriate $Q10$ for PLA, the degradation rates for different temperatures were obtained from the mentioned studies. The condition of RH = 50% was selected, since at a constant RH of 100%, water uptake and hydrolysis become much more significant on degradation, and it is actually aimed to evaluate how the thermodegradation processes are intensified. In addition, the results of the study of Ho, Pometto, and Hinz (1999) taken into account referred to a PLA with mw = 2 x 10^5 g $\cdot$ mol^{-1}, as the PLA used in the study of Copinet et al. (2004).

Thus, the degradation rates, in terms of molecular weight variation per week (Δmw/week), were found by approximating the mw x time curves to linear equations and calculating their respective slopes (angular coefficients). To determine $Q10$, it is necessary to compare the degradation rate for temperatures 10 °C apart; therefore, two pairs of temperatures were considered: 30 – 40 °C, and 45 – 55 °C. In addition, the data for times up to 5 weeks were considered, a period in which the molecular weight decay shows linear behavior and which comprises the exposure time to be employed in the present work.

The degradation rates (k) calculated for the four temperatures, as well as the reaction rate coefficients for 10 °C increases ($Q10$) – obtained by the ratio between the k values for 30 and 40 °C, and for 45 and 55 °C – are given in Table 2.

Table 2 - Degradation rates (k) of PLA under different temperatures and $Q10$ values obtained by the ratio between k values for temperatures 10 °C apart.

Temperature	**Degradation Rate (k) [Δmw/week]**	**$Q10$**	**Bibliographic Reference**
30 °C	4.57	2.96	Copinet et al. (2004)
40 °C	13.55		Ho, Pometto, and Hinz (1999)
45 °C	8.78	2.99	Copinet et al. (2004)
55 °C	26.24		Ho, Pometto, and Hinz (1999)

Source: Author.

It can be seen that the $Q10$ value for PLA is approximately 3. Therefore, specifically for this material, the acceleration factor for accelerated weathering by temperature control ($F_{a(T)}$) would be given by Equation (5) (considering a T_r = 25 °C).

$$F_{a(T)} = 3^{\left(\frac{T_{aw}-25}{10}\right)} \quad (5)$$

By determining the time for failure in the accelerated weathering test ($t_{aw(T)}$), it is possible to estimate the time for failure in natural weathering ($t_{nw(T)}$), i.e., the product shelf life, using Equation (6).

$$t_{nw(T)} = t_{aw(T)} \cdot A_{F(T)} \quad (6)$$

3.7.2 Temperature, Humidity, and UV Radiation Control

Another artificial weathering technique used to promote the accelerated degradation of polymers (in order to allow the rapid determination of their durability), considering more weathering variables, consists of the application of severe conditions of temperature, humidity, and ultraviolet radiation – and ASTM G154 (2016) is one of the technical standards most commonly taken as a basis for this purpose. One of the application areas in which this accelerated weathering methodology is applied consists of medical devices made of polymeric raw materials, such as silicone and PLA (LACERDA; RIBEIRO, 2016; SHIHAB; ABDUL-AMEER, 2018; ZARDAWI, 2012).

As previously explained in 3.5.2, the ASTM G154 (2016) methodology consists of subjecting the material to controlled cycles of temperature, condensation, and ultraviolet light, in order to simulate critical conditions of heating/cooling, humidity, and solar exposure. Again, to determine the product's shelf life, it is necessary to assess the time required for its functional failure under accelerated weathering and use a mathematical model that establishes the relationship between artificial and natural conditions, in order to predict the time for failure in a real situation.

Lv et al. (2015) conducted accelerated weathering tests with a polymeric material – specifically polypropylene (PP) – and they proposed an equation to obtain the acceleration factor that indicates the correspondence between the tests and natural weathering. It was based on the two-parameter Arrhenius equation for photochemical degradation reactions (Equation (7)), in which the rate (k) depends on the irradiance (I) – associated with an exponent α – and the temperature (T) to which the material is exposed (RAJPUT; SASTRY; TIWARI, 2017).

$$k = (I)^{\alpha} e^{\frac{-E_a}{R \cdot T}} \quad (7)$$

In Lv et al. (2015) study, there were three environmental variables of interest in the accelerated weathering tests: radiation (whose impact on the specimen is given by irradiance I), temperature (T), and oxygen pressure (O) – associated with an exponent β. Therefore, to include the influence of a third variable on the model in question, based on the addition law (GU et al., 2009), the two-parameter equation (Equation (7)) was extended to a three-parameter

equation (Equation (8)), which allows obtaining the degradation rate under influence of radiation, temperature and oxygen pressure ($k_{R,T,O}$).

$$k_{R,T,O} = (I)^{\alpha} e^{\frac{-E_a}{R \cdot T}} (O)^{\beta} \quad (8)$$

Considering that the present work is based on artificial weathering tests whose variables of interest are radiation, temperature, and humidity, Equation (8) can be adapted to include relative humidity (Equation (9)), obtaining the reaction rate under influence of temperature, humidity, and radiation ($k_{T,H,R}$).

$$k_{T,H,R} = (I)^{\alpha} e^{\frac{-E_a}{R \cdot T}} (H)^{\gamma} \quad (9)$$

The exponents α and β (or γ), to be used in the equation, are material-specific and depend on the existing relationship between the intensity of the variables to which they are associated and the degradation rate. For example, in Lv et al. (2015) study, α and β were defined as ½ and 1, respectively; since, for PP, it was found in the literature that the degradation rate varies with the square root of the irradiance (or light intensity) and varies linearly with the oxygen pressure.

The correlation between artificial weathering and natural weathering – regarding tests with temperature, humidity, and radiation control – can be established by means of an acceleration factor ($F_{a(T,H,R)}$) expressed by Equation (10), where 1 and 2 represent natural weathering and accelerated weathering, respectively.

$$F_{a(T,H,R)} = \frac{k_{T,R,H_2}}{k_{T,R,H_1}} = \left(\frac{I_2}{I_1}\right)^{\alpha} \cdot e^{\frac{-E_a}{R} \cdot \left(\frac{1}{T_2} - \frac{1}{T_1}\right)} \cdot \left(\frac{H_2}{H_1}\right)^{\beta} \quad (10)$$

It is necessary to assess the relationship between irradiance and degradation rate, as well as between relative humidity and degradation rate, specifically for PLA. According to Ho, Pometto, and Hinz (1999) study, the PLA degradation rate increases linearly with the increase of relative humidity to which it is exposed; therefore, γ is defined as 1.

Regarding irradiance, there are few studies in the literature dedicated to the understanding of how a polymer degradation rate is intensified with increasing light intensity, possibly due to the difficulties of performing this type of experiment in conventional weathering

equipment (MARTIN; CHIN; NGUYEN, 2003; PICKETT et al., 2019) Consequently, there is even less information regarding this relationship specifically for PLA.

A study conducted by Pickett, Gibson, and Gardner (2008) aimed to assess, for a series of thermoplastic polymers (although not PLA specifically), the validity of Schwarzchild's Reciprocity Law, which presumes a proportional relationship between light intensity and degradation rate (CROLL, 2019): the closer the p coefficient is to 1, the closer to linear is the relationship is. When $p < 1$, the degradation rate increases more slowly with increasing light intensity. Good linearity was observed in the study for five out of the six tested materials.

As demonstrated by Philippart, Sinturel, and Gardette (1997) study (used as a basis for Lv et al. (2015) study), with increasing irradiance, the degradation rate of PP – which is a thermoplastic and aliphatic polymer like PLA – grows more slowly than a linear relationship; increasing, in fact, with the square root of light intensity. Therefore, PP would be associated with a coefficient p lower than 1. In addition, in the literature review conducted by Martin, Chin, and Nguyen (2003), it was observed that all aliphatic hydrocarbons found had coefficients p coefficients lower than 1.

Therefore, it is expected that PLA, as an aliphatic polymer, would present, from a certain increase in light intensity, an acceleration on its degradation less drastic than what a linear function would determine. Thus, as a more critical condition, a linear relationship can be assumed to characterize the influence of irradiance on PLA degradation, i.e., that α (in Equation (10)) would be 1.

Furthermore, $F_{a(T,H,R)}$ depends on the activation energy (E_a) for thermal degradation of the polymer under evaluation. According to Patnaik, Panda, and Kumar (2020) study, PLA presents a E_a of 21-23 kJ $\cdot$ mol^{-1}. The average value of 22 kJ $\cdot$ mol^{-1} will be used to calculate $F_{a(T,H,R)}$.

Therefore, the correlation between accelerated weathering by temperature, humidity, and radiation control and PLA natural weathering can be established by means of the acceleration factor calculated with Equation (11). The final value of $F_{a(T,H,R)}$ will depend on irradiance, temperature, and humidity associated with the tests, as well as the values of environmental variables, assumed as natural conditions.

$$F_{a(T,H,R)} = \left(\frac{I_2}{I_1}\right)^1 \cdot e^{\frac{-25}{8,13}\cdot\left(\frac{1}{T_2}-\frac{1}{T_1}\right)} \cdot \left(\frac{H_2}{H_1}\right)^1 \qquad (11)$$

Therefore, determining the time for failure in accelerated weathering tests under temperature, humidity, and radiation control ($t_{aw(T,H,R)}$), it is possible to estimate the time for failure in natural weathering ($t_{nw(T,H,R)}$), i.e., the shelf life of the product, using Equation (12).

$$t_{nw(T,H,R)} = t_{aw(T,H,R)} \cdot F_{a(T,H,R)} \tag{12}$$

4 MATERIALS AND METHODS

4.1 MATERIALS

A transparent 1.75 mm thick PLA filament – Ingeo™ 3D850 (NatureWorks, Blair, United Sates) – was used as raw material for manufacturing the specimens used in this study. Based on the χc measurement for the specimen in the initial condition (section 5.3.1) and the classification of Lu and Mikos (1999), it was possible to determine which PLA stereoisomer was the one used in this work. Table 3 exhibits some properties given by the manufacturer in the technical data sheet of the used material (NatureWorks, 2022).

Table 3 – Typical Properties of Ingeo™ 3D850 3D printing filament.

Specific Gravity [g/cc]	Relative Viscosity	Melting Point [°C]	Tensile Strength [MPa]	Tensile Modulus [MPa]	Tensile Elongation [%]	Heat Distortion Temperature (0.45 MPa) [°C]
1.24	4.0	165-180	50	2315	3.31	80-90

Source: Author.

4.2 METHODS

4.2.1 Scaffolds Manufacturing by FFF

The scaffolds were manufactured by the FFF 3D printing technique, using PLA monofilament as raw material. The printing parameters were employed based on a previous work carried out at LINDEN Laboratory, Federal University of Santa Catarina, which aimed to develop a scaffold geometry with adequate mechanical and biological properties. After testing different layer infill percentages (20 or 40%) for the porous region and different infill angles (45°/-45° or 0°/90°), it was found that the best combination of parameters was 20% infill percentage and 45°/-45° infill angles.

The printed pieces present an almost cylindrical shape (since three longitudinal cuts were made in a cylinder, allowing its further attachment to the collet of the equipment for torque strength measurement), 1 cm diameter, and 1 cm height. Moreover, they have a porous external structure – in order to promote osseointegration – and a solid, centrally perforated internal area

– to accommodate a dental screw (implant) – as shown in Figure 9, which presents the computational model used to print the scaffolds.

Figure 9 - Computational model used to print the scaffolds.

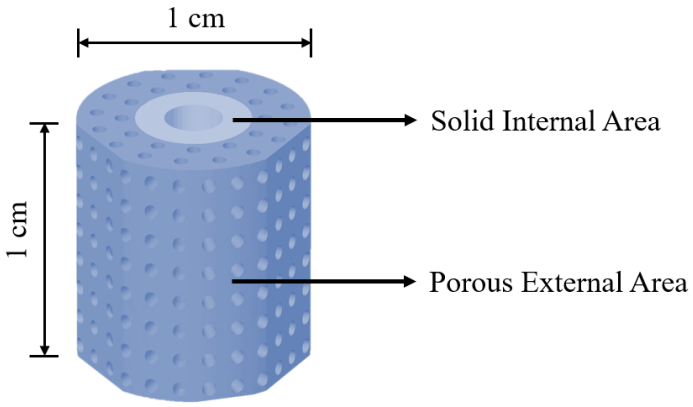

Source: Author.

A 3D printer (Minibot 130, Figure 10), from the LINDEN Laboratory, Federal University of Santa Catarina, and a 0.3 mm diameter printer nozzle made of brass were used. The printing temperature was 200 °C, the printing platform was without heating, and the flow rate (or extrusion multiplier) – which specifies the rate at which the polymer is extruded (amount of polymer extruded per unit length) – was 100% i.e., the printer extruded the filament once every 1 mm of movement. The layer height was 0.1 mm and the print speed – which refers to the nozzle's horizontal speed on the build platform (in the x/y direction) during extrusion – was 100 mm/s. The time to print each specimen was approximately 30 minutes.

Figure 10 - FFF 3D printer.

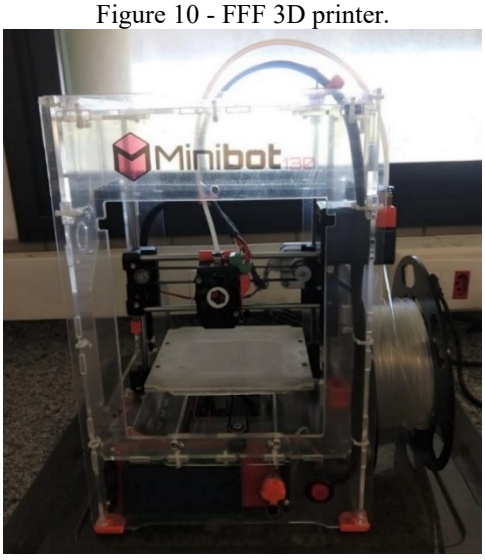

Source: Author.

The porous portion was printed with 20% infill and the solid portion, with 100% infill, both with 45°/-45° infill angles; the external fill pattern was concentric and the internal fill pattern, was rectilinear. To avoid detachment between the piece and the platform during printing, a skirt support was used: an initial double layer printed around the piece (6 contours were made on each layer). The other parameters are detailed in Table 17 of APPENDIX A - 3D Printing Parameters. To facilitate its identification in this work, the scaffold is referred to hereafter as M20_45.

A 3D modeling software (SolidWorks 2015) was used to design the scaffold 3D model and a slicer software (Ultimaker Cura 4.10.0) was used to generate the G-Code file, which gives the necessary commands for printing. The slicer software has, therefore, the function of dividing the piece into several layers and defining the coordinates that the 3D printer must follow, according to the printing parameters determined within the software itself. The G-Code can be transmitted to the printer either via USB connection or via a memory stick.

4.2.2 Accelerated Weathering Tests

4.2.2.1 Temperature Control

For accelerated weathering tests under temperature control (which will also be referred to as T tests), a microprocessor-controlled drying oven model Q317M-22 (Quimis, Diadema, Brazil) – from Processing Ceramics Laboratory (ProCer), Federal University of Santa Catarina – was used, using temperatures of 25, 35, and 45° C. The ABNT NBR 16469 (2020) recommendation that the temperatures selected for accelerated weathering should be below any transition temperature of the material and limited to a maximum of 60°C was followed: according to the DSC result obtained for the PLA scaffold in its initial condition (presented in section 5.3.1), its T_g is 64.1 °C.

Before placing the specimens in the oven, the temperature was set and stabilized for one hour. The specimens to be subjected to one of the defined temperatures were stored in closed Petri dishes and then placed inside the oven.

Five different exposure times were defined for 25 and 35 °C: 24, 96, 168, 240, and 336 h, and the specimens necessary for the foreseen analyses were gradually removed from the oven as the exposure times were reached. In the case of 45 °C, more exposure times were applied: eight in total (24, 96, 168, 240, 33, 408, 456, and 528 h), since it was intended to reach the minimum mechanical resistance defined as acceptance criterion (as explained in detail in

4.2.3.4), for shelf life determination, and it was observed that the mechanical resistance after the maximum exposure time under 35 °C did not reach the criterion. After being removed from the oven, the specimens were stored in a vacuum desiccator until performing characterization tests.

According to ABNT NBR 16469 (2020), it is necessary to report the limitation of the equipment used, in terms of lack of relative humidity control. In such cases, the standard recommends the absolute humidity (water content in air) during the tests to be constant under the selected temperature values and that there should be compliance with the humidity values expected for the application environment.

The operation of the oven is based on using ambient air, heating it, and forcing it through the chamber, without adding water to or removing it from the system. Therefore, the absolute humidity inside the equipment does not change, and there is only a reduction in the relative humidity, inherently to the increase in temperature – as explained in section 3.5.3.3.

The relative humidity in the laboratory where the oven was located remained between 60-65% during the tests, which – considering an average room temperature of 25 °C, an altitude of approximately 12 m at the test site[3] , and average relative humidity of 62.5% – corresponds to an absolute humidity of 0.014 kg steam/m^3 air and a mixing ratio of 12.41 g steam/kg dry air[4].

According to the integrative literature review conducted by Bruna and Graziano (2012) about the temperature and relative humidity conditions for storage of health care materials, most documents from competent associations or independent authors recommend that the relative humidity should be up to 70%. Therefore, the relative humidity in the accelerated weathering tests by temperature control is in accordance with the ambient condition expected for an actual storage situation.

4.2.2.2 Temperature, Humidity, and UV Radiation Control

For the accelerated weathering tests under temperature, humidity, and UV radiation control (which will also be referred to hereafter as T-H-R tests), a UVA/UVB weathering

[3] Determined by means of the altitude map of Florianópolis, available at <https://pt-br.topographic-map.com/maps/f5qk/Florian%C3%B3polis/>. Accessed 13 July 2022.

[4] Determined using the psychometric properties calculator, available at <https://www.agais.com/toolbox/psicrometria3.php>. Accessed 13 July 2022.

chamber, UUV model (Bass, Barueri, Brazil), from SENAI Technology Institute, in Criciúma (Brazil), was used. The Cycle 1 methodology defined by ASTM G154 (2016) was employed. The parameters can be found in Table 1.

Five different exposure times were defined: 24, 96, 168, 240, and 336 h. The specimens required for the foreseen analyses were progressively removed from the weathering chamber as the exposure times were reached and stored in a vacuum desiccator until the characterization tests were performed.

4.2.3 Scaffolds Characterization

4.2.3.1 Visual Color Analyses

With unaided eye, it was evaluated if the accelerated weathering tests were able to cause some kind of coloration change on the PLA scaffolds, which were originally translucent. It was aimed to correlate possible changes to the effects of the applied environmental variables and, therefore, to the triggered degradation mechanisms.

4.2.3.2 Differential Scanning Calorimetry (DSC) Analyses

Differential Scanning Calorimetry (DSC) is a material characterization technique in which the difference between the heat flows in the specimen of interest and the reference material are measured as a function of the specimen temperature – both being subjected to a controlled linear heating program. The energy required to maintain the specimen and the reference at the same temperature varies continuously and depends on the thermal effects associated with the specimen, so that the curve obtained in the analysis shows variations of heat flow with temperature when a reaction or transition occurs in the specimen, allowing the identification of whether the phenomenon is exothermic or endothermic (CANEVAROLO, 2004).

The PLA scaffolds were characterized by DSC, using a Jade-DSC model equipment (Perkin Elmer, Waltham, MA), from the Analysis Center of the Chemical and Food Engineering Department, Federal University of Santa Catarina. It was aimed to determine the properties of specimens in their initial condition and after different exposure times to accelerated weathering, under temperature control, and under temperature, humidity, and radiation control. The specimens, for this specific analysis, were printed in a modified way, as 10 × 10 × 3 cm plates

(with the same infill percentage and infill angles of the scaffold porous region: 20% and 45°/-45°), so they could be posteriorly cut to the proper size to fit the DSC specimen holder. Two specimens were analyzed for each condition/time exposure to accelerated weathering.

DSC analyses were conducted under a heating rate of 10 °C·min^{-1}, over a temperature range of 0 to 210 °C, using a nitrogen atmosphere under a flow rate of 20 ml·min^{-1}, 40 µl aluminum pots as specimen holders, and 10 mg specimen in each analysis, as described by Araque-Monrós et al. (2013), in which PLA was also studied. The objective was to determine characteristic transition temperatures of polymeric materials: glass transition temperature (T_g) and melting temperature (T_m), in addition to the degree of crystallinity (χc), which can be obtained through Equation (13), proper for polymers that present cold crystallization, such as PLA (the extra heat absorbed by crystallites formed in the cold crystallization should be subtracted from the total melting enthalpy, due to the melting of the crystallites) (MARTÍN DEL CAMPO et al., 2020; PILLA et al., 2008; SAWPAN et al., 2019).

$$\chi c = \frac{\Delta H_m - \Delta H_{cc}}{\Delta H_m^*} \cdot 100 \qquad (13)$$

where:

ΔH_m is the melting enthalpy obtained from the polymer analysis;

ΔH_{cc} is the cold crystallization enthalpy obtained from the polymer analysis;

ΔH_m^* is the melting enthalpy corresponding to the polymer in its 100% crystalline state.

According to Prapruddivongs and Sombatsompop (2012), ΔH_m^* for 100% crystalline PLA is 93.7 J/g, and this value was used in the crystallinity calculations for PLA specimens in the initial condition and after the accelerated weathering tests. T_g and T_m, as well as ΔH_m and ΔH_{cc}, were measured using Pyris software (version 9.0), suitable for quantification of thermal analysis results.

4.2.3.3 X-Ray Diffraction (XRD) Analyses

The X-ray diffraction characterization technique consists of irradiating a certain material with X-rays and measuring the intensity, as well as the angle of the rays scattered by the material. The X-ray tube generates a polychromatic beam that passes through a collimator, which turns the rays parallel and the beam, narrower.

Thereafter, X-rays reach the specimen and undergo diffraction at various angles. The refracted rays are captured by a detector positioned at a certain angle. The intensity of the scattered rays is plotted as a function of the scattering angle (2θ) – generating a diffractogram – and the material structure is determined by analyzing the angles corresponding to scattered rays' intensity peaks (BLEICHER; SASAKI, 2000).

X-ray diffraction analyses were performed to identify the presence or absence of characteristic peaks of PLA crystalline planes. This way, it would be possible to confirm the effects of accelerated weathering tests on the material crystallinity, quantified through the DSC technique. Analyses were performed for the initial condition and for exposure times of 168 and 336 h, for each accelerated weathering configuration. The specimens, for this specific analysis, were printed as 10 x 10 x 3 cm plates (with the same infill percentage and infill angles of the scaffold porous region: 20% and 45°/-45°), so they could be posteriorly cut to the proper size to fit the XRD specimen holder.

A Rigaku MiniFlex 600 diffractometer, from the LINDEN Laboratory, Federal University of Santa Catarina, was used. The equipment operates with Cu-Kα radiation (λ = 1.5418 Å), a coupled sodium iodate detector, a potential difference of 40 kV, and an electrical current of 15 mA. A scanning range of 10° to 30° was employed, under 3°/min speed. One specimen was analyzed for each selected accelerated weathering condition/exposure time.

4.2.3.4 Mechanical Torque Strength Tests

Considering that M20_45 is intended to be used as a graft for a dental implant, it is relevant to assess whether the scaffold presents sufficient mechanical strength to withstand the torsional loading expected for screw implantation, to be manually performed by the dentist. Thus, by establishing a minimum limit for the mechanical strength of the polymeric scaffold, its failure under accelerated weathering can be determined, i.e., the exposure time that results in M20_45 failure and that, therefore, is associated with its shelf life.

As explained in section 3.7, the degradation and the failure of polymeric materials subjected to weathering tests should be evaluated by means of a key property for its functional application. Considering that an adequate mechanical strength to support the insertion loads of a dental screw is a requirement of the scaffold functionality, it is pertinent to assess this mechanical property as a parameter to determine its shelf life.

The mechanical-functional evaluation of M20_45 was based on ABNT ISO/TS 13498 (2013), in order to measure, for different accelerated weathering conditions, the maximum

torque strength of the connection between a metallic screw and the polymeric scaffold. The standard establishes a method for applying torsional loading on a screw to insert it into a dental endosseous substrate (in this case, the scaffold) until failure of one of the components or the assembly occurs, being an appropriate method to evaluate new types of dental screw/endosseous substrate coupling, as well as new materials.

For torque strength measurements, 2 mm diameter pre-drilled holes were made in the specimens (polymeric scaffolds), and 3 mm diameter self-tapping screws were used. The tests were conducted in the LINDEN Laboratory, Federal University of Santa Catarina, using a torque applicator device developed in previous works (EIRADO, 2009; STARES, 2010), whose configuration can be seen in Figure 11.

Figure 11 - Torque strength test setup. In the bottom left, the front view of the collet with the scaffold attached.

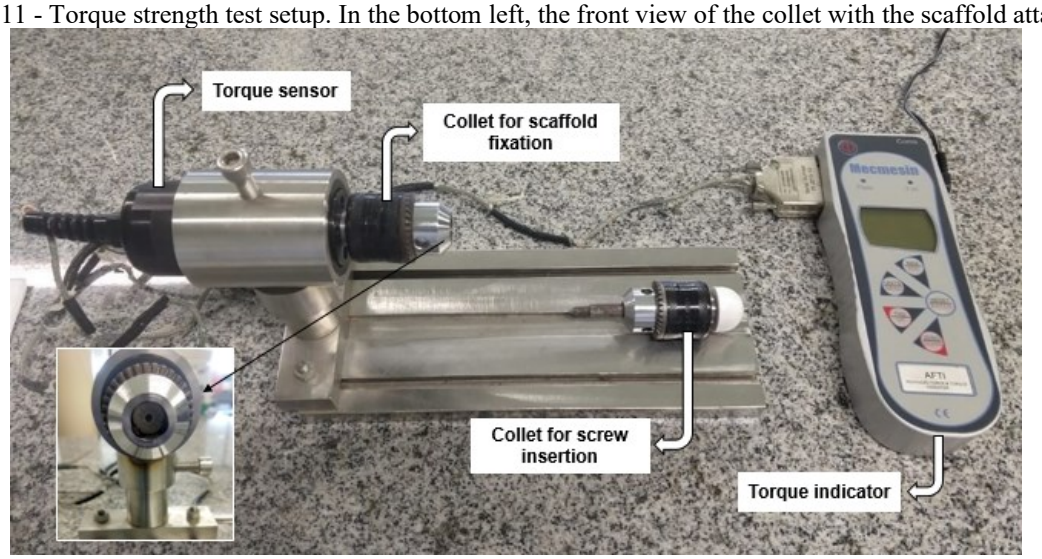

Source: Author.

Initially, the specimen was fixed to a collet coupled to a torque sensor, connected to an Advanced Force and Torque Indicator (AFTI) (Mecmesin, Slinfold, United Kingdom), which displays the momentary torque applied on the screw/scaffold assembly. A drill was fixed to another collet and posteriorly assembled to the screw head so that it could be inserted into the scaffold. Then, torque was applied so that the screw could rotate with an approximately constant angular speed of 10 rpm.

The test was conducted until specimen failure was identified, and the final value shown on the torque meter was recorded as the maximum torque strength of the tested specimen. The failure modes presented by each specimen were also recorded. For each weathering

condition/exposure time combination (23 in total) applied to M20_45, five specimens were tested, and the average value was defined as the final torque strength.

For each weathering test with temperature control – under 25, 35, and 45 °C – and for T-H-R test, statistical analysis through paired Student's t-test was performed to find out which exposure times caused significant changes in mechanical strength compared to M20_45 in its initial condition. A two-tailed distribution and a 5% significance level (α) were considered, i.e., a significant change was defined for p-value < 0.05.

In addition, an analysis of variance (ANOVA) followed by a Tukey's multiple comparisons test was performed to determine the significant differences between the mechanical strength values associated with each weathering test, specifically for each exposure time (from 24 to 336 h). Again, a α = 5% was considered (p-value < 0.05). For all data statistical treatment tests, Excel 2013 (Microsoft Office) was used.

4.2.3.5 Fourier Transform Infrared Spectroscopy (FTIR) Analyses

The Fourier transform infrared spectroscopy (FTIR) through attenuated total reflection (ATR) is a non-destructive technique of easy application, relatively low cost, and rapid analysis time. It is based on the internal reflectance of infrared (IR) light incident on a material and, consequently, on the changes in the characteristic intensities of the light at all wavelengths of its spectrum, which is associated with chemical bonds present in the sample, since they absorb specific frequencies of the light. Therefore, this technique allows to obtain an infrared spectrum characteristic of the analyzed material and its chemical composition, by identifying the existing functional groups (CANEVAROLO, 2004; LEE; LIONG; JEMAIN, 2017).

The samples before and after the different accelerated weathering tests were characterized through FTIR analyses, using a spectrophotometer (Bruker, Tensor 27) – from the Polymers and Composites Laboratory (POLICOM), Federal University of Santa Catarina. The spectra were recorded employing the attenuated total reflectance (ATR) technique, scanning from 4000 to 600 cm^{-1}, with an average of 32 scans at a resolution of 2 cm^{-1}. The FTIR analyses were performed for the scaffolds in the initial condition and for 168 and 336 h exposure times under each accelerated weathering type, aiming to assess possible changes in the characteristic spectrum, associated with PLA degradation mechanisms.

4.2.3.6 Viscosimetry Analyses

Solution viscosimetry can be used to perform average molecular weight measurements since the relationship between viscosity and concentration of a polymeric solution is dependent on the chain length of the polymer. This technique stands out as an effective, simple, and low-cost method to obtain information about the size of solubilized macromolecules, based on physicochemical interactions between a polymer and a solvent at a certain temperature (BOAVENTURA et al., 2009; DA SILVA et al., 2009; THOMAS M. SCHMITT, 2012).

In this method, the inherent viscosities of polymer solutions with different concentrations are obtained, in order to determine the polymer's intrinsic viscosity, which can be applied to the Mark-Houwink Equation (14) to finally calculate the viscosity-average molecular weight of the material (KACZMAREK et al., 2013; THOMAS M. SCHMITT, 2012).

$$[\eta] = \mathrm{K} \cdot {M_v}^{a} \tag{14}$$

where:

$[\eta]$ is the intrinsic viscosity;

K and a are constants related to a given polymer-solvent-temperature system;

M_v is the viscosity-average molecular weight.

The relative viscosity for a polymer solution at a certain concentration is obtained from the times taken by the solution and by the pure solvent to flow between the meniscuses of a capillary viscometer (Equation (15)). Then, Equation (16) is used to obtain the inherent viscosity of each solution concentration (SILVESTRINI, 2020).

Finally, the intrinsic viscosity is defined by extrapolation of the curve obtained for inherent viscosity x concentration to $C = 0$, according to Equation (17), which represents an infinitely diluted polymer solution, resulting in parameters related to the isolated chain (BOAVENTURA et al., 2009; SILVESTRINI, 2020).

$$\eta_{rel} = \frac{t}{t_0} \tag{15}$$

where:

η_{rel} is the relative viscosity;

t is the flow time presented by the solution;

t_0 is the flow time presented by the solvent.

$$\eta_{inh} = \frac{\ln(\eta_{rel})}{C} \tag{16}$$

where:

η_{inh} is the inherent viscosity;

C is the solution concentration.

$$[\eta] = \lim_{C \to 0} \frac{\ln(\eta_{inh})}{C} \tag{17}$$

For viscosity-average molecular weight measurements, based on ASTM D2857 (2016), a Cannon-Fenske n° 100 capillary viscometer was used – from the Polymers and Composites Laboratory (POLICOM), Federal University of Santa Catarina – immersed in a bath maintained at 25 °C. Chloroform 99.8% PA ACS (Hexis Científica, Jundiaí, Brazil) was used as solvent. Since the PLA isomer used in this work is PLLA (as explained in section 5.3.1), the constants K and a for PLLA in chloroform at 25 °C (5 x 10^{-4} and 0.73, respectively) were used, according to the literature review of Garlotta (2001).

Analyses were performed for the initial condition and for exposure times of 168 and 336 h, under each accelerated weathering type of test. For each exposure time/accelerated weathering combination, three flow time measurements were performed and the average value was used to define the viscosity-average molecular weight. The following solution concentrations were used: 0.2; 0.4; 0.6 and 1 g/dL.

For each measurement of viscosity-average molecular weight, first the average flow times were used to calculate the values of relative viscosity and inherent viscosity. After plotting the values of inherent viscosity as a function of concentration, the curves were approximated to linear equations, used to calculate the intrinsic viscosity (through the linear coefficient) for each combination of weathering type and exposure time. Finally, each intrinsic viscosity was used to calculate the viscosity-average molecular weight for each condition.

4.2.3.7 Scanning Electron Microscopy (SEM) Analyses

Scanning electron microscopy allows obtaining surface images of a specimen with magnification ranging from the order of hundreds to thousands of times, through accelerated electrons bombardment on the material surface. The electron-specimen interaction generates several possible signals, among which secondary electrons (SE) and backscattered electrons (BSE) are the most interesting for imaging. As the primary electrons (incident) beam sweeps out the specimen, the mentioned signals suffer modifications, according to variations presented by the surface (MALISKA, 2018).

SE are generated from inelastic interactions between primary electrons and low-energy electrons from the conduction band (in metals) or valence band (in semiconductors or insulators), being responsible for providing topographic images with high resolution. The BSE, on the other hand, result from elastic and inelastic collisions, being generated in deeper layers of the material and being influenced by the atomic number (Z) of the element on which they are incident: the higher the Z, the higher the BSE emission coefficient. Thus, images generated by BSE allow the identification of specimen regions with different chemical compositions through differences in contrast (MALISKA, 2018).

The M20_45 specimens were characterized, in terms of microstructure, by scanning electron microscopy, in order to identify cracks or other imperfections generated by the accelerated weathering tests. The specimens, for this specific analysis, were printed in a modified way, that is, the piece was sectioned longitudinally, in order to observe the modifications in the external porous region. In total, four scaffold specimens were subjected to SEM analysis: in the initial condition, after 336 h under 35 °C, after 336 h under 45 °C, and after 336 h under temperature, humidity, and radiation[5]. Because they were polymeric specimens, it was necessary to give them conductive properties to allow the SEM analyses, by depositing a thin gold layer on each specimen.

A JEOL JSM-6390LV microscope from the Central Laboratory for Electron Microscopy (LCME), Federal University of Santa Catarina, was used for the analyses. The equipment operates with a Tungsten filament and an acceleration potential of 10 kV was used. For surface defects measurements, ImageJ *software* (version Java 1.8.0_172) was used.

[5] It was not considered relevant to analyze the specimen related to the weathering under 25 °C, since it is room temperature, not capable of generating considerable surface defects on the specimens within the times defined for this study.

4.2.4 Shelf Life Prediction

In order to determine and compare shelf life results associated with the T test and the T-H-R test, a criterion to define a product's failure must be defined. It was established that the functional property to be used as a parameter for failure determination would be the torque strength of the screw/scaffold assembly. Therefore, it is necessary to assign a minimum acceptance criterion to this property, in terms of safety during application.

The loading generated during the insertion of a dental screw may damage both the screw and the bone or, for cases in which it is necessary to use, the endosseous substrate (such as a polymeric scaffold). The indication for maximum insertion torque to be used, in order to avoid loss of stability and even implant breakage, should be given by each manufacturer. However, it is also possible to find information in the scientific literature regarding torque levels that are considered safe for implantation.

Some studies report torque values that may cause tissue damage or loss of rigidity on the fixed system and, therefore, should be avoided. Torques in the range of 50 N·cm are associated with possible compression necrosis – when excessive compressive loads hinder local microcirculation, leading to necrosis (MOEEN et al., 2014).

According to Trisi et al. (2009), who related different insertion torque values with posterior implant micromovements, torques equal to or greater than 45 N·cm are associated with greater primary stability than those lower than 45 N·cm. On the other hand, when torques up to 45 N·cm are employed, secondary stability shows a statistically significant increase, which does not occur for higher torque values, so it is often inadvisable to exceed 45 N·cm during dental implant insertion. The Verrastro Neto et al. (2018) study suggests that inserting dental implants at low torques (< 30 N·cm) favors new blood vessel growth and microcirculation, essential to the healing process. Furthermore, Benic, Mir-Mari, and Hämmerle (2014) conducted a systematic review and meta-analysis of implants inserted with torques between 20 and 45 N·cm and found that, for this range of values, there is no significant difference between immediate or delayed loading on implants, in terms of adjacent bone loss and implant success.

Therefore, it is pertinent to establish 45 N·cm as the maximum recommended insertion torque for dental implant insertion, i.e., this value can be defined as a minimum strength requirement that the screw/scaffold assembly must present to be suitable for its application. Considering that even lower torque levels are used and recommended, there is a safety margin

associated with the defined criterion. Thus, it is defined that M20_45 will fail when its torque strength by screw insertion is equal to or lower than 45 N·cm.

4.2.4.1 Temperature Control

For shelf life prediction through the accelerated weathering with temperature control, the calculation was based on the 45 °C test, i.e, T_{aw} = 45 °C. It was necessary to employ exposure times longer than the maximum one defined for 25 and 35 °C weathering tests, aiming to reach the functional failure of M20_45 under 45 °C (when the torque strength would reach the minimum requirement of 45 N·cm).

As exposed in section 3.7.1, the time for M20_45 failure under natural weathering conditions based on accelerated weathering tests under temperature control ($t_{nw(T)}$) can be defined through its time for failure under accelerated weathering conditions ($t_{aw(T)}$) and the acceleration factor $F_{a(T)}$, obtained from Equation (5). Therefore, by defining $t_{aw(T)}$, the shelf life based on accelerated weathering under temperature control was determined by using Equation (18).

$$t_{nw(T)} = t_{aw(T)} \cdot 3^2 \tag{18}$$

4.2.4.2 Temperature, Humidity, and UV Radiation Control

For shelf life prediction through the accelerated weathering with temperature, humidity, and UV radiation control – according to Cycle 1 specifications, defined by ASTM G154 (2016) – the same torque strength criterion (45 N·cm) was used to establish the M20_45 failure.

As exposed in section 3.7.2, the time for M20_45 failure under natural weathering conditions based on accelerated weathering tests under temperature, humidity, and UV radiation control ($t_{nw(T,H,R)}$) can be defined by the time for failure under accelerated weathering conditions ($t_{aw(T,H,R)}$) and the acceleration factor $F_{a(T,H,R)}$, obtained from Equation (11). Therefore, by defining $t_{aw(T,H,R)}$, the shelf life based on accelerated weathering under temperature, humidity and UV radiation was determined by using Equation (19).

$$t_{nw(T,H,R)} = t_{aw(T,H,R)} \cdot \left[\left(\frac{I_2}{I_1} \right)^1 \cdot e^{\frac{-25}{8,13} \cdot \left(\frac{1}{T_2} - \frac{1}{T_1} \right)} \cdot \left(\frac{H_2}{H_1} \right)^1 \right] \tag{19}$$

Following ASTM G154 (2016) specifications for Cycle 1, UVA-340 nm lamps with a typical irradiance of 0.89 $W \cdot m^{-2}$ (I_2) were used. The determination of the typical irradiance of the real condition (I_1), associated with natural weathering, was based on ASTM D5272 (2008). The solar radiation data of Florida (United States) was taken into account. The reference site presents approximately 26°N of latitude and a subtropical, hot, and humid climate, i.e., climatic conditions close to those of Florianópolis (SC), whose latitude is approximately 27°S.

According to the mentioned technical standard, the annual solar radiation in this region is 305.5 $MJ \cdot m^{-2}$ (295-385 nm). Considering that the radiation energy corresponding to the 340 nm wavelength (emitted by the UV lamps used in this work) represents 1% of the entire UV radiation band emitted by the Sun ($\mathrm{UV(total)}_{year}$) (CHÁVEZ-MONTES et al., 2015), Equation (20) can be used to calculate the total annual energy coming from 340 nm UV radiation ($\mathrm{UV340}_{year}$) that reaches the considered reference site.

$$\mathrm{UV(340)}_{year} = \mathrm{UV(total)}_{year} \cdot 1\% \tag{20}$$

Therefore, the annual UV-340 nm radiation on the considered region is 3.055 x 10^3 $KJ \cdot m^{-2}$. As given by Equation (1), the irradiance (I) can be calculated by dividing the total radiation energy (ε_t) – in this case, 3.055 x 10^3 $KJ \cdot m^{-2}$ – by the exposure time (t) – which, in this case, is one year, i.e. 3.1536 x 10^7 s. Therefore, the typical sunlight irradiance at the selected reference location (I_1) – is approximately 0.097 $W \cdot m^{-2}$.

The temperature for natural weathering conditions (T_1) was defined as 25 °C. As the applied temperature in the accelerated weathering test is not constant, the average temperature was considered as T_2. Therefore, as each cycle consists of 8 h at 60 °C and 4 h at 50 °C, the average temperature of accelerated weathering (T_2) is 56.67 °C.

The relative humidity (RH) for real conditions (natural weathering), i.e, H_1, was defined as 70% – according to recommendations found in the literature regarding the RH for health products storage (BRUNA; GRAZIANO, 2012). As the RH used for accelerated weathering is also not constant, the average value was considered as H_2. Each cycle consists of 4 h at 100% relative humidity (saturation) and 8 h without humidity control. However, since the weathering chamber uses ambient air, it is possible to estimate the RH during these eight hours, inside the equipment, through the temperature and the RH kept in the room where the test is performed, in addition to the temperature inside the equipment (60 °C) – by considering that the water

content in the air, i.e., absolute humidity (AH) will be the same inside and outside the equipment.

A temperature of 25 °C and an RH of 70% were measured in the test room. Using a relative humidity/absolute humidity calculator, AH was estimated and then the RH inside the equipment for 8 h at 60 °C was calculated. The average barometric pressure of Criciúma (test site) was taken into account: 1015 hPa[6]. This way, a water content in the air of 0.0162 kg/m^3 was found, which resulted in an RH inside the equipment of 12.4% during 8 hours at 60 °C. Therefore, the average RH of the test (RH_2) was 41.6%.

By substituting these values in Equation (19):

$$t_{nw(T,H,R)} = t_{aw(T,H,R)} \cdot \left[\left(\frac{0{,}89}{0{,}097} \right)^1 \cdot e^{\frac{-25}{8{,}13} \cdot \left(\frac{1}{56{,}67} - \frac{1}{25} \right)} \cdot \left(\frac{41{,}6}{70} \right)^1 \right] \quad (21)$$

$$t_{nw(T,H,R)} = t_{aw(T,H,R)} \cdot 5{,}84 \quad (22)$$

[6] AccuWeather data – Criciúma. Available at: <https://www.accuweather.com/pt/br/crici%C3%BAma/35956/current-weather/35956>. Accessed 02 July 2022.

5 RESULTS AND DISCUSSION

5.1 SCAFFOLDS MANUFACTURING BY FFF[7]

Although a relatively high printing speed was used (ALGARNI; GHAZALI, 2021), the time to print each specimen was approximately 30 min, due to the high level of details of the porous structure. 3D printing can sometimes arise some challenges to produce good quality objects. The main difficulties found during the specimens manufacturing were related to detachment from the print bed, hot end clogging and failed extrusion.

In order to avoid the printing object to detach from the surface, it was necessary to carefully perform the bed leveling before printing each batch (of six specimens) and adjust the distance between the nozzle and the print bed, to assure they were not too close. Otherwise, the extrusion of first layers is impaired and once the filament does have space to extrude, the object does not firmly stick to the surface. Another measure taken was to employ a skirt support i.e., an initial double layer printed around the piece (six contours were made on each layer), which also avoids detachment.

The bed leveling and the nozzle-bed distance adjustment also prevent possible clogging. If the distance is too low, there can be a backup of the melted filament in the hot end, leading to material build-up. Moreover, considering the relatively small nozzle diameter that was used, despite the better accuracy it provides for complex objects (such as the scaffold here studied), sometimes it can facilitate residual particles from the filament to build up and make the extrusion more difficult. This required periodical good cleaning or even replacement of the nozzle.

Failed extrusions i.e., when no filament or a defective filament is extruded from the hot end, could also be minimized by bed leveling and control of the nozzle-bed distance. This should not be too low so the nozzle does not scrape off the molten filament; and neither too high, so that no loose filaments are extruded, hindering sticking between filaments and between object and print bed. In addition, it was important to always assure the filament spool was free to rotate while being pulled by the extruder. Otherwise, the hot end would not be properly fed, which interrupted the printing.

[7] DOI: <https://doi.org/10.1016/j.mtcomm.2022.104140>.

5.2 VISUAL COLOR ANALYSIS[8]

The accelerated weathering tests under temperature control did not cause noticeable color changes in the specimens. The specimens that underwent the test under temperature, humidity, and UV radiation control (Cycle 1 of ASTM G154 (2016)) became noticeably brittle (requiring careful handling), and acquired a matted color (close to white) from 168 h exposure onwards – as indicated in the test report No: 32680.2021.B- V.0, issued by SENAI Technology Institute, in Criciúma (APPENDIX B – T-H-R Test Report) – which reflected in the more pronounced decrease in mechanical strength for the T-R-H test (section 5.5). Figure 12 compares M20_45 in its initial condition (before weathering) and specimens subjected to 336 h exposure under the 35 and 45 °C T tests (which remained with practically the same translucent color), as well as under the T-R-H test (for which a color change and embrittlement were more evident).

Figure 12 - PLA scaffolds before and after accelerated weathering: (a) initial condition, (b) 336 h under 35 °C, (c) 336 h under 45 °C, (d) 336 h under temperature, UV radiation, and humidity control.

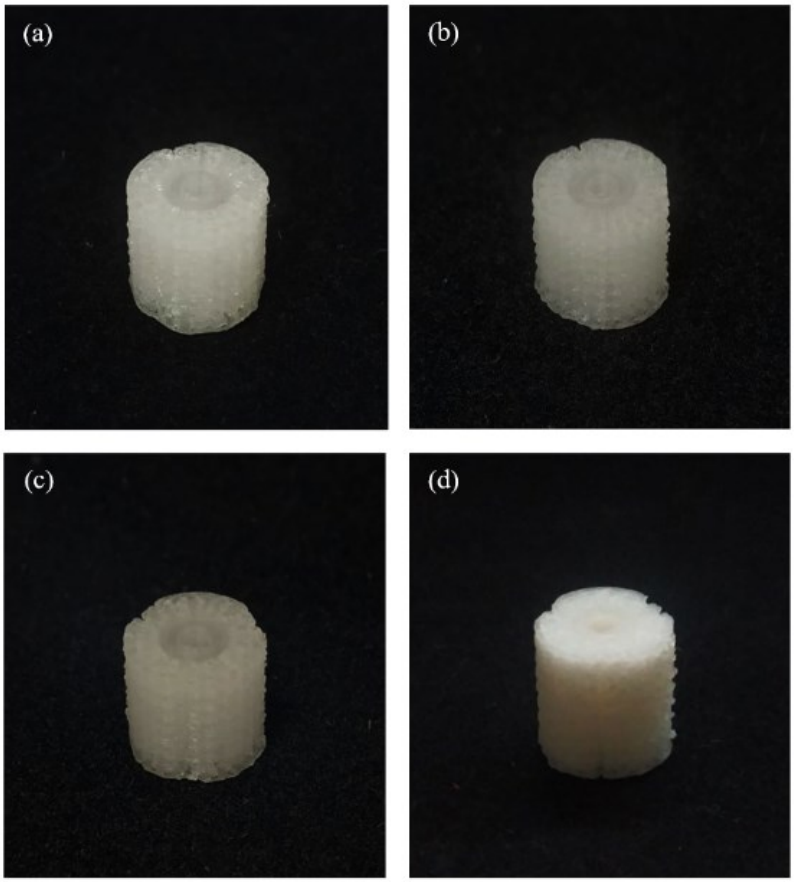

Source: Author.

[8] DOI: <https://doi.org/10.1016/j.mtcomm.2022.104821>.

The matting of pure PLA specimens or PLA-based composites, turning them whiter and/or yellowish, is frequently reported in the literature about accelerated weathering tests under UV radiation application (ISADOUNENE et al., 2018; LIM; CHOW; PUNG, 2019; LIN; XIE; QIU, 2019; LIZÁRRAGA-LABORÍN et al., 2018). The phenomenon can be attributed to the fact that PLA structure has chromophore groups (that provide color to the material) of carbonyl type (C=O), which absorb UV radiation, triggering the polymer photodegradation (LIN; XIE; QIU, 2019; LIZÁRRAGA-LABORÍN et al., 2018; YEW et al., 2009) and, consequently, increasing the number of carbonyl groups – according to the photolytic degradation mechanism schematized in Figure 6.

5.3 DIFFERENTIAL SCANNING CALORIMETRY (DSC) ANALYSES[9]

5.3.1 Initial Condition

For the initial condition, a T_g of 64.12 °C, a T_m of 176.74 °C and a χc of 23.89% (Table 4) were found, corresponding to expected values for PLA in the semi-crystalline form. Therefore, the material used in this work consists of PLLA stereoisomer (LU; MIKOS, 1999).

Table 4 - DSC analysis results for the PLA scaffold in its initial condition (without accelerated weathering).

Sample	T_g [°C]	χc [%]
1	63.78	23.66
2	64.45	24.13
Average	64.12	23.89
Standard Deviation	0.47	0.33

Source: Author.

5.3.2 Accelerated Weathering under 35 °C

Table 5 presents the results of T_g and χc (calculated through Equation (13)) obtained for specimens in the initial condition and those subjected to accelerated weathering under 35 °C[10].

[9] DOI: <https://doi.org/10.1016/j.mtcomm.2022.104821>.

[10] The heat flow curves (mW) as a function of temperature (°C), obtained for the two batches of specimens are shown in Figure 29 and Figure 30 of APPENDIX C – DSC Curves.

Table 5 - DSC analysis results for the PLA scaffold in its initial condition and after different exposure times to accelerated weathering under 35 °C.

Exposure Time [h]	**0**		**24**		**96**		**168**		**240**		**336**	
Properties	T_g [°C]	χc [%]	T_g [°C]	χc [%]	T_g [°C]	χc [%]	T_g [°C]	χc [%]	T_g [°C]	χc [%]	T_g [°C]	χc [%]
Sample 1	63.78	23.66	66.61	26.09	67.64	26.03	67.82	27.83	66.63	29.10	67.45	29.08
Sample 2	64.45	24.13	68.29	28.03	68.46	31.89	68.6	34.00	66.63	32.22	68.62	36.54
Average	64.12	23.89	67.45	27.06	68.05	28.96	68.21	30.92	66.63	30.66	68.04	32.81
Standard Deviation	0.47	0.33	1.19	1.37	0.58	4.14	0.55	4.36	0.00	2.20	0.83	5.28

Source: Author.

5.3.2.1 Crystallinity Degree (χc)

As indicated in Table 5, there is a predominantly increasing behavior of M20_45 average crystallinity with increasing exposure time under 35 °C. After the maximum exposure time (336 h), it can be seen that the χc of the material rose by 8.92%, which represents a relatively increase of 37.34% over the χc of the specimen in its initial condition (23.89%). Figure 13A shows χc values plotted as a function of exposure times to this accelerated weathering test.

The χc increase after accelerated weathering tests is a phenomenon commonly reported in the scientific literature for PLA, which can be explained by the preferable degradation of amorphous (less ordered) parts of the polymer, which leads to an increase in crystalline phase/amorphous phase ratio on the material – also as a result of reduction of molecular entanglements (that characterize amorphous parts) and increase on the mobility of the chains, allowing them to slowly reorganize and become crystalline. Consequently, there is an increase in the crystalline phase/amorphous phase ratio of the material (YATIGALA; BAJWA; BAJWA, 2018; YUAN; MAK; YAO, 2002).

Ahmad and Sawpan et al. (2019) reported approximately 22% (from 7.9% to 29.9%) and 42.7% (from 7.9% to 50.6%) increases in χc after 384 and 576 h[11], respectively, for accelerated weathered PLA specimens (ASTM G154 (2016) – UV-A). Isadounene et al. (2018) obtained a 9.6% increase (from 20.4% to 30%) in χc after 480 h exposure of PLA specimens under ASTM G154 (UV-A) accelerated weathering. Martín del Campo et al. (2020) reported a 31% increase (from 20% to 51%) in χc of PLA specimens subjected to 600 h exposure to ASTM G154 (UV-A) tests.

All the aforementioned studies refer to PLA specimens produced by injection or compression molding – which, although different from 3D printing, are also based on melting and subsequent solidification of a polymeric material in the desired shape. The literature focused on accelerated weathering tests with 3D-printed PLA specimens is scarce, and the few existing studies' results refer basically to tensile tests, coloration changes, water absorption, deformations, and micrographic analysis (ALDEEN; OWAID, 2020; GRASSI; SPAGNOLO; PAOLETTI, 2019; LIN; XIE; QIU, 2019).

[11] The values were estimated from the graph presented in the publication, by using the online tool that allows extracting data from graph images *WebPlotDigitizer*. Available at: <https://apps.automeris.io/wpd/>. Accessed 21 July 2022.

In addition, most studies, such as those already mentioned, refer to accelerated weathering tests combining temperature, humidity, and ultraviolet radiation, being rare those that report the effects of temperature alone or combined with humidity. Copinet et al. (2004) evaluated the effects of different temperatures combined with different relative humidity values on PLA and, although they did not provide values for crystallinity variation, the authors stated that the results of material degradation are associated with an increase in χc, due to accelerated weathering.

Some studies have reported decreases in χc of PLA specimens subjected to accelerated weathering, although not quantitatively; but by observing the reduction or non-identification of characteristic crystalline peaks of the polymer, in diffractograms (from XRD analyses). Lv et al. (2017) reported the gradual decrease of crystalline peaks as a function of exposure time, while Lv et al. (2018) pointed out, initially, the appearance of crystalline peaks after 900 h of exposure, followed by a decrease of such peaks at 1200 h.

Therefore, many studies of the scientific literature corroborate the effect of increasing χc in M20_45 specimens due to exposure to temperatures higher than room temperature. The phenomenon can be explained by preferential degradation over the less organized regions (amorphous) leading to an increase in the percentage of crystalline regions in the polymer specimen.

5.3.2.2 Glass Transition Temperature (T_g)

According to the obtained results, there is a predominantly increasing behavior of the glass transition temperature as the exposure time under 35 °C increases. Figure 13B shows T_g values plotted as function of exposure times under 35 °C. After the maximum exposure time (336 h), the average T_g rose by 3.92 °C, which represents a relatively increase of 6.11% over the T_g of M20_45 in its initial condition (64.12 °C).

The increase in the T_g of PLA after accelerated weathering tests is also a phenomenon documented in the literature regarding PLA specimens. Ahmad Sawpan et al. (2019), after performing accelerated weathering tests under temperature, humidity, and UVA radiation (Cycle 7 of ASTM G154 (2016)) with PLA specimens, obtained a 7 °C increase (from 57.8 to 64.8 °C) in the T_g of the specimens after 576 h exposure – and an approximately 4 °C increase

after 384 h exposure[12]. Isadounene et al. (2018) also conducted ASTM G154 (2016) accelerated weathering tests with PLA specimens, and a 3 °C increase (from 60 to 63 °C) was observed on the T_g after 480 h exposure. The results found by Lv et al. (2017) regarding ASTM G154 (2016) tests show 1.2, 1.6, and 4.4 °C increases on the T_g of PLA specimens after 300, 600 and 1200 h exposures, respectively (the initial T_g was 60.7 °C).

Again, the studies mentioned above refer to PLA specimens produced by injection or compression molding, and not by 3D printing (as performed in this work), due to the scarcity of results available in the literature about PLA specimens produced by 3D printing and subjected to accelerated weathering tests. In addition, the cited studies are based on the combined application of temperature, humidity, and radiation, because researches evaluating the isolated effect of temperature are rare.

Copinet et al. (2004) evaluated the effects of different temperatures combined with different relative humidity values on PLA, and there was a decrease on T_g in all cases, contrary to the results found in the present work for 35 °C weathering. However, the study of Copinet et al. (2004) used PLA in the form of films, produced by the tape casting technique, which considerably differs from 3D printing and could, therefore, have an influence on the kinetics of degradation in the material. Concerning studies based on ASTM G154 (2016), a few of them point out the non-modification or the reduction on the T_g of PLA specimens after accelerated weathering tests (BOLIO-LOPEZ et al., 2013; LV et al., 2018).

Therefore, scientific literature corroborates the increasing effect of the M20_45 T_g due to exposure to temperatures higher than room temperature. This phenomenon occurs due to the volume relaxation caused by chains segmental motion that results from the degradation induced by accelerated weathering. The volume relaxation leads to densification of amorphous regions and, thus, to reduction of the free volume. Therefore, the glass transition of the material becomes more difficult, i.e. more energy is required, so it occurs at higher temperatures (LV et al., 2017; SAWPAN et al., 2019).

[12] The value was estimated from the graph presented in the publication, by using an online tool that allows extracting data from graph images *WebPlotDigitizer*. Available at: <https://apps.automeris.io/wpd/>. Accessed 21 July 2022.

5.3.3 Accelerated Weathering under 45 °C

Table 6 presents the results of T_g and χc (calculated through Equation (13)) obtained for specimens in the initial condition and those subjected to accelerated weathering under 45 °C[13].

5.3.3.1 Crystallinity Degree (χc)

As indicated in Table 6, there is an increasing behavior of M20_45 crystallinity up to 240 h exposure under 45 °C, and then there is a decay from 336 h onwards. After 240 h, the material χc rose by 14.08%, which represents a relatively increase of 58.94% over the χc of the specimen in the initial condition (23.89%). At subsequent exposure times, χc began to progressively decrease, until it reached 28.82% at 528 h. Figure 13A shows χc values plotted as a function of exposure times to this accelerated weathering test.

Therefore, the χc increasing effect for accelerated weathering under 45 °C was faster and more pronounced when compared to 35 °C accelerated weathering. In addition, there was a second stage variation of this property (with its decay over time).

In studies that reported a decrease in the crystalline phase of PLA specimens subjected to accelerated weathering (although in a non-quantitative manner), the authors associated the phenomenon to chain reorganization and degradation of the polymer crystalline regions (LV et al., 2017, 2018).

Therefore, based on the results for χc variation, each of the behaviors observed for M20_45 χc could be associated with a different degradation step:

1) similar to what was observed for 35 °C weathering, degradation under 45 °C initially affected the amorphous portion of the specimens, also facilitating, with the reduction of chain entanglements, their reorganization into crystalline form – which justifies the initial increase of χc up to 240 h exposure;

2) the subsequent reduction in χc (from 240 to 528 h) can be understood as a result of the degradation now affecting crystalline regions, which leads to an increase in the proportion of less ordered (amorphous) regions and consequently leads to a decrease in the crystalline phase/amorphous phase ratio (LV et al., 2017, 2018; YATIGALA; BAJWA; BAJWA, 2018).

[13] The heat flow curves (mW) as a function of temperature (°C), obtained for the two batches of specimens are shown in Figure 31 and Figure 32 of APPENDIX C – DSC Curves.

Table 6 - DSC analysis results for the PLA scaffold in its initial condition and after different exposure times to accelerated weathering under 45 °C.
(continue)

Exposure Time [h]	**0**		**24**		**96**		**168**		**240**		**336**	
Properties	**T_g [°C]**	**χc [%]**	**T_g [°C]**	**χc [%]**	**T_g [°C]**	**χc [%]**	**T_g [°C]**	**χc [%]**	**T_g [°C]**	**χc [%]**	**T_g [°C]**	**χc [%]**
Sample 1	64.45	24.13	66.82	22.25	67.66	24.67	67.97	31.16	69.46	32.16	70.78	29.53
Sample 2	63.78	23.66	69.47	28.04	71.49	36.93	71.17	40.54	70.84	43.78	70.49	38.10
Average	64.12	23.89	68.15	25.14	69.58	30.80	69.57	35.85	70.15	37.97	70.64	33.82
Standard Deviation	0.47	0.33	1.87	4.09	2.71	8.66	2.26	6.63	0.98	8.22	0.21	6.06

Table 6 - DSC analysis results for the PLA scaffold in its initial condition and after different exposure times to accelerated weathering under 45 °C.
(conclusion)

Exposure Time [h]	**408**		**456**		**528**	
Properties	**T_g [°C]**	**χc [%]**	**T_g [°C]**	**χc [%]**	**T_g [°C]**	**χc [%]**
Sample 1	69.62	26.76	64.33	23.31	64.8	24.62
Sample 2	74.16	34.76	69.32	33.18	66.68	33.02
Average	71.89	30.76	66.83	28.24	65.74	28.82
Standard Deviation	3.21	5.66	3.53	6.98	1.33	5.94

Source: Author.

5.3.3.2 Glass Transition Temperature (T_g)

According to the results obtained for the 45 °C weathering, a faster increase on the T_g occurred, compared to the 35 °C weathering, up to 408 h exposure – at higher levels than what was observed for 336 h under 35 °C (as can be seen in Figure 13B) – followed by a predominantly decreasing behavior up to 528 h. At 408 h exposure, the T_g rose by 7.77 °C, which represents an 12.12% relatively increase. At subsequent exposure times, the T_g started to progressively decrease, until it reached 65.74 °C at 528 h.

In studies that reported a decrease on the T_g of PLA specimens after accelerated weathering tests, the authors associated the phenomenon with the scission of long chains, as a result, for example, of the hydrolysis of ester bonds and the penetration of water between the chains, increasing their mobility. Consequently, decreases in the molecular mass of the polymer were also observed (BOLIO-LOPEZ et al., 2013; COPINET et al., 2004; LV et al., 2018).

It can be seen that the 45 °C weathering has considerably accelerated the increasing effect on the material T_g, when compared to the results for the 35 °C weathering. Moreover, similarly to what happened to χc, a second stage of T_g variation was observed, with its decay over time.

Since the χc reduction was not associated to a T_g reduction between 240 and 408 h, it can be assumed that, in fact, three distinct degradation stages occurred for 45 °C weathering (instead of only two stages, as previously concluded through results for χc variation):

1) initially, up to 240 h, degradation may have predominantly affected amorphous parts of the scaffold; which, associated with the reduction of chain entanglements, facilitates their reorganization into crystalline structures. Associated to that, volume relaxation may have caused the densification of amorphous regions, hindering the material's glass transition. Consequently, there was an initial increase in both χc and T_g;

2) the subsequent reduction in χc accompanied by T_g increase, between 240 and 408 h, may result from two phenomena at this stage: degradation started to act on crystallites of the material (leading to χc decrease) and volume relaxation induced by chains segmental motion continued to be intensified (which explains why T_g continued to increase);

3) the χc reduction also accompanied by T_g reduction, from 408 h onwards, may indicate that degradation over the crystalline parts continued to occur, which implies higher ratios of amorphous/crystalline phases; and that scission of long chains due to hydrolysis and water entrance between chains became more significant than volume relaxation, leading to higher

chain mobility – consequently, the material becomes more susceptible, when heated, to switch to a more "malleable" condition, i.e., to the glass transition (BOLIO-LOPEZ et al., 2013; COPINET et al., 2004; LV et al., 2018; YATIGALA; BAJWA; BAJWA, 2018).

The degradation of PLA specimens, in cases of 35 and 45 °C weathering tests occurs predominantly by thermooxidation mechanisms, because the experiments are performed in a laboratory oven, under temperature control, and without significant presence of light (RASSELET et al., 2014). In addition, the hydrolysis mechanism is also present due to the existence of environmental humidity, being also intensified by temperature and mainly affecting amorphous parts, more susceptible to reacting with the water in the air (COPINET et al., 2004; DE JONG et al., 2001; ELSAWY et al., 2017; YUAN; MAK; YAO, 2002).

Figure 13 - (a) Degree of crystallinity (χc) as a function of exposure time of the PLA scaffolds to accelerated weathering under 35 and 45 °C. (b) Glass transition temperature (T_g) as a function of exposure time of the PLA scaffolds to accelerated weathering under 35 and 45 °C.

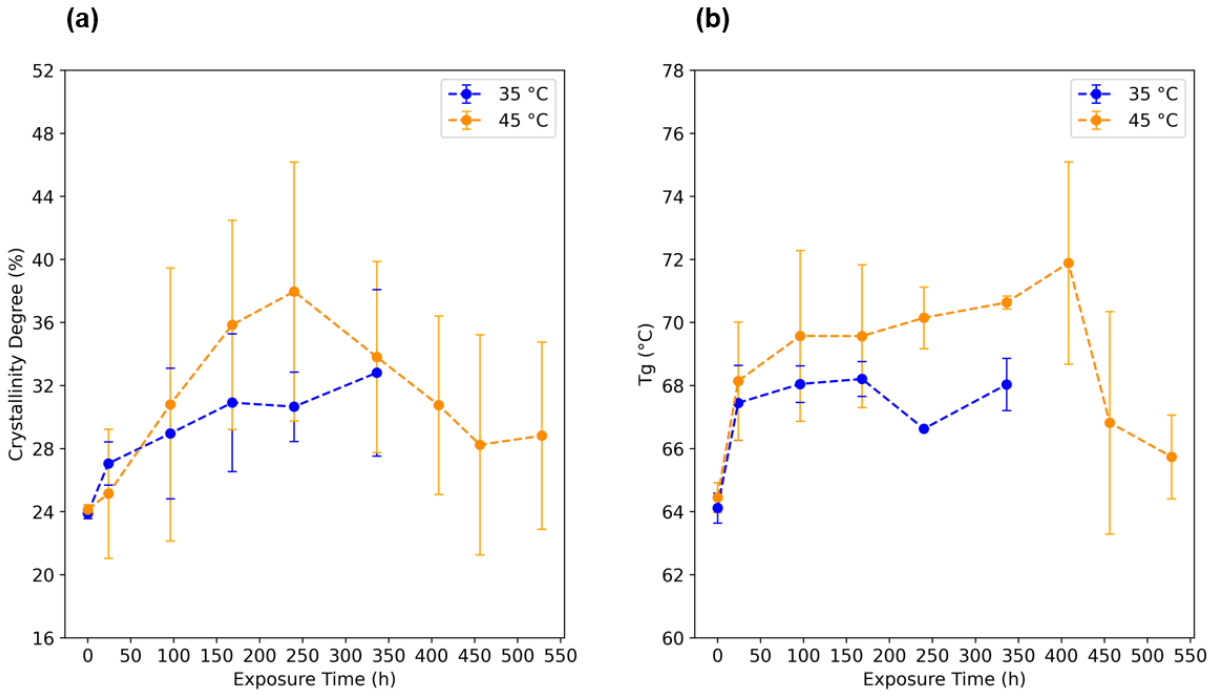

Source: Author.

5.3.4 Accelerated Weathering under Temperature, Humidity, and Radiation

Figure 14 shows the heat flow curves (mW) as a function of temperature (°C), obtained through DSC analyses, of M20_45 specimens subjected to accelerated weathering under temperature, humidity, and radiation (T-H-R) control – Cycle 1 of ASTM G154 (2016). Each

curve corresponds to a single specimen in the initial condition and subjected to the five established exposure times: 24, 96, 168, 240, and 336 h[14].

The endothermic T_g peak and the exothermic ΔH_{cc} peak could not be identified – i.e., the enthalpies for these transitions became zero. The only visible peak in the DSC curves for the T-H-R tests was T_m. Therefore, T_g measurements were disabled, and it was only possible to calculate χc for the different time exposures.

Sawpan et al. (2019) also reported the non-identification of the glass transition peak of pure PLA specimens subjected to ASTM G154 (2016) accelerated weathering tests. The authors associated the phenomenon with intense chain scission on the amorphous portion of the polymer into low molecular weight chains.

To present χc calculated values – through Equation (13) – as well as for better visualization of the other results, the measured properties are shown in Table 7.

Figure 14 - DSC curves obtained for different exposure times of the PLA scaffold to accelerated weathering under temperature, UV radiation, and humidity control.

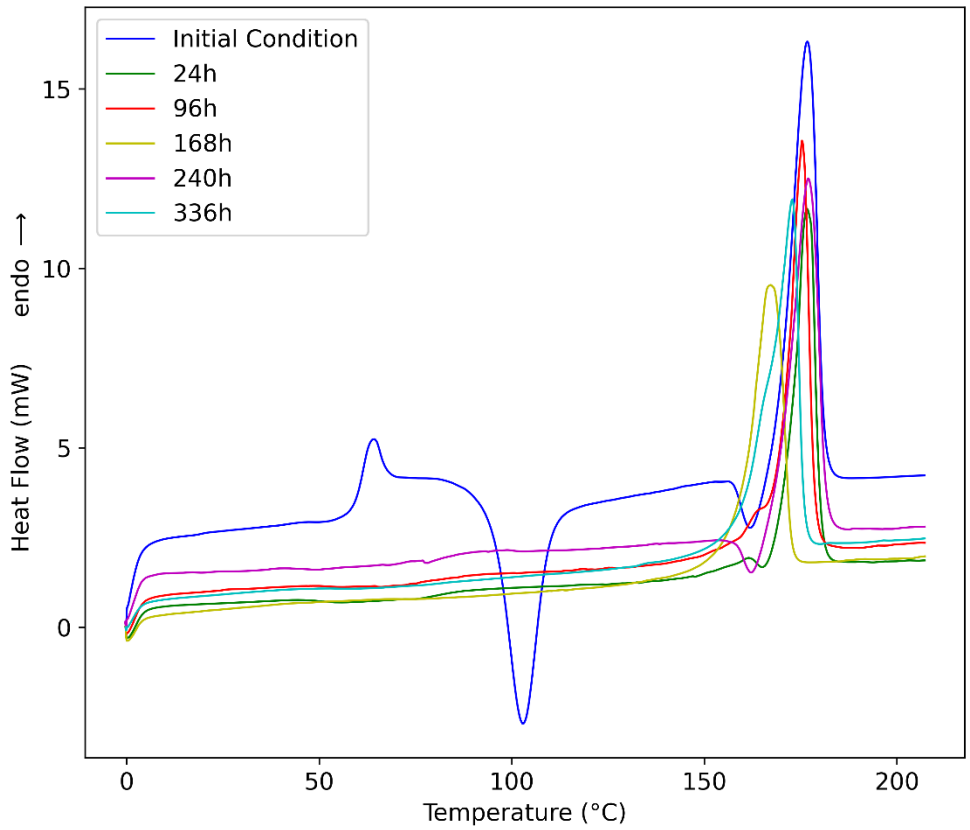

Source: Author.

[14] The curves for the second batch of specimens are shown in Figure 34 of APPENDIX C – DSC Curves.

Table 7 - DSC analysis results for the PLA scaffold in its initial condition and after different exposure times to accelerated weathering under temperature, UV radiation, and humidity control.

Exposure Time [h]	**0**	**24**	**96**	**168**	**240**	**336**
Properties	**χc [%]**	**χc [%]**	**χc [%]**	**χc [%]**	**χc [%]**	**χc [%]**
Specimen 1	23.66	55.12	55.18	57.77	59.38	62.24
Specimen 2	24.13	47.34	53.56	56.48	59.65	63.32
Average	23.89	51.23	54.37	57.12	59.51	62.78
Standard Deviation	0.33	5.50	1.14	0.91	0.19	0.76

Source: Author.

5.3.4.1 Crystallinity Degree (χc)

As indicated in Table 7, the M20_45 average χc presented a sharp increase between the initial condition and 24 h exposure (from 23.89 to 51.23%) and a milder increase up to 336 h, reaching 62.78%. Therefore, at 336 h, the average χc rose by 38.89%, which represents a relatively increase of 162.79% between the final and the initial condition. Figure 15 shows χc values plotted as a function of exposure times to T-H-R accelerated weathering.

Therefore, the χc increase, for T-H-R accelerated weathering, was the most pronounced among all the accelerated weathering tests, showing the expressive and rapid effect of high humidity and radiation when combined with high temperature. There was not a decreasing stage of χc for the T-H-R test, as occurred for 45 °C AW, indicating that the degradation strongly affected the amorphous regions of the polymeric specimens, because they are less ordered and, consequently, more susceptible to degradation.

In addition, there is a reduction of the characteristic chain entanglements of amorphous regions, which increases the molecular mobility and their slow reorganization into crystalline form (YATIGALA; BAJWA; BAJWA, 2018; YUAN; MAK; YAO, 2002). Most of the studies mentioned in the section regarding DSC results for 35 °C weathering (5.3.2) indicate χc increases after accelerated weathering, also corroborating the results regarding the increase in χc in the weathering tests under temperature, humidity, and radiation.

Therefore, the more severe conditions imposed by the T-H-R tests led to rapid degradation of the most sensitive regions of the polymer (amorphous), with relatively little degradation over crystalline regions. In fact, the maximum average χc measured for the tests

under temperature, humidity, and radiation was 62.78%; while for the tests under 45 °C, it was 37.97%.

The degradation of PLA specimens, in the case of the T-H-R accelerated weathering test occurs by thermooxidation (effect of temperature), hydrolysis (mainly effect of humidity), and photodegradation (effect of UV radiation). Hydrolysis is also intensified by temperature, and the amorphous regions of the polymer are more susceptible to reacting with the water in the air (COPINET et al., 2004; DE JONG et al., 2001; ELSAWY et al., 2017; IKADA, 1997; RASSELET et al., 2014; YUAN; MAK; YAO, 2002).

Figure 15 - Crystallinity degree (χc) as a function of exposure time of the PLA scaffold to accelerated weathering under temperature, UV radiation, and humidity control.

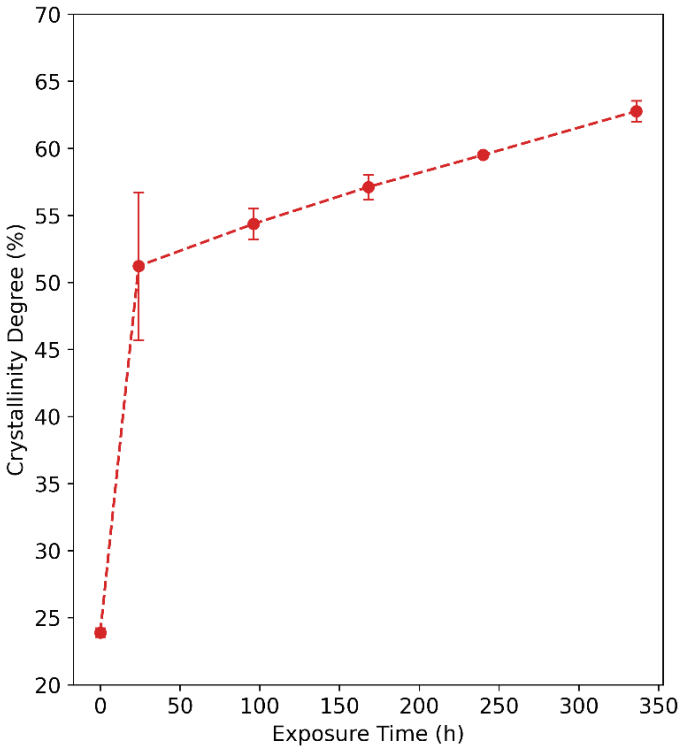

Source: Author.

5.4 X-RAY DIFFRACTION (XRD) ANALYSES[15]

5.4.1 Initial Condition

PLA crystallizes as an orthorhombic α phase and there are two characteristic peaks of PLA crystalline planes (when it is semicrystalline): the most intense one is located at 2θ = 16.3°

[15] DOI: <https://doi.org/10.1016/j.mtcomm.2022.104821>.

– assigned to (200) and (110) planes and the less intense one is located at 2θ = 18.65° – corresponding to (203) plane (SAWPAN et al., 2019).

Figure 16 shows the diffractogram obtained for M20_45 in its initial condition. Only the peak at ~16.3°, assigned to the crystalline planes (200) and (110) – in addition to a visible amorphous band below the peak – was identified, which may be due to the low crystallinity of the PLA in its initial condition, so that only the most intense characteristic peak was evident. Islam, Pickering, and Foreman (2010), in XRD analyses with PLA-based composites before accelerated weathering, identified only one PLA peak at 16.4°.

5.4.2 Accelerated Weathering under 35 °C

For the 35 °C accelerated weathering test, at both 168 and 336 h exposure, the diffractograms also presented only the characteristic peak at ~16.3° – planes (200) and (110) – and the amorphous band below the peak, similar to the peak identified for the initial condition. It can be assumed that effects on the crystallinity degree of the specimens subjected to 35 °C accelerated weathering were not able to produce significant changes in the diffractograms (compared to the one obtained for the scaffold in the initial condition). The peak at ~16.3° remained visible, corroborating the DSC results that point out the non-significant degradation of PLA crystallites (section 5.3.2). Figure 16 shows the curves obtained for the initial condition, 168, and 336 h exposures.

Figure 16 - Diffractograms for the PLA scaffold in its initial condition, after 168 h and after 336 h exposure to accelerated weathering under 35 °C.

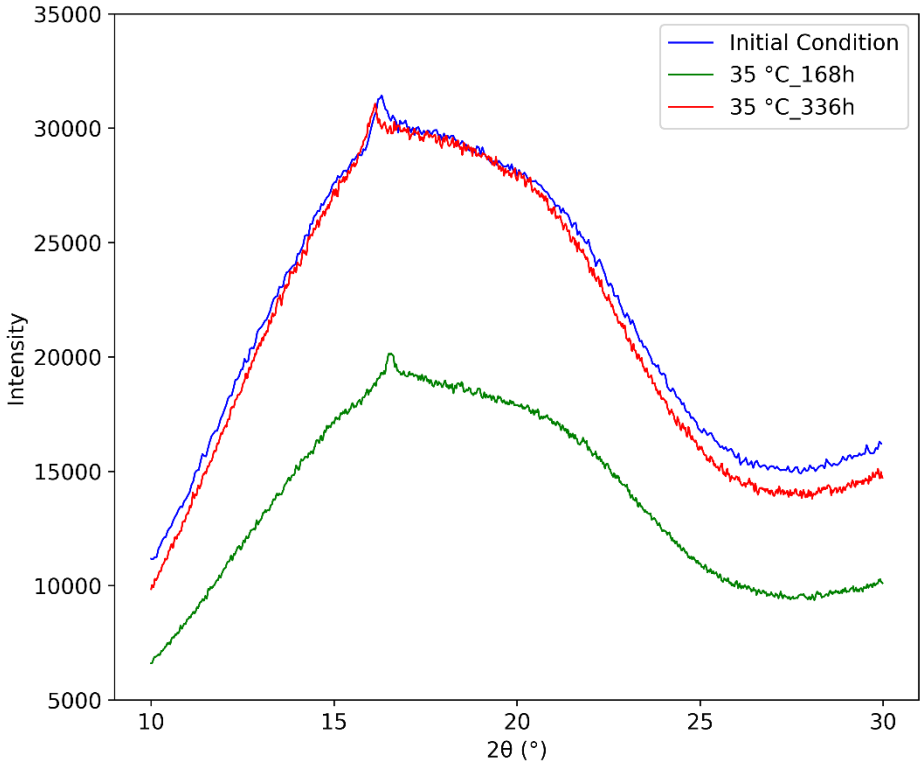

Source: Author.

5.4.3 Accelerated Weathering under 45 °C

For the 45 °C accelerated weathering test, the characteristic peak of the (200) and (110) planes, at ~16.3°, was not identified for both 168 and 336 h exposure (only the amorphous band remained visible), as can be seen in Figure 17. This effect may be associated with the degradation of the crystalline parts of the scaffold, identified through DSC results for these tests. The χc values did not become null, but the partial degradation over the crystallites may have been enough to suppress the peak at ~16.3° in the diffractograms.

Figure 17 - Diffractograms for the PLA scaffold in its initial condition, after 168 h and after 336 h exposure to accelerated weathering under 45 °C.

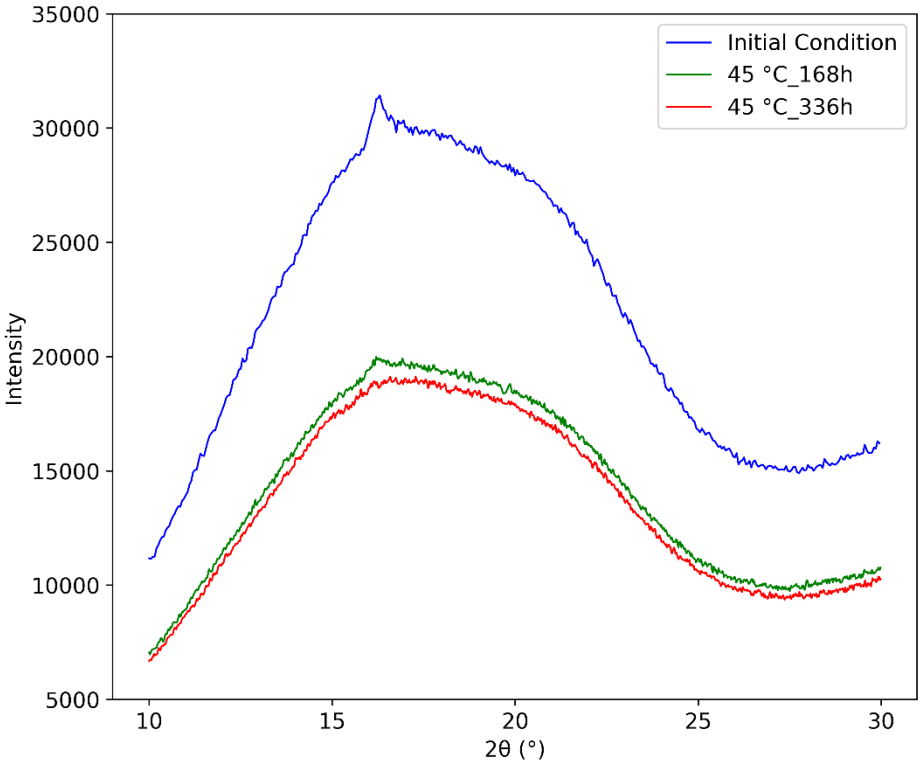

Source: Author.

5.4.4 Accelerated Weathering under Temperature, Humidity, and Radiation

Figure 18 presents the diffractograms obtained for the scaffold in its initial condition, 168, and 336 h exposure to T-H-R accelerated weathering. Since the curves are in very different intensity ranges, the visibility of the peak previously identified in the diffractogram for the scaffold in its initial condition was compromised.

For both 168 and 336 h exposure, the intensity of the characteristic peak of (200) and (110) crystalline planes (at ~16.3°) considerably increased. In addition, the characteristic peak of (203) crystalline plane (at ~18.65°) became also visible. The intensities of both peaks increased from 168 to 336 h exposure.

Both peaks, for the two exposure times, became much more prominent, with a considerable reduction in noise and amorphous band, compared to the diffractograms of the initial condition, the 35 °C weathering, and the 45 °C weathering. XRD analyses conducted by Islam, Pickering, and Foreman (2010), for PLA-based composite specimens, before and after accelerated weathering according to ASTM G154 (2016), show similar results regarding the

presence of noise and an amorphous band before the weathering tests, and their drastic reduction after the tests, in addition to the evidencing of narrow and sharp peaks.

Figure 18 - Diffractograms for the PLA scaffold in its initial condition, after 168 h and after 336 h exposure to accelerated weathering under temperature, UV radiation, and humidity control.

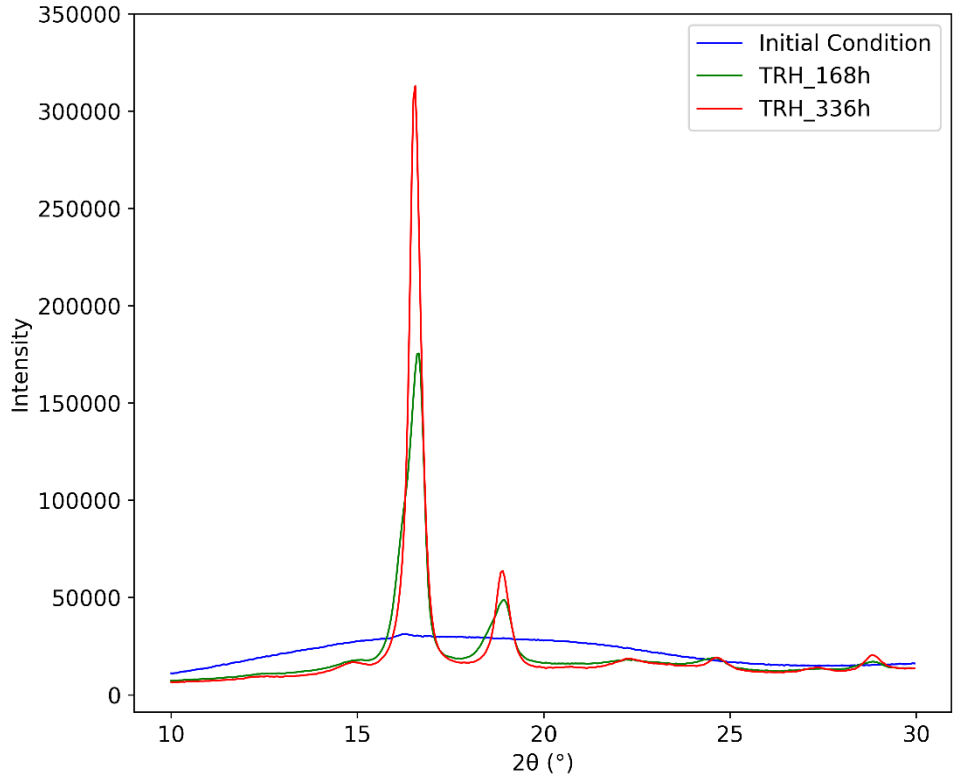

Source: Author.

5.5 MECHANICAL TORQUE STRENGTH TESTS[16]

5.5.1 Initial Condition

The PLA scaffold, in its initial condition, presented a torque strength (ABNT ISO/TS 13498, 2013) of 54.4 ± 3. N·cm. The results of the tests for these specimens are presented in Table 8. It can be seen that the failure mode of four of the specimens was stripping torque (ST), which occurs when, during screw insertion, the formed thread fails – which allows the screw to freely rotate in the polymeric specimen, with no resulting axial force between the screw and the substrate (EDWARDS et al., 2005). The failure mode of one of the specimens was the breakage of the scaffold.

[16] DOI: <https://doi.org/10.1016/j.mtcomm.2022.104140>.

Table 8 - Torque strength (ABNT ISO/TS 13498, 2013) results for the PLA scaffold in its initial condition.

Specimen	Torque Resistance [N·cm]	Failure Mode*
1	50.2	ST
2	50.9	ST
3	55.3	ST
4	57.2	B
5	58.6	ST
Average	54.4	-
Standard Deviation	3.7	-

*ST: stripping torque. B: breakage.
Source: Author.

5.5.2 Weathering under 25 °C

The results for the 25 °C weathering are presented in Table 9. Figure 19 shows the torque strength values plotted as a function of exposure time, for the different T tests, including the one under 25 °C. There was no considerable reduction in mechanical resistance, as expected for room temperature since no accelerating factors are acting on the degradation process.

Table 9 - Torque strength (ABNT ISO/TS 13498, 2013) results for the PLA scaffold subjected to weathering under 25 °C.

(continue)

Exposure Time	24 h		96 h		168 h	
Specimen	**Torque Resistance [N·cm]**	**Failure Mode***	**Torque Resistance [N·cm]**	**Failure Mode***	**Torque Resistance [N·cm]**	**Failure Mode***
1	62.1	ST	58.6	ST	57.1	ST
2	51.2	B	53.2	B	53.5	ST
3	59.3	ST	48.4	ST	52.0	B
4	50.2	ST	57.3	B	59.1	ST
5	50.8	B	52.7	ST	54.3	ST
Average	54.7	-	54.0	-	55.2	-
Standard Deviation	5.6	-	4.0	-	2.9	-

Table 9- Results of mechanical resistance to torque (ABNT ISO/TS 13498, 2013) for M20_45 subjected to weathering tests at 25 °C.

(conclusion)

Exposure Time	**240 h**		**336 h**	
Specimen	**Torque Resistance [N·cm]**	**Failure Mode***	**Torque Resistance [N·cm]**	**Failure Mode***
1	58.6	ST	59.3	ST
2	53.2	B	60.1	ST
3	49.4	B	53.2	ST
4	56.3	ST	48.8	B
5	52.9	B	49.4	B
Average	54.1	-	54.2	-
Standard Deviation	3.5	-	5.3	-

*ST: stripping torque. B: breakage.
Source: Author.

5.5.3 Accelerated Weathering under 35 °C

The results for the specimens that underwent the 35 °C accelerated weathering test are presented in Table 10. Figure 19 shows the torque strength values plotted as a function of exposure time, for the different T tests performed, including for the 35 °C accelerated weathering. The acceptance criterion of 45 N·cm was not reached; the torque strength decreased until it reached 47.9 ± 1.9 N·cm, at 336 h exposure.

Table 10 - Torque strength (ABNT ISO/TS 13498, 2013) results for the PLA scaffold subjected to accelerated weathering under 35 °C.

(continue)

Exposure Time	**24 h**		**96 h**		**168 h**	
Specimen	**Torque Resistance [N·cm]**	**Failure Mode***	**Torque Resistance [N·cm]**	**Failure Mode***	**Torque Resistance [N·cm]**	**Failure Mode***
1	58.1	ST	49.1	B	47.9	ST
2	49.1	B	56.7	ST	50.6	ST
3	50.2	ST	53.2	ST	60.6	ST
4	56.2	ST	52.5	ST	44.3	B
5	52.3	ST	48.6	B	49.8	B
Average	53.2	-	52.0	-	50.6	-
Standard Deviation	3.9	-	3.3	-	6.1	-

Table 10 - Torque strength (ABNT ISO/TS 13498, 2013) results for the PLA scaffold subjected to accelerated weathering under 35 °C.

(conclusion)

Exposure Time	**240 h**		**336 h**	
Specimen	**Torque Resistance [N·cm]**	**Failure Mode***	**Torque Resistance [N·cm]**	**Failure Mode***
1	44.1	B	48.2	ST
2	48.8	B	50.2	ST
3	56.6	ST	45.3	B
4	53.5	B	49.2	B
5	47.6	ST	46.7	B
Average	50.1	-	47.9	-
Standard Deviation	4.9	-	1.9	-

* ST: stripping torque. B: breakage.
Source: Author.

5.5.4 Accelerated Weathering under 45 °C

The results for the specimens that underwent the 45 °C accelerated weathering test are presented in Table 11. Figure 19 shows the torque strength values plotted as a function of exposure time, for the different T tests performed, including for the 45 °C accelerated weathering. The torque strength obtained for the last exposure time (528 h) was below the acceptance criterion (45 N.cm). Thus, 456 h was defined as the time for failure, although the average value (47.0 N.cm) was slightly above 45 N.cm.

Table 11 - Torque strength (ABNT ISO/TS 13498, 2013) results for the PLA scaffold subjected to accelerated weathering under 45 °C.

(continue)

Exposure Time	**24 h**		**96 h**		**168 h**		**240 h**	
Specimen	**Torque Resistance [N·cm]**	**Failure Mode***	**Torque Resistance [N·cm]**	**Failure Mode***	**Torque Resistance [N·cm]**	**Failure Mode***	**Torque Resistance [N·cm]**	**Failure Mode***
1	53.7	ST	49.1	ST	57.5	ST	47.7	ST
2	49.3	ST	48.7	B	54.8	B	44.6	ST
3	57.8	ST	53.6	ST	44.7	ST	53.5	ST
4	50.6	B	51.8	ST	50.4	B	51.5	ST
5	52.9	ST	49.3	ST	49.9	ST	49.3	ST
Average	52.9	-	50.5	-	51.5	-	49.3	-
Standard Deviation	3.3	-	2.1	-	4.9	-	3.4	-

Torque strength (ABNT ISO/TS 13498, 2013) results for the PLA scaffold subjected to accelerated weathering under 45 °C.

(conclusion)

Exposure Time	336 h		408 h		456 h		528 h	
Specimen	**Torque Resistance [N·cm]**	**Failure Mode***	**Torque Resistance [N·cm]**	**Failure Mode***	**Torque Resistance [N·cm]**	**Failure Mode***	**Torque Resistance [N·cm]**	**Failure Mode***
1	48.7	B	45.1	B	46.1	ST	40.4	B
2	51.8	ST	46.6	B	48.7	ST	43.2	ST
3	46.2	B	49.9	ST	47.5	B	47.2	ST
4	45.6	B	49.0	ST	47.9	ST	44.6	ST
5	52.4	ST	47.5	ST	44.6	B	48.5	ST
Average	48.9	-	47.6	-	47.0	-	44.8	--
Standard Deviation	3.1	-	1.9	-	1.6	-	3.2	-

* ST: stripping torque. B: breakage.
Source: Author.

Figure 19 - Torque strength as a function of exposure time, for different tests under temperature control (25, 35, and 45 °C).

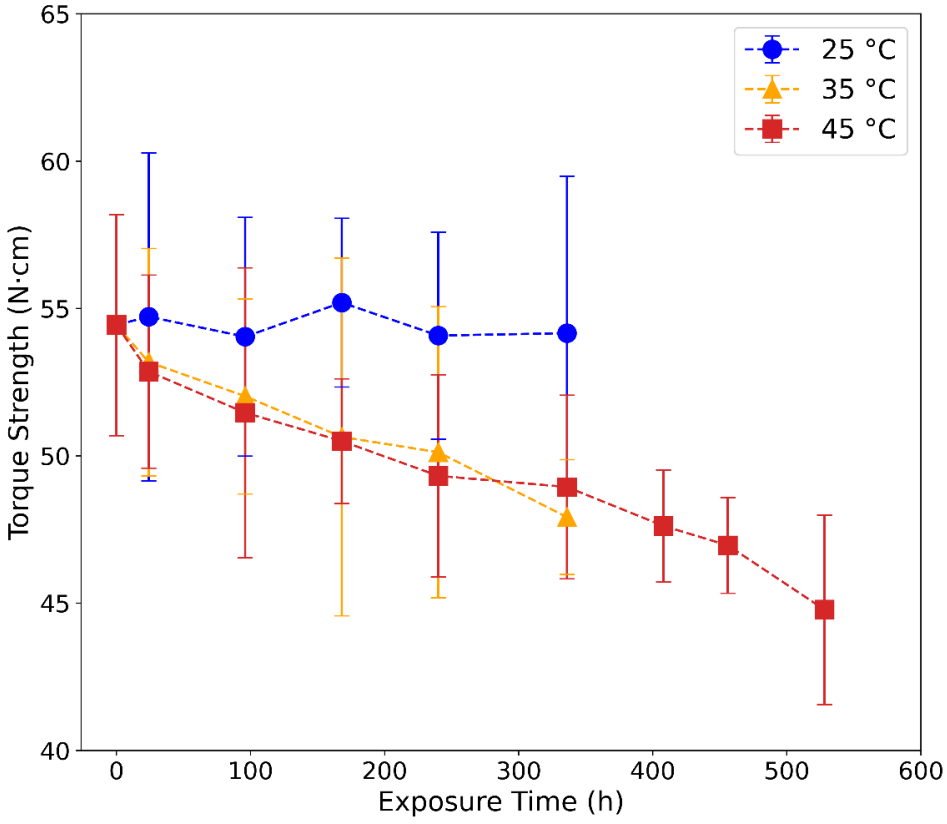

Source: Author.

5.5.5 Accelerated Weathering under Temperature, Humidity, and Radiation

The results for the specimens that underwent accelerated weathering under temperature, humidity, and radiation control (Cycle 1 of ASTM G154 (2016)) are presented in Table 12. Figure 20 shows the torque strength values plotted as a function of exposure time, for the T-H-R accelerated weathering test.

The torque strength sharply decreased from 168 to 240 h exposure, with more than a 10 N.cm difference. Since at 240 h the measured strength was below the acceptance criterion (45 N.cm), 168 h was defined as the time for failure, although the average mechanical strength (47.4 N.cm) was slightly above the acceptance criterion.

Table 12 - Torque strength (ABNT ISO/TS 13498, 2013) results for the PLA scaffold subjected to accelerated weathering under temperature, radiation, and humidity control.

(continue)

Exposure Time	**24 h**		**96 h**		**168 h**	
Specimen	**Torque Resistance [N·cm]**	**Failure Mode***	**Torque Resistance [N·cm]**	**Failure Mode***	**Torque Resistance [N·cm]**	**Failure Mode***
1	59.2	ST	51.8	B	45.7	B
2	57.0	B	46.6	B	49.1	B
3	54.7	B	50.3	B	46.8	B
4	52.2	B	49.1	B	44.9	B
5	48.3	B	56.2	ST	50.3	B
Average	54.3	-	50.8	-	47.4	-
Standard Deviation	4.2	-	3.6	-	2.3	-

Table 12 - Torque strength (ABNT ISO/TS 13498, 2013) results for the PLA scaffold subjected to accelerated weathering under temperature, radiation, and humidity control.

(conclusion)

Exposure Time	**240 h**		**336 h**	
Specimen	**Torque Resistance [N·cm]**	**Failure Mode***	**Torque Resistance [N·cm]**	**Failure Mode***
1	29.2	B	18.4	B
2	28.0	B	23.4	B
3	31.4	B	25.1	B
4	34.4	B	22.1	B
5	36.2	B	17.9	B
Average	31.8	-	21.4	-
Standard Deviation	3.4	-	2.8	-

* ST: stripping torque. B: breakage.
Source: Author.

Figure 20 - Torque strength as a function of exposure time for the PLA scaffold subjected to accelerated weathering under temperature, radiation, and humidity control.

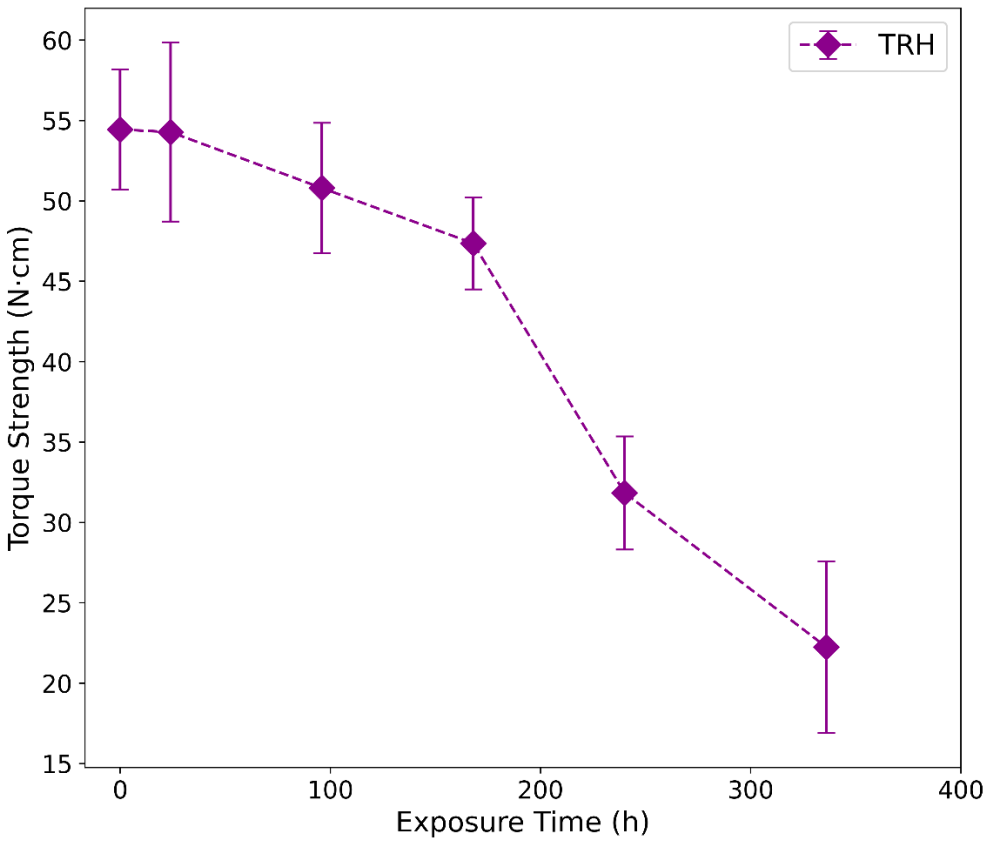

Source: Author.

For both accelerated weathering test types, T tests, and T-H-R tests, the torque strength decreased as exposure time increased, with the T-H-R test presenting the most drastic decrease. At 336 h, for example, the mechanical strength reduction (compared to the PLA scaffold in its initial condition) for 45 °C accelerated weathering was 10.10%, meanwhile, for the T-H-R test, it was 60.73%.

To the best of our knowledge, there are no studies in the literature presenting the same mechanical test performed in this study. However, other types of mechanical tests are usually performed to characterize PLA specimens undergoing AW, especially tensile, flexural, and fracture toughness tests.

Isadounene et al. (2018) reported a reduction in tensile strength, tensile modulus, and elongation at break of pure PLA specimens as a function of exposure time to combined temperature, humidity, and UV-A radiation (ASTM G154 (2016)). Lv et al. (2018) also reported a reduction in the tensile strength of pure PLA specimens subjected to ASTM G154 (2016) tests (UV-A) after different exposure times (up to 1200 h). Martín Del Campo et al. (2020) performed measurements of tensile strength, tensile modulus, flexural strength, flexural modulus, and impact strength, before and after 600 h under ASTM G154 (2016) tests (using UV-A) and a decrease in all the mentioned mechanical properties was observed for the pure PLA specimens. Measurements of tensile strength, tensile modulus, flexural strength, and flexural modulus conducted by Islam, Pickering, and Foreman (2010), for up to 1000 h of accelerated weathering (ASTM G154 (2016)), using UV-A, also indicated a decrease for all these mechanical properties.

In addition, Copinet et al. (2004) reported a decrease in elongation at break of PLA films subjected to accelerated weathering tests under temperature and humidity control, both with and without the application of UV-B radiation. Lin, Xie, and Qiu (2019) performed accelerated weathering tests by applying UV radiation under different temperatures, and a decrease in tensile strength was observed under all conditions.

The aforementioned studies associated the gradual reduction in mechanical strength as exposure time to accelerated weathering increases with phenomena such as plasticization, swelling (water absorption), and photodegradation (in cases of UV application). In addition, chain cleavage and hydrolysis of PLA ester bonds are also mentioned.

5.5.6 Statistical Analysis

By performing paired Student's t-tests for each type of weathering test, it was obtained that, under 25 °C, none of the exposure times caused significant change (p-value < 0.05) in mechanical strength compared to the initial value. For the 35 °C accelerated weathering, only at 336 h exposure, there was a significant change (from 54.4 ± 3.7 N·cm to 47.9 ± 1.9 N·cm, p-value = 0.0419). For the 45 °C accelerated weathering, there was a significant change at 240 h (49.3 ± 3.4 N·cm, p-value = 0.0198), 336 h (48.9 ± 3.1 N·cm, p-value = 0.0767), 408 h (47.6 ± 1.9 N·cm, p-value = 0.0056), 456 h (47.0 ± 1.6 N·cm, p-value = 0.0223) and 528 h (44.8 ± 3.2 N·cm, p-value = 0.0004). For the T-H-R test, there was significant variation at 168 h (47.4 ± 2.3 N·cm, p-value = 0.0173), 240 h (31.8 ± 3.4 N·cm, p-value = 0.00000112), and 336 h (21.4 ± 2.8 N·cm, p-value = 0.0001).

By performing an ANOVA test followed by a Tukey's multiple comparisons test to compare the different weathering tests regarding the mechanical resistance obtained for each exposure time, it was found that, for 24 and 96 h, the different weathering methods did not differ significantly (p-value < 0.05). For 168 h, the result for the T-H-R test (47.4 ± 2.3 N·cm) differed significantly from that obtained for weathering under 25 °C (55.2 ± 2.9 N·cm). Regarding 240 and 336 h, the results for T-H-R test (31.8 ± 3.4 N·cm and 21.4 ± 2.8 N·cm, respectively) differed significantly from those obtained for specimens maintained under 25 °C (54.1 ± 3.5 N·cm and 54.2 ± 5.3, respectively), under 35 °C (50.1 ± 4.9 N·cm and 47.9 ± 1.9 N·cm, respectively), and under 45 °C (49.3 ± 3.4 N·cm and 48.9 ± 3.1 N·cm, respectively). For none of the exposure times compared, there was a significant difference between the T tests results (25, 35, and 45 °C).

5.6 FOURIER TRANSFORM INFRARED SPECTROSCOPY (FTIR) ANALYSES[17]

Figure 21 compares the FTIR spectra of the scaffolds in the initial condition and subjected to 168 and 336 h at 35 and 45 °C, and under T-R-H accelerated weathering. PLA presents six distinctive infrared (IR) bands corresponding to its chemical bond structure, which could be clearly identified in the first spectra (of the unweathered PLA scaffold); at 868 cm^{-1}, corresponding to the C–C stretching peak; at 1043, 1080, 1128, 1180, and 1267 cm^{-1}, corresponding to the C–O stretching peaks; at 1361 and 1381 cm^{-1}, corresponding to the C–H

[17] DOI: <https://doi.org/10.1016/j.mtcomm.2022.104821>.

deformation peak; at 1452 cm^{-1}, corresponding to the deformation vibration of –CH3; at 1747 cm^{-1}, corresponding to the ester carbonyl stretching groups C=O; and at 2852, 2920, 2997 cm^{-1}, corresponding to the C–H stretching peaks (COPINET et al., 2004; ISADOUNENE et al., 2018; LIZÁRRAGA-LABORÍN et al., 2018; LV et al., 2017; MARTÍN DEL CAMPO et al., 2020; VARSAVAS; KAYNAK, 2017).

As already mentioned, the main photolytic degradation of PLA occurs through the Norrish II reaction. This mechanism leads to chain scission, resulting in the formation of C=C bond and hydroperoxides (O–H) (ISHIKAWA et al., 2015; WANG et al., 2021), and this effect was significant enough to cause a change only in the spectra of the scaffold subjected to 336 h under the T-R-H accelerated weathering, for which, similarly to what was reported by Varsavas and Kaynak (2017), new peaks of C=C (at 1653 cm^{-1}) and O–H (at 3734 and 3751 cm^{-1}), appeared, as can be seen in Figure 22.

Some studies regarding the accelerated weathering of PLA samples report changes in the intensity of the IR bands combined with their shift to lower wavenumbers (COPINET et al., 2004; VARSAVAS; KAYNAK, 2017), while others only report variations in peak intensities (ISADOUNENE et al., 2018; LIZÁRRAGA-LABORÍN et al., 2018; LV et al., 2017; MARTÍN DEL CAMPO et al., 2020). In the present work, none of the wavenumbers of the characteristic IR bands significantly shifted to lower or higher wavenumbers.

However, a phenomenon that could be observed in the spectra for all AW types was the decrease in intensity of all typical IR peaks with increasing exposure time to AW, as also observed by Varsavas and Kaynak (2017) for neat PLA samples subjected to ASTM G154 (UV-B) tests. This phenomenon can be explained as a result of the significant level of chain scission in the PLA structure, triggered by degradation mechanisms of photolysis – present in the T-R-H test – and hydrolysis – present in all AW tests performed, being also intensified by temperature (GONZÁLEZ-LÓPEZ et al., 2020; COPINET et al., 2004; VARSAVAS; KAYNAK, 2017).

Therefore, it could be also verified that the level of decrease in the intensity of IR peaks was potentialized following the order of criticality of the tests (35 °C < 45 °C < T-H-R), and the peaks became especially broader for samples exposed to 336 h at 45 °C and to 168 and 336 h under the T-H-R accelerated weathering – which corroborates the observed decay in mechanical strength along with the exposure time since chain scissions lead mechanical properties to decrease (GONZÁLEZ-LÓPEZ et al., 2020). Additionally, for none of the AW types, an increase in peak intensities was observed, as reported for some studies in the literature (LIZÁRRAGA-LABORÍN et al., 2018; LV et al., 2017; MARTÍN DEL CAMPO et al., 2020).

Figure 21 - FTIR spectra of the PLA scaffolds in the initial condition, after 168 and 336 h exposure to accelerated weathering under 35 and 45 °C, and under temperature, UV radiation, and humidity control.

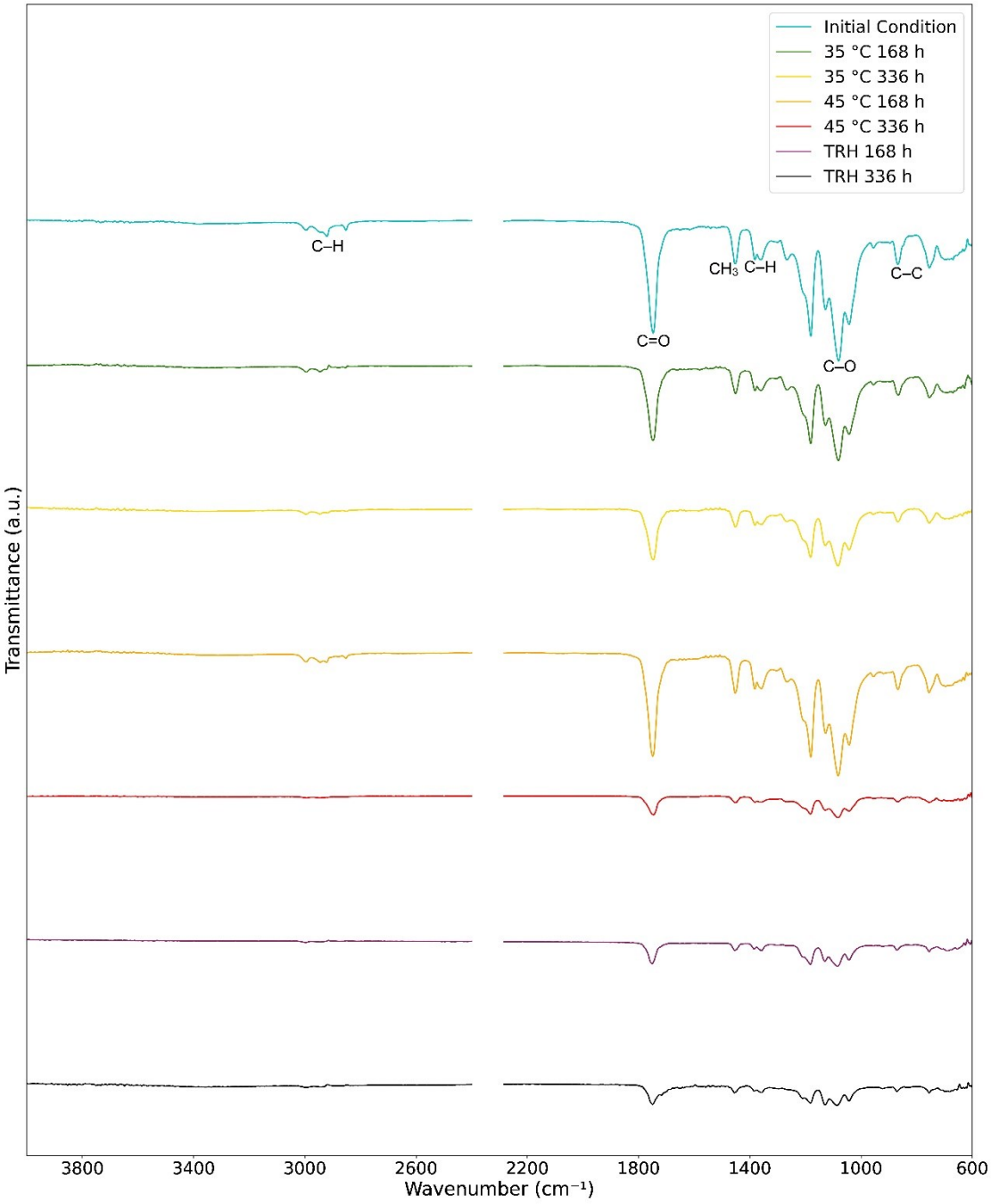

Source: Author.

Figure 22 - Expanded FTIR spectra of the PLA scaffold subjected to 336 h under temperature, UV radiation, and humidity control.

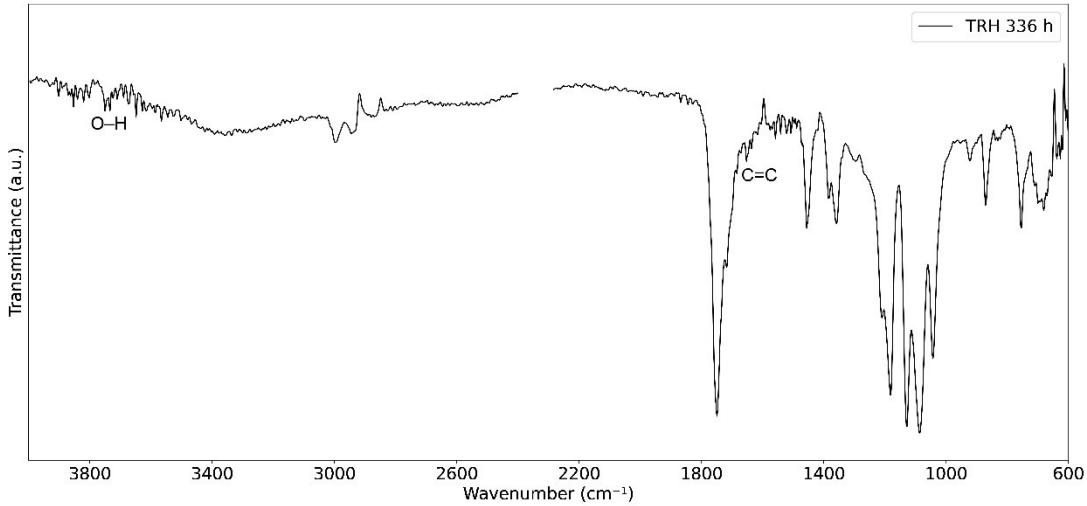

Source: Author.

5.7 VISCOSIMETRY ANALYSES

5.7.1 Initial Condition

For the PLA scaffold in its initial condition, a viscosity-average molecular weight of 70,158.75 g/mol was found. It was considered a pertinent value for the material, since PLLA molecular weight was reported to vary between 23,000 and 66,000 g/mol when measured through viscosimetry analysis (PEREGO; CELLA; BASTIOLI, 1996), in addition to values reported for weight-average molecular weight between approximately 100,000 and 370,000 g/mol when assessed by different techniques – in the context of PLA used for FFF processes and PLA specimens subjected to accelerated weathering tests (AMBONE; TORRIS; SHANMUGANATHAN, 2020; BHAGIA et al., 2021; HO; POMETTO; HINZ, 1999; COPINET et al., 2004; CHÁVEZ-MONTES et al., 2015; LV et al., 2018; KAYNAK; SARI, 2016; VARSAVAS; KAYNAK, 2017). Table 13 shows the flow times measured for the solvent and the different concentrations related to the initial condition, as well as the calculated values of η_{rel}, η_{inh}, $[\eta]$, and M_v.

Table 13 – Viscosimetry results for the PLA scaffold in its initial condition.

	Flow Time [s]				
	Solvent	**Initial Condition**			
Concentration [g/dL]	**0**	**0.2**	**0.4**	**0.6**	**1**
1	41.089	54.017	65.030	67.038	106.026
2	42.030	52.014	63.011	66.047	103.099
3	43.045	54.050	67.091	63.060	105.039
Average [s]	42.055	53.360	65.044	65.382	104.721
Standard Deviation [s]	0.978	1.166	2.040	2.071	1.489
η_{rel}	–	1.269	1.547	1.555	2.490
η_{inh} **[dL/g]**	–	1.1905	1.0902	0.7355	0.9123
$[\eta]$ **[dL/g]**	–	1.1909			
M_v **[g/mol]**	–	70,158.75			

Source: Author.

5.7.2 Accelerated Weathering under 35 °C

For the 35 °C accelerated weathering, viscosity-average molecular weights of 65,648.34 and 54,533.77 g/mol were found for 168 and 336 h exposure, respectively. Table 14 shows the flow times measured for the solvent and the different concentrations for 35 °C accelerated weathering (168 and 336 h), as well as the calculated values of η_{rel}, η_{inh}, $[\eta]$, and M_v. Figure 23 shows molecular weight values plotted as a function of exposure time, for the different accelerated weathering tests performed, including those under 35 °C.

5.7.3 Accelerated Weathering under 45 °C

For the 45 °C accelerated weathering, viscosity-average molecular weights of 32,424.40 and 22,889.27 g/mol were found for 168 and 336 h exposures, respectively. Table 15 shows the flow times measured for the solvent and the different concentrations for 45 °C accelerated weathering (168 and 336 h), as well as the calculated values of η_{rel}, η_{inh}, $[\eta]$, and M_v. Figure

23 shows molecular weight values plotted as a function of exposure time, for the different accelerated weathering tests performed, including those under 45 °C.

5.7.4 Accelerated Weathering under Temperature, Humidity, and Radiation

For the T-H-R accelerated weathering, viscosity-average molecular weights of 8,249.09 and 4,595.01 g/mol were found for 168 and 336 h exposure, respectively. Table 16 shows the flow times measured for the solvent and the different concentrations for T-H-R accelerated weathering (168 and 336 h), as well as the calculated values of η_{rel}, η_{inh}, $[\eta]$, and M_v. Figure 23 shows molecular weight values plotted as a function of exposure time, for the different accelerated weathering tests performed, including those under T-H-R control.

Table 14 – Viscosimetry results for the PLA scaffold subjected to accelerated weathering under 35 °C.

	Flow Time [s]								
	Solvent	**168 h under 35 °C**				**336 h under 35 °C**			
Concentration [g/dL]	**0**	**0.2**	**0.4**	**0.6**	**1**	**0.2**	**0.4**	**0.6**	**1**
1	41.089	54.003	63.038	72.051	101.086	50.078	60.000	73.087	97.079
2	42.03	52.014	65.098	68.095	97.066	52.062	56.015	69.031	99.058
3	43.045	51.064	64.010	67.099	103.065	52.077	63.002	66.016	100.043
Average [s]	42.055	52.360	64.049	69.082	100.406	51.406	59.672	69.378	98.727
Standard Deviation [s]	0.978	1.500	1.031	2.619	3.057	1.150	3.505	3.548	1.510
η_{rel}	–	1.245	1.523	1.643	2.388	1.222	1.419	1.650	2.348
η_{inh} **[dL/g]**	–	1.0959	1.0517	0.8272	0.8702	1.0039	0.8747	0.8343	0.8534
$[\eta]$ **[dL/g]**	–	1.1315				0.9809			
M_v **[g/mol]**		65,648.34				54,533.77			

Source: Author.

Table 15 – Viscosimetry results for the PLA scaffold subjected to accelerated weathering under 45 °C.

	Flow Time [s]								
	Solvent	**168 h under 45 °C**				**336 h under 45 °C**			
Concentration [g/dL]	**0**	**0.2**	**0.4**	**0.6**	**1**	**0.2**	**0.4**	**0.6**	**1**
1	41.089	48.081	54.061	60.066	76.065	46.08	52.05	56.001	68.017
2	42.03	49.040	54.005	59.06	73.075	47.036	49.081	57.006	66.051
3	43.045	47.032	52.045	61.02	77.083	46.096	52.079	55.002	65.057
Average [s]	42.055	48.051	53.370	60.049	75.408	46.404	51.070	56.003	66.375
Standard Deviation [s]	0.978	1.004	1.148	0.980	2.083	0.547	1.723	1.002	1.506
η_{rel}	–	1.143	1.269	1.428	1.793	1.103	1.214	1.332	1.578
η_{inh} **[dL/g]**	–	0.6665	0.5957	0.5936	0.5839	0.4921	0.4856	0.4774	0.4564
$[\eta]$ **[dL/g]**	–	0.6573				0.5027			
M_v **[g/mol]**		32,424.40				22,889.27			

Source: Author.

Table 16 – Viscosimetry results for the PLA scaffold subjected to accelerated weathering under temperature, humidity, and radiation control.

	Flow Time [s]								
	Solvent	**168 h under T-H-R**				**336 h under T-H-R**			
Concentration [g/dL]	**0**	**0.2**	**0.4**	**0.6**	**1**	**0.2**	**0.4**	**0.6**	**1**
1	41.089	45.016	47.053	46.084	50.086	43.086	43.052	46.058	48.023
2	42.03	43.071	44.027	48.038	53.031	43.079	44.051	46.005	47.076
3	43.045	44.064	46.068	48.004	51.092	44.096	45.046	43.092	48.055
Average [s]	42.055	44.050	45.716	47.375	51.403	43.420	44.050	45.052	47.718
Standard Deviation [s]	0.978	0.973	1.543	1.118	1.497	0.585	0.997	1.697	0.556
η_{rel}	–	1.047	1.087	1.127	1.222	1.032	1.047	1.071	1.135
η_{inh} **[dL/g]**	–	0.2318	0.2087	0.1986	0.2007	0.1598	0.1159	0.1147	0.1263
$[\eta]$ **[dL/g]**	–	0.2291				0.146			
M_v **[g/mol]**		8,249.09				4,595.01			

Source: Author.

Figure 23 – Viscosity-average molecular weight as a function of exposure time for PLA scaffolds subjected to accelerated weathering under temperature control (35 or 45 °C) and under temperature, radiation, and humidity control.

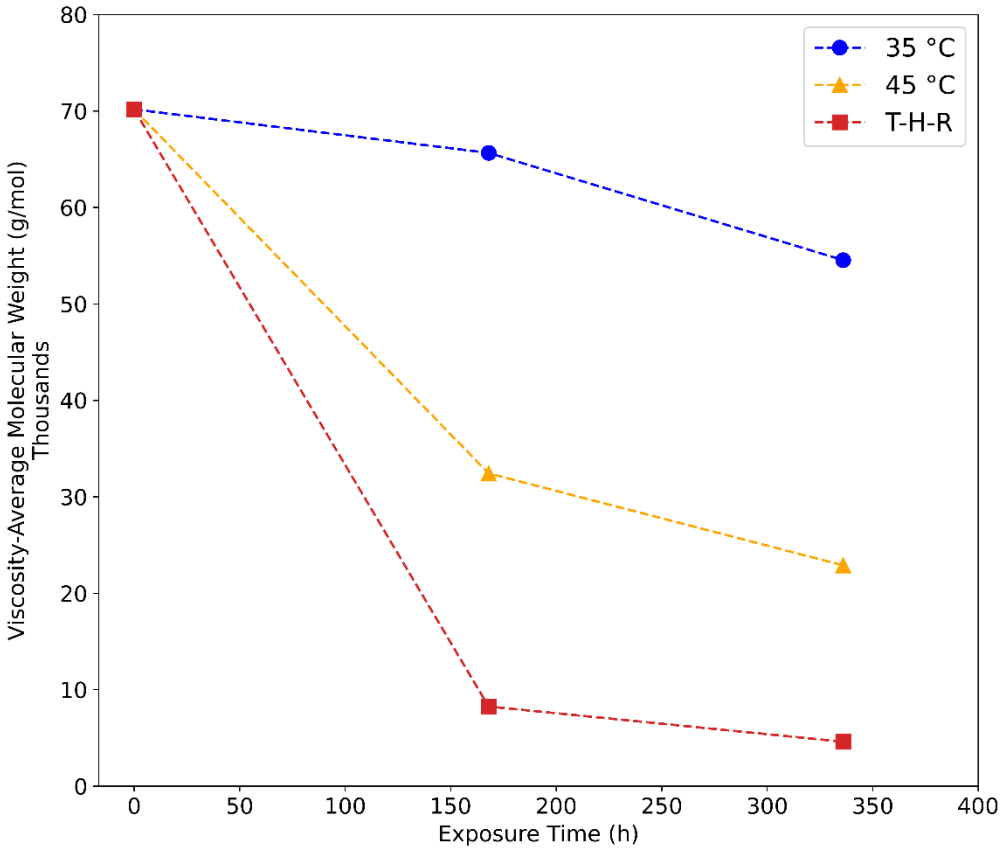

Source: Author.

Based on the results obtained with the viscosimetry analyses, it was possible to observe that there was a progressive decay of the molecular weight of the PLA scaffold with the exposure time to accelerated weathering, corroborating the expected phenomena of degradation by chain scission – originated by photolysis and hydrolysis (which is intensified by temperature) (GONZÁLEZ-LÓPEZ et al., 2020; COPINET et al., 2004). It is also possible to verify that the reduction in molecular weight was greater when the exposure temperature increased and even more drastic for weathering with the application of high temperature, humidity, and radiation. Therefore, the results are in accordance with the gradually higher criticality levels of the mentioned tests and they also corroborate the results of mechanical strength decay along with the exposure time, since chain scission leads to a decrease in mechanical properties (GONZÁLEZ-LÓPEZ et al., 2020).

Approximating the obtained curves to linear equations, the following degradation rates were found through the slopes: 7.81, 23.64, and 32.78 mw/week, for the tests under 35 °C, 45 °C, and T-H-R, respectively. Through the results for the T tests, a $Q10$ of 3.03 was found –

very close to the values found through the literature review presented in section 3.7.1, corroborating the equation defined for obtaining the shelf life by the correlation between the T tests and the natural weathering of the scaffold.

At the maximum exposure time analyzed (336 h), the molecular weight of the PLA scaffold subjected to the 35 °C accelerated weathering decreased by 15,624.98 g/mol, which is 22.27% less than the initial value (70,158.75 g/mol). For the 45 °C accelerated weathering, there was a decay of 32.62% (or 47,269.48 g/mol) at the same exposure time. For the T-H-R test, the molecular weight decreased 93.45% (or 65,563.74 g/mol) at 336 h.

The decrease in molecular weight is a phenomenon commonly reported in the scientific literature regarding polymers subjected to accelerated weathering tests, such as PLA, even though techniques other than viscosimetry are commonly employed for the measurements. Ho, Pometto, and Hinz (1999) compared the effects in the molecular weight – through high-performance size-exclusion chromatography (HPSEC) – of PLA films subjected to different temperatures (25, 40 and 55 °C) and humidity levels (10, 50, and 100%), with or without UV application. In all cases, the molecular weight decreased along with the exposure time, the degradation rate had a positive correlation with the temperature and the humidity, and it was also enhanced by UV radiation. After two weeks under 40 °C/50% RH, for example, the molecular weight decayed by approximately 10 and 30% for PLA samples with nearly 200,000 and 115,000 g/mol, respectively.

Copinet et al. (2004) applied different combinations of temperature (30, 45, and 60 °C) and humidity (30, 50, and 100%), with or without UV application, to PLA films and evaluated the effects on the molecular weight – through size-exclusion chromatography (SEC) – of the samples. The authors also observed a faster decrease in molecular weight for higher levels of temperature and humidity, and when UV radiation was present. After five weeks (first assessed exposure time) under 30 °C/50% RH and under 45 °C/50% RH (without UV), for example, the molecular weight decayed by approximately 15% and 25% from the initial value of almost 200,000 g/mol.

Some studies assessed the variation of molecular weight of PLA samples subjected to controlled cycles of temperature, humidity, and UV radiation. Chávez-Montes et al. (2015) aimed to study the effect of ASTM G154 tests (using UV-A) on the molecular weight decay for different PLA composites films – by gel permeation chromatography (GPC) – and in all cases a considerable decrease in weight average molecular weight (M_w) and the number average molecular weight (M_n) was observed as exposure time increased (up to 360 h). Lv et al. (2018) reported M_w and M_n decay (assessed by GPC analysis) on injection molded PLA samples after

ASTM G154 tests (using UV-A): 2,000 and 59,000 g/mol decrease (from 142,000 g/mol) in M_w after 600 and 1200 h, respectively; and 26,500 and 55,100 g/mol decrease (from 94,500 g/mol) in M_n, for the same exposure times.

Kaynak and Sari (2016) conducted static light scattering (SLS) analysis to assess the variation on M_w of PLA injection molded parts subjected to ASTM G154 tests (using UV-B) and observed a decay from 370,000 to 270,000 g/mol (for 50 h exposure), to 130,000 (for 100 h), to 100,000 (for 150 h), and finally to 80,000 (for 200 h). Varsavas and Kaynak (2017) also applied UV-B ASTM G154 cycles to PLA samples produced by injection and performed molecular weight measurements through the same technique. The authors reported a decrease from 370,000 to 130,000 after 100 h exposure and to 10,000 g/mol after 400 h.

Therefore, according to previous scientific literature, PLA is sensitive to temperature, humidity, and UV radiation, so its degradation rate increases as the intensity of these variables are also increased. The results obtained for the viscosity-average molecular weight of the PLA scaffolds subjected to the different accelerated weathering configurations are in accordance with this behavior commonly described, since the degradation in terms of ΔM_w/week was potentialized following the order of criticality of the tests (35 °C < 45 °C < T-H-R), reaching final molecular weights progressively lower.

5.8 SCANNING ELECTRON MICROSCOPY (SEM) ANALYSES[18]

Figure 24, Figure 25, Figure 26, and Figure 27 show the micrographs obtained for M20_45 in its initial condition, after 336 h under 35 °C accelerated weathering, after 336 h under 45 °C accelerated weathering, and after 336 h under T-H-R accelerated weathering, respectively – with x100 and x2000 magnifications. There were no noticeable surface defects on the specimens that underwent T tests, the visible discontinuities are supposed to be originated from impurities deposited on the specimens or even from printing defects.

On the other hand, T-H-R accelerated weathering resulted in the appearance of surface defects – micropores and microcracks – that can be better visualized by employing x5000 magnification (Figure 28). From twenty quasi-rounded pores found in the micrograph of Figure 25, an average pore size of $4.2 \times 10^{-1} \pm 2.1 \times 10^{-1}$ µm (between 8.1×10^{-2} µm and 7.3×10^{-1} µm) was measured.

[18] DOI: <https://doi.org/10.1016/j.mtcomm.2022.104821>.

Figure 24 - Micrographs obtained for the PLA scaffold in its initial condition. Left: View of a pore of the specimen, 100x magnification. Right: Specimen's surface at 2000x magnification.

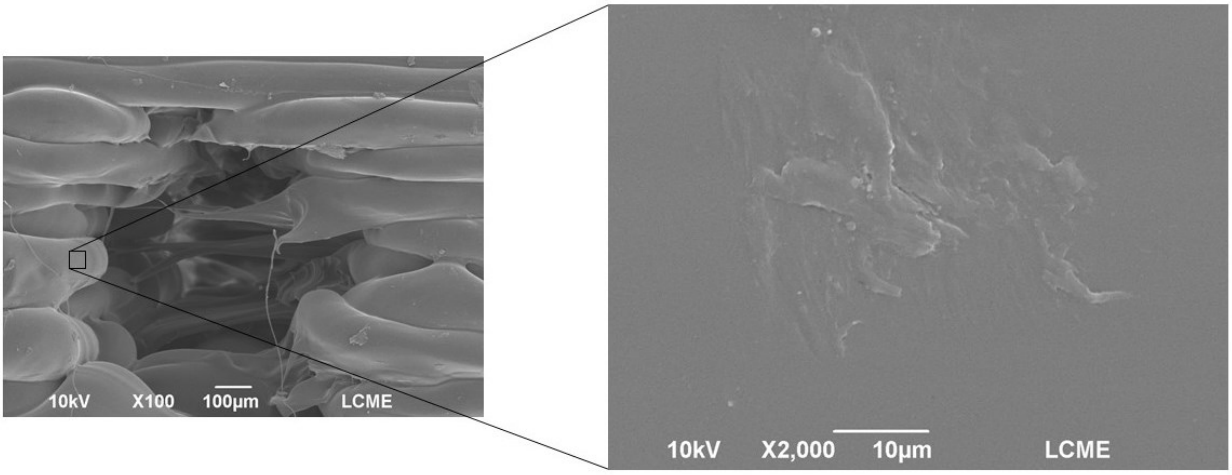

Source: Author.

Figure 25 - Micrographs obtained for the PLA scaffold after 336 h of accelerated weathering under 35 °C. Left: View of a pore of the specimen, 100x magnification. Right: Specimen's surface at 2000x magnification.

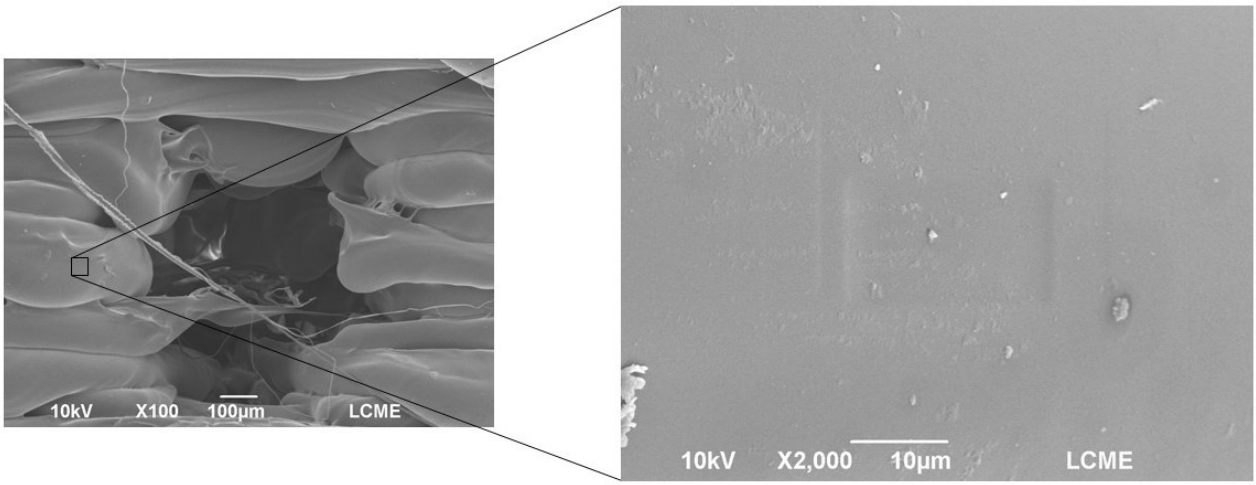

Source: Author.

Figure 26 - Micrographs obtained for the PLA scaffold after 336 h of accelerated weathering under 45 °C. Left: View of a pore of the specimen, 100x magnification. Right: Specimen's surface at 2000x magnification.

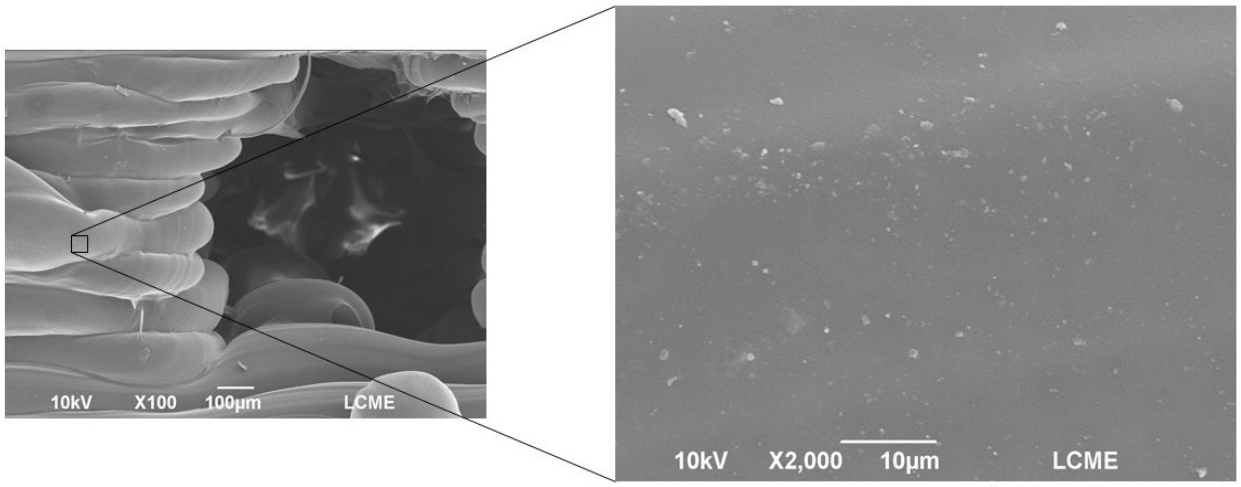

Source: Author.

Figure 27 - Micrographs obtained for the PLA scaffold after 336 h of accelerated weathering under temperature, UV radiation, and humidity control. Left: View of a pore of the specimen, 100x magnification. Right: Specimen's surface at 2000x magnification.

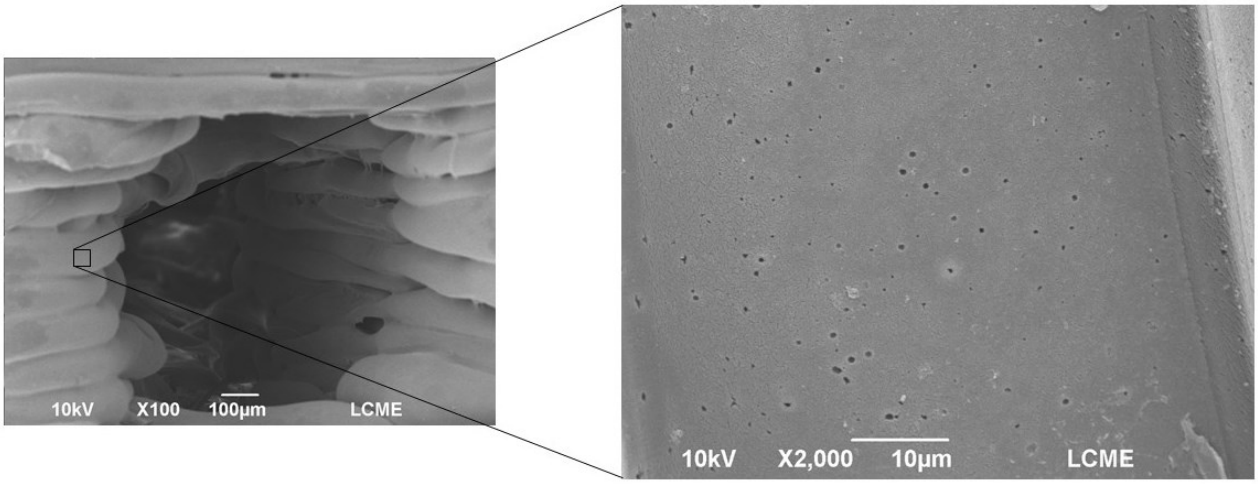

Source: Author.

Figure 28 - Micrographs obtained for the PLA scaffold after 336 h of accelerated weathering under temperature, UV radiation, and humidity control at 5000x magnification.

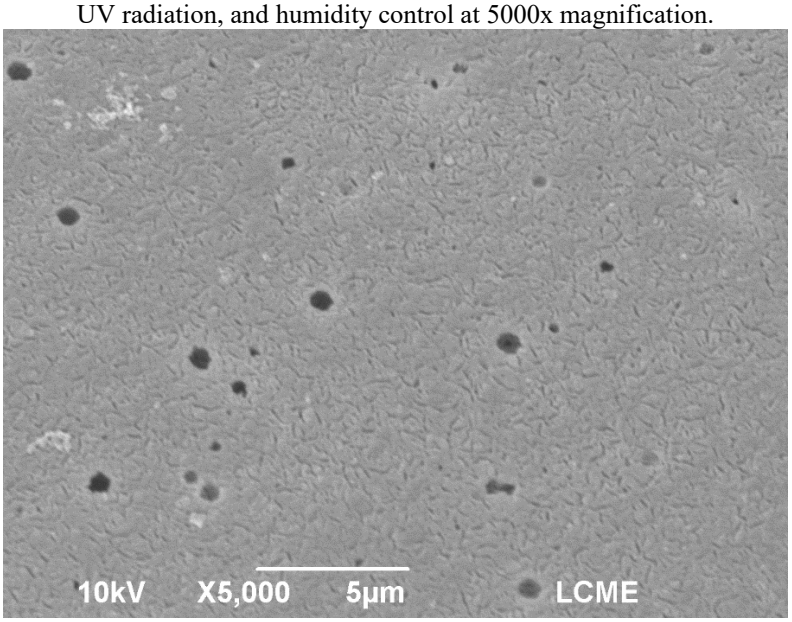

Source: Author.

Some studies reported that accelerated weathering of PLA specimens under controlled temperature, humidity, and UV-A radiation only gave the specimens' surface a rougher texture than the original condition (more homogeneous) when analyzed by scanning electron microscopy (ISADOUNENE et al., 2018; LIZÁRRAGA-LABORÍN et al., 2018). Islam, Pickering, and Foreman (2010) on the other hand, reported the appearance of surface cracks on pure PLA specimens subjected to ASTM G154 (2016) tests, using UV-A. Lin, Xie, and Qiu (2019), after performing tests with UV radiation and temperature application, have reported pores formation, similar to what was observed for the scaffold subjected to the T-H-R test in this work. Even though the specimens tested by Lin, Xie, and Qiu (2019) are composites (PLA and wood powder), the phenomenon has been associated with the polymeric matrix. According to the authors, heat and radiation effects lead PLA to degrade into its monomer, lactic acid, which is volatile and, therefore, caused the appearance of pores in the polymer’s structure.

5.9 SHELF LIFE PREDICTION[19]

5.9.1 Temperature Control

The time for failure for accelerated weathering under temperature control (at 45 °C) – determined through the results of the mechanical tests – was 456 h. Using Equation (18), a $F_{a(T)}$ of 9 was obtained, so that the shelf life would be 4104 hours, or 171 days – by multiplying the time for failure for 45 °C accelerated weathering and $F_{a(T)}$.

5.9.2 Temperature, Humidity, and Radiation Control

The time for failure for accelerated weathering under temperature, radiation, and humidity control, was 168 h. Using Equation (22), a $F_{a(T,H,R)}$ of 5.84 was obtained, so that the shelf life would be 918.12 hours, or approximately 38 days – by multiplying the time for failure for the T-H-R test and $F_{a(T,H,R)}$.

Therefore, the combined action of temperature, radiation, and humidity has a great impact on polymeric products, expressively triggering degradation mechanisms that lead to a decrease in physicochemical properties and, consequently, to a gradual loss of functionality. Therefore, the scaffold's functionality – in terms, in this case, of torque strength, by insertion of a metallic screw – may be considerably impaired in a relatively short exposure time.

[19] DOI: <https://doi.org/10.1016/j.mtcomm.2022.104140>.

6 CONCLUSIONS

Polymeric biomaterials are of great relevance in the market of implantable medical devices, such as those used in tissue engineering. PLA is an advantageous material because, besides being biocompatible and sustainable, it is a thermoplastic polymer and, therefore, suitable for additive manufacturing processes, such as FFF. Dental scaffolds consist of synthetic structures important for surgical procedures involving metallic implants to be inserted in patients whose bone quality is compromised and does not guarantee, by itself, the necessary stabilization for the osseointegration process.

The development of new healthcare devices raises the demand to characterize the time during which these products can be stored before their application, that is, their shelf life. This characterization is especially necessary for polymeric products, due to their inherent susceptibility to being affected by external environmental agents.

Different methodologies have been developed and employed for this purpose, and different methods of correlating accelerated weathering to natural weathering have been proposed. In the present work, two different normative methodologies have been selected to apply critical conditions that lead to accelerated weathering: under temperature control (according to the ABNT NBR 16469 (2020) and under temperature, relative humidity, and UV radiation control (according to ASTM G154 (2016).

It was observed that, under 35 °C accelerated weathering, the degradation only affected amorphous regions of the PLA scaffolds, with a gradual increase in the degree of crystallinity and the glass transition temperature. Under the most critical temperature, 45 °C, there was a stage in which degradation also started to affect crystalline regions of the polymer, with stages of growth and decay of the χc and the T_g, which was also corroborated by the non-identification of a peak of crystalline planes in XRD.

The results for accelerated weathering under temperature, relative humidity, and UV radiation (T-H-R) are in accordance with the higher criticality expected for this type of test. The no n-identification of the T_g peak was observed, as well as the rapid increase of χc (indicating the intense action of degradation on amorphous regions of the polymer), corroborated by XRD results, in which the characteristic crystalline plane peaks of PLA became more evident with a huge increase in intensity, along with the disappearance of the amorphous band.

PLA scaffolds maintained at 25 °C did not present significant changes in maximum torque strength, as expected for room temperature. Accelerated weathering at 35 °C caused a significant change in mechanical strength after 336 h. For accelerated weathering at 45 °C and for ASTM G154 accelerated weathering, a significant decrease in torque strength decreased occurred earlier: from 240 and 168 h forward, respectively – in accordance with the highest levels of the criticality of the tests. In the case of the ASTM G154 test, noticeable embrittlement to the touch and a matting effect of the specimens could also be observed. The decrease in mechanical resistance is consistent as a result of phenomena expected for weathered PLA specimens, mainly related to chain scission due to triggered thermal, hydrolytic, and photolytic degradation.

The FTIR analyses confirmed degradation was triggered by photolytic and hydrolytic mechanisms so that the reduction in the intensity of characteristic peaks could be observed in the spectra due to intensified chain scissions. The level of degradation presented a positive correlation with the criticality of the weathering tests, with greater intensity reductions for the T-H-R test, followed by the tests under 45 °C, and, finally, under 35 °C.

According to the viscosimetry results, the degradation rate of the PLA scaffolds also presented a positive correlation with the intensity of the weathering variables applied, being potentialized following the order of criticality of the tests (35 °C < 45 °C < T-H-R). Consequently, the most pronounced decay in molecular weight, at 336 h exposure, was also observed for the T-H-R test, followed by the T tests under 45 °C and 35 °C. These results can be explained by the intensification of phenomena like photolysis and hydrolysis when the temperature is increased and by the combined application of high temperature, humidity, and radiation.

Therefore, the viscosimetry and FTIR results are in accordance with the observed decrease in mechanical strength (with the same order of criticality) of the PLA scaffolds, since the rate of polymeric chain scission is associated with the rate of decay in mechanical properties.

In addition, the T tests did not cause the formation of noticeable defects on the surface of the PLA scaffolds, while the T-R-H test generated micropores and microcracks on the specimen, as a result of degradation of the polymer into volatile lactic acid monomers.

The time for functional failure associated with the test under temperature control was 456 h, which corresponded to a 171 days shelf life, in natural weathering. For the test under temperature, relative humidity, and UV radiation control, the time for functional failure was 168 h, which corresponded to a shelf life of 38 days (4.5 smaller than the shelf life obtained through the T test).

Therefore, relative humidity and UV radiation, combined with temperature application, present severe degradation effects on the stability of polymeric samples, such as the PLA scaffolds studied in this work, being critical variables for their functionality maintenance.

Considering the shelf life obtained by the weathering test under temperature control is an acceptable time for storage prior to use, it is defined that the PLA scaffolds must be stored and transported away from sunlight, in addition to maintaining the temperature and humidity conditions as commonly recommended for health care products: under 25 °C and up to 70%, respectively. Under these conditions, the product's shelf life can be defined as 150 days (five months) – thus establishing a safety margin regarding the period after manufacturing within which the product should be used.

7 SUGGESTIONS FOR FUTURE WORK

It is suggested to perform sterilization processes by applying gamma radiation (using Cobalt-60 as the radioisotope) in order to evaluate whether it has a significant influence on the mechanical strength and chemical properties of the PLA scaffolds. The mentioned method is reported in studies about PLA specimens produced by 3D printing, and 25 kGy is a typical dosage employed in Co-60 sterilization of medical devices and equipment (ALSABBAGH et al., 2021; GREMARE et al., 2018; WEST et al., 2019). Different sterilization dosages can be selected and the intensity to which the specimen properties are preserved can be assessed – by analyses such as Differential Scanning Calorimetry (DSC), Thermogravimetric Analysis (TGA), and Fourier Transform Infrared Spectroscopy (FTIR).

Another suggestion is to combine polymeric scaffolds with a ceramic biomaterial, aiming to optimize the ability to promote osseointegration – considering its potential use in tissue engineering – perform its physicochemical characterization, as well as conduct accelerated weathering tests and determine its shelf life. This demand comes from the relatively low cell adhesion and proliferation reported for scaffolds made entirely of polymers, such as PLA (GUO et al., 2012). Examples of manufacturing methods for composite scaffolds are the incorporation of a ceramic material into the polymeric filament and the subsequent printing of the specimen, or the coating of a finished polymeric structure with the ceramic material. Examples of ceramic biomaterials used for this purpose are hydroxyapatite, chitosan, and bioglass (MONDAL et al., 2020; NIAZA et al., 2016; ROETHER et al., 2002; WANG et al., 2018).

8 REFERENCES

ABNT NBR 16469 – **Implantes para cirurgia – Projeto de produto – Orientações para avaliação da vida útil em prateleira por envelhecimento acelerado**, Associação Brasileira de Normas Técnicas, Rio de Janeiro, 2020.

ALDEEN, N. A.; OWAID, B. Effect of ultraviolet and temperature on mechanical properties of three dimension printed materials. **AIP Conference Proceedings. AIP Publishing LLC**, p. 020184, 2020.

ALGARNI, M.; GHAZALI, S. Comparative study of the sensitivity of PLA, ABS, PEEK, and PETG's mechanical properties to FDM printing process parameters. **Crystals**, v. 11, n. 8, p. 995, 2021.

ALSABBAGH, A. et al. Effects of gamma irradiation on 3D-printed polylactic acid (PLA) and high-density polyethylene (HDPE). **Polymer Bulletin**, v. 78, n. 9, p. 4931-4945, 2021.

AMBONE, T.; TORRIS, A.; SHANMUGANATHAN, K. Enhancing the mechanical properties of 3D printed polylactic acid using nanocellulose. **Polymer Engineering & Science**, v. 60, n. 8, p. 1842-1855, 2020.

AOYAGI, Y.; YAMASHITA, K.; DOI, Y. Thermal degradation of poly [(R)-3-hydroxybutyrate], poly [ε-caprolactone], and poly [(S)-lactide]. **Polymer Degradation and Stability**, v. 76, n. 1, p. 53-59, 2002.

ARAQUE-MONRÓS, M. C. et al. Study of the degradation of a new PLA braided biomaterial in buffer phosphate saline, basic and acid media, intended for the regeneration of tendons and ligaments. **Polymer degradation and stability**, v. 98, n. 9, p. 1563-1570, 2013.

ASTM Standard D1435 – **Standard Practice for Outdoor Weathering of Construction Seals and Sealants**, PA, ASTM International, West Conshohocken, 2020.

ASTM Standard D2857 – **Standard Practice for Dilute Solution Viscosity of Polymers**, PA, ASTM International, West Conshohocken, 2016.

ASTM Standard D5272 – **Standard Practice for Outdoor Exposure Testing of Photodegradable Plastics**, PA, ASTM International, West Conshohocken, 2008.

ASTM Standard E490 – **Solar Constant and Zero Air Mass Solar Spectral Irradiance Tables**, PA, ASTM International, West Conshohocken, 2019.

ASTM Standard F1980 – **Standard Guide for Accelerated Aging of Sterile Barrier Systems for Medical Devices**, PA, ASTM International, West Conshohocken, 2016.

ASTM G7 – **Standard Practice for Atmospheric Environmental Exposure Testing of Nonmetallic Materials**, PA, ASTM International, West Conshohocken, 2013.

ASTM G24 – **Standard Practice for Conducting Exposures to Daylight Filtered Through Glass**, PA, ASTM International, West Conshohocken, 2013.

ASTM G90 – **Standard Practice for Performing Accelerated Outdoor Weathering of Nonmetallic Materials Using Concentrated Natural Sunlight**, PA, ASTM International, West Conshohocken, 2017.

ASTM G151 – **Standard Practice for Exposing Nonmetallic Materials in Accelerated Test Devices that Use Laboratory Light Sources**, PA, ASTM International, West Conshohocken, 2019.

ASTM G152 – **Standard Practice for Operating Enclosed Carbon Arc Light Apparatus for Exposure of Nonmetallic Materials**¸ PA, ASTM International, West Conshohocken, 2013.

ASTM G153 – **Standard Practice for Operating Enclosed Carbon Arc Light Apparatus for Exposure of Nonmetallic Materials**, PA, ASTM International, West Conshohocken, 2013.

ASTM G154 – **Standard Practice for Operating Fluorescent Ultraviolet (UV) Lamp Apparatus for Exposure of Nonmetallic Materials**, PA, ASTM International, West Conshohocken, 2016.

ASTM G155 – **Standard Practice for Operating Xenon Arc Light Apparatus for Exposure of Non-Metallic Materials**, PA, ASTM International, West Conshohocken, 2013.

ASTM G177 – **Standard Tables for Reference Solar Ultraviolet Spectral Distributions: Hemispherical on 37° Tilted Surface**, PA, ASTM International, West Conshohocken, 2020.

AUDOUIN, L. et al. "Close loop" mechanistic schemes for hydrocarbon polymer oxidation. **Journal of Polymer Science Part A: Polymer Chemistry**, v. 33, n. 6, p. 921–927, 1995.

BENIC, G. I.; MIR-MARI, J.; HÄMMERLE, C. H. F. Loading protocols for single-implant crowns: a systematic review and meta-analysis. **The International Journal of Oral & Maxillofacial Implants**, v. 29, n. Supplement, p. 222–238, 2014.

BHAGIA, S. et al. Critical review of FDM 3D printing of PLA biocomposites filled with biomass resources, characterization, biodegradability, upcycling and opportunities for biorefineries. **Applied Materials Today**, v. 24, p. 101078, 2021.

BLEICHER, L.; SASAKI, J. M. **Introdução à Difração de Raios-X em Cristais**. Fortaleza: Universidade Federal do Ceará, 2000.

BOAVENTURA, A. A. et al. Estudo físico-químico de poli(butadieno-co-undeceno) por viscosimetria. In: **Anais do 10º Congresso Brasileiro de Polímeros**, Foz do Iguaçu, PR, Brasil. 2009.

BOLIO-LOPEZ, G. I. et al. Weathering and biodegradation of polylactic acid composite reinforced with cellulosewhiskers. **Revista Mexicana De Ingeniería Química**, v. 12, n. 1, p. 143–153, 2013.

BRUNA, C. Q. DE M.; GRAZIANO, K. U. Temperatura e umidade no armazenamento de materiais autoclavados: revisão integrativa. **Revista da Escola de Enfermagem da USP**, v. 46, n. 5, p. 1215–1220, 2012.

CAI, Y. et al. Novel biodegradable three-dimensional macroporous scaffold using aligned electrospun nanofibrous yarns for bone tissue engineering. **The Scientific World Journal**, v. 100, n. 5, p. 1187–1194, 2012.

CAMINERO, M. Á. et al. Additive manufacturing of PLA-based composites using fused filament fabrication: effect of graphene nanoplatelet reinforcement on mechanical properties, dimensional accuracy and texture. **Polymers**, v. 11, n. 5, p. 799, 2019.

CANEVAROLO JR, Sebastião V. et al. **Técnicas de caracterização de polímeros**. São Paulo: Artliber, 2004.

CARLETTI, E. et al. Microfabrication of PDLLA scaffolds. **Journal of Tissue Engineering and Regenerative Medicine**, v. 5, n. 7, p. 569-577, 2011.

CHA, H.-S. et al. Frequency of bone graft in implant surgery. **Maxillofacial Plastic and Reconstructive Surgery**, v. 38, n. 1, p. 2–5, 2016.

CHANDRAHASA, S.; MURRAY, P. E.; NAMEROW, K. N. Proliferation of mature ex vivo human dental pulp using tissue engineering scaffolds. **Journal of Endodontics**, v. 37, n. 9, p. 1236–1239, 2011.

CHÁVEZ-MONTES, W. M. et al. Effect of artificial weathering on PLA/nanocomposite molecular weight distribution. **Polymers**, v. 7, n. 4, p. 760–776, 2015.

CHEN, S. et al. Fabrication and evaluation of 3D printed poly(L-lactide) scaffold functionalized with quercetin-polydopamine for bone tissue engineering. **ACS Biomaterials Science & Engineering**, v. 5, n. 5, p. 2506-2518, 2019.

CHOI, W. J. et al. Rapid development of dual porous poly(lactic acid) foam using fused deposition modeling (FDM) 3D printing for medical scaffold application. **Materials Science & Engineering C**, v. 110, p. 110693, 2020.

COPINET, A. et al. Effects of ultraviolet light (315 nm), temperature and relative humidity on the degradation of polylactic acid plastic films. **Chemosphere**, v. 55, n. 5, p. 763–773, 2004.

CROLL, S. G. Reciprocity in weathering exposure and the kinetics of property degradation. **Progress in Organic Coatings**, v. 127, p. 140-150, 2019.

DA SILVA, L. et al. Determinação de peso molecular e efeito polieletrolítico por viscosimetria. In: **Anais do 10º Congresso Brasileiro de Polímeros**, Foz do Iguaçu, PR, Brasil. 2009.

DE JONG, S. J. et al. New insights into the hydrolytic degradation of poly(lactic acid): Participation of the alcohol terminus. **Polymer**, v. 42, n. 7, p. 2795–2802, 2001.

EDWARDS, T. R. et al. Stripping torque as a predictor of successful internal fracture fixation. **ANZ Journal of Surgery**, v. 75, n. 12, p. 1096–1099, 2005.

EIRADO, S. R. A. **Análise da influência da esterilização por irradiação gama nas propriedades mecânicas do osso cortical bovino**. Bachelor's dissertation (Materials Engineering), Federal University of Santa Catarina, 2009.

ELSAWY, M. A. et al. Hydrolytic degradation of polylactic acid (PLA) and its composites. **Renewable and Sustainable Energy Reviews**, v. 79, p. 1346–1352, 2017.

FARAH, S.; ANDERSON, D. G.; LANGER, R. Physical and mechanical properties of PLA, and their functions in widespread applications - a comprehensive review. **Advanced Drug Delivery Reviews**, v. 107, p. 367–392, 2016.

FARRÉ-GUASCH, E. et al. Application of additive manufacturing in oral and maxillofacial surgery. **Journal of Oral and Maxillofacial Surgery**, v. 73, n. 12, p. 2408–2418, 2015.

FARSI, M.; ASEFNEJAD, A.; BAHARIFAR, H. A hyaluronic acid/PVA electrospun coating on 3D printed PLA scaffold for orthopedic application. **Progress in Biomaterials**, v. 11, n. 1, p. 67-77, 2022.

Shelf Life of Medical Devices, Food and Drug Administration, White Oak, MD, 1991. https://www.fda.gov/regulatory-information/search-fda-guidance-documents/shelf-life-medical-devices (accessed 02 June 2022).

GARLOTTA, D. A literature review of poly(lactic acid). **Journal of Polymers and the Environment**, v. 9, n. 2, p. 63–84, 2001.

GEBHARDT, M. et al. Cell survival within pulp and periodontal constructs. **Journal of Endodontics**, v. 35, n. 1, p. 63–66, 2009.

GENDVILIENE, I. et al. Effect of extracellular matrix and dental pulp stem cells on bone regeneration with 3D printed PLA/HA composite scaffolds. **European Cells and Materials**, v. 41, p. 204–215, 2021.

GONZÁLEZ-LÓPEZ, M. E. et al. Accelerated weathering of poly(lactic acid) and its biocomposites: a review. **Polymer Degradation and Stability**, v. 179, 2020.

GORDON, D. A. et al. Multivariate multiple regression models of poly(ethylene-terephthalate) film degradation under outdoor and multi-stressor accelerated weathering exposures. **PLoS ONE**, v. 13, n. 12, p. 1–30, 2018.

GOTTARDI, R. et al. Application of a Hyperelastic 3D Printed Scaffold for Mesenchymal Stem Cell-Based Fabrication of a Bizonal Tendon Enthesis-like Construct. **Frontiers in Materials**, v. 8, p. 613212, 2021.

GRASSI, G.; SPAGNOLO, S. L.; PAOLETTI, I. Fabrication and durability testing of a 3D printed façade for desert climates. **Additive Manufacturing**, v. 28, p. 439–444, 2019.

GREMARE, A. et al. Characterization of printed PLA scaffolds for bone tissue engineering. **Journal of Biomedical Materials Research Part**, v. 106, n. 4, p. 887–894, 2018.

GUO, C. et al. Novel fabrication method of porous poly(lactic acid) scaffold with hydroxyapatite coating. **Materials Letters**, v. 74, p. 197–199, 2012.

GUPTA, B.; REVAGADE, N.; HILBORN, J. Poly(lactic acid) fiber: an overview. **Progress in Polymer Science (Oxford)**, v. 32, n. 4, p. 455–482, 2007.

HO, K. L. G.; POMETTO, A. L.; HINZ, P. N. Effects of temperature and relative humidity on polylactic acid plastic degradation. **Journal of Environmental Polymer Degradation**, v. 7, n. 2, p. 83–92, 1999.

HU, J. et al. Porous nanofibrous PLLA scaffolds for vascular tissue engineering. **Biomaterials**, v. 31, n. 31, p. 7971–7977, 2011.

HUKINS, D. W. L.; MAHOMED, A.; KUKUREKA, S. N. Accelerated aging for testing polymeric biomaterials and medical devices. **Medical Engineering and Physics**, v. 30, n. 10, p. 1270–1274, 2008.

HULME, A.; COOPER, J. Life prediction of polymers for industry. **Sealing Technology**, v. 2012, n. 9, p. 8–12, 2012.

HUTMACHER, D. W. et al. Mechanical properties and cell cultural response of polycaprolactone scaffolds designed and fabricated via fused deposition modeling. **Journal of Biomedical Materials Research**, v. 55, n. 2, p. 203–216, 2001.

ISHIKAWA, D. et al. High-speed monitoring of the crystallinity change in poly(lactic acid) during photodegradation by using a newly developed wide area NIR imaging system (Compovision). **Analytical and bioanalytical chemistry**, v. 407, n. 2, p. 397-403, 2015.

IKADA, E. Photo- and bio-degradable polyesters. photodegradation behaviors of aliphatic polyesters. **Journal of Photopolymer Science and Technology**, v. 10, n. 2, p. 265–270, 1997.

Ingeo Biopolymer 3D850 Technical Data Sheet 3D Printing Monofilament – High Heat Grade; MSDS No. NW3D850_090716V1; NatureWorks: Minnetonka, MN. https://www.natureworksllc.com/~/media/Files/NatureWorks/Technical-Documents/Technical-Data-Sheets/TechnicalDataSheet_3D850_monofilament_pdf.pdf?la=en (accessed 02 June 2022).

INUI, A. et al. Potency of double-layered poly l-lactic acid scaffold in tissue engineering of tendon tissue. **International Orthopaedics**, v. 34, n. 8, p. 1327–1332, 2010.

ISADOUNENE, S. et al. Accelerated ageing of alkali treated olive husk flour reinforced polylactic acid (pla) biocomposites: physico-mechanical properties. **Polymers and Polymer Composites**, v. 26, n. 3, p. 223–232, 2018.

ISLAM, M. S.; PICKERING, K. L.; FOREMAN, N. J. Influence of accelerated ageing on the physico-mechanical properties of alkali-treated industrial hemp fibre reinforced poly(lactic acid) (PLA) composites. **Polymer Degradation and Stability**, v. 95, n. 1, p. 59–65, 2010.

ISO 4892-1 – **Plastics – Methods of exposure to laboratory light sources – Part 1: General guidance**, International Organization for Standardization, Vernier, GVA, 2016.

ISO TS 13498 – **Dentistry – Torsion test of implant body/connecting part joints of endosseous dental implant systems**, International Organization for Standardization, Vernier, GVA, 2011.

JACQUES, L. F. E. Accelerated and outdoor/natural exposure testing of coatings. **Progress in Polymer Science (Oxford)**, v. 25, n. 9, p. 1337–1362, 2000.

JANORKAR, A. V.; METTERS, A. T.; HIRT, D. E. Degradation of poly(l-lactide) films under ultraviolet - induced photografting and sterilization conditions. **Journal of Applied Polymer Science**, v. 106, n. 2, p. 1042–1047, 2007.

JAZAYERI, H. E. et al. Polymeric scaffolds for dental pulp tissue engineering: a review. **Dental Materials**, v. 36, n. 2, p. e47–e58, 2020.

JEON, H. J.; KIM, M. N. Biodegradation of poly(l-lactide) (PLA) exposed to UV irradiation by a mesophilic bacterium. **International Biodeterioration and Biodegradation**, v. 85, p. 289–293, 2013.

JEONG, H. J. et al. Fabrication of three-dimensional composite scaffold for simultaneous alveolar bone regeneration in dental implant installation. **International Journal of Molecular Sciences**, v. 21, n. 5, 2020.

JIANG, Xiping et al. 3D printing of multilayered scaffolds for rotator cuff tendon regeneration. **Bioactive materials**, v. 5, n. 3, p. 636-643, 2020.

JU, Y. M. et al. Beneficial effect of hydrophilized porous polymer scaffolds in tissue-engineered cartilage formation. **Wiley Periodicals, Inc.**, v. 85, n. 1, p. 252-260, 2008.

KACZMAREK, H. et al. Crosslinked blends of poly(lactic acid) and polyacrylates: AFM, DSC and XRD studies. **Journal of Polymer Research**, v. 20, n. 3, p. 1-12, 2013.

KARBASIAN, M. et al. Therapy with new generation of biodegradable and bioconjugate 3D printed artificial gastrointestinal lumen. **Iranian Journal of Basic Medical Sciences**, v. 24, n. 3, p. 391, 2021.

KAYNAK, C.; SARI, B. Accelerated weathering performance of polylactide and its montmorillonite nanocomposite. **Applied Clay Science**, v. 121–122, p. 86–94, 2016.

KIM, B. S.; MOONEY, D. J. Development of biocompatible synthetic extracellular matrices for tissue engineering. **Trends in Biotechnology**, v. 16, n. 5, p. 224–230, 1998.

KOCKOTT, D. Natural and artificial weathering of polymers. **Polymer Degradation and Stability**, v. 25, n. 2–4, p. 181–208, 1989.

KOPINKE, F. D. et al. Thermal decomposition of biodegradable polyesters - II. poly(lactic acid). **Polymer Degradation and Stability**, v. 53, n. 3, p. 329–342, 1996.

LANGER, R.; VACANTI, J. P. Tissue engineering. **Science**, v. 260, p. 920, 1993.

LEE, L. C.; LIONG, C.-Y.; JEMAIN, A. A. A contemporary review on Data Preprocessing (DP) practice strategy in ATR-FTIR spectrum. **Chemometrics and Intelligent Laboratory Systems**, v. 163, p. 64-75, 2017.

LEVI, B. et al. Stem cells: update and impact on craniofacial surgery. **Journal of Craniofacial Surgery**, v. 23, n. 1, p. 319–322, 2012.

LI, G. et al. Electrospun fibers for dental and craniofacial applications. **Current Stem Cell Research & Therapy**, v. 9, n. 3, p. 187–195, 2014.

LI, J. et al. Computer-aided design and manufacturing and rapid prototyped nanoscale hydroxyapatite/polyamide (n-HA/PA) construction for condylar defect caused by mandibular angle ostectomy. **Aesthetic Plastic Surgery**, v. 35, n. 4, p. 636–640, 2011.

LILA, M. K. et al. Accelerated thermal ageing behaviour of bagasse fibers reinforced poly(lactic acid) based biocomposites. **Composites Part B: Engineering**, v. 156, p. 121–127, 2019.

LIM, K.; CHOW, W. S.; PUNG, S. Y. Accelerated weathering and UV protection-ability of poly(lactic acid) nanocomposites containing zinc oxide treated halloysite nanotube. **Journal of Polymers and the Environment**, v. 27, n. 8, p. 1746–1759, 2019.

LIN, W.; XIE, G.; QIU, Z. Effects of ultraviolet aging on properties of wood flour-poly(lactic acid) 3D printing filaments. **BioResources**, v. 14, n. 4, p. 8689–8700, 2019.

LIU, F. et al. Poly(l-lactide-co-caprolactone)/tussah silk fibroin nanofiber vascular scaffolds with small diameter fabricated by core-spun electrospinning technology. **Journal of Materials Science**, v. 55, n. 16, p. 7106-7119, 2020.

LIZÁRRAGA-LABORÍN, L. L. et al. Accelerated weathering study of extruded polyethylene/poly(lactic acid)/chitosan films. **Polymer Degradation and Stability**, v. 155, p. 43–51, 2018.

L. Lu, A.G. Mikos, Poly(lactic acid), in: **Polymer Data Handbook**, Oxford University Press, New York, p. 627-633, 1999.

LUNT, J. Large-scale production, properties and commercial applications of poly lactic acid polymers. **Polymer Degradation and Stability**, v. 59, n. 1–3, p. 145–152, 1998.

LV, S. et al. Effect of glycerol introduced into PLA based composites on the UV weathering behavior. **Construction and Building Materials**, v. 144, p. 525–531, 2017.

LV, S. et al. Enhanced durability of sustainable poly(lactic acid)-based composites with renewable starch and wood flour. **Journal of Cleaner Production**, v. 203, p. 328–339, 2018.

LV, Y. et al. Outdoor and accelerated laboratory weathering of polypropylene: a comparison and correlation study. **Polymer Degradation and Stability**, v. 112, p. 145–159, 2015.

MALISKA, A. M. **Microscopia Eletrônica de Varredura e Microanálise**. Florianópolis: Universidade Federal de Santa Catarina, 2018.

MAN, C. et al. Poly(lactic acid)/titanium dioxide composites: preparation and performance under ultraviolet irradiation. **Polymer Degradation and Stability**, v. 97, n. 6, p. 856–862, 2012.

MARTÍN DEL CAMPO, A. S. et al. Accelerated weathering of polylactic acid/agave fiber biocomposites and the effect of fiber–matrix adhesion. **Journal of Polymers and the Environment**, v. 29, n. 3, p. 937–947, 2020.

MELEK, L. N. Tissue engineering in oral and maxillofacial reconstruction. **Tanta Dental Journal**, v. 12, n. 3, p. 211–223, 2015.

MICHEL, A. T.; BILLINGTON, S. L. Characterization of poly-hydroxybutyrate films and hemp fiber reinforced composites exposed to accelerated weathering. **Polymer Degradation and Stability**, v. 97, n. 6, p. 870–878, 2012.

MOEEN, F. et al. Effect of variations in buccal bone thickness, implant diameter and thread pitch on stress distributions upon implant placements at high insertion torques: a three-dimensional finite element analysis. **Pakistan Oral & Dental Journal**, v. 34, n. 2, 2014.

MOHANDESNEZHAD, S. et al. In vitro evaluation of zeolite-nHA blended PCL/PLA nanofibers for dental tissue engineering. **Materials Chemistry and Physics**, v. 252, p. 123152, 2020.

MONDAL, S. et al. Hydroxyapatite nano bioceramics optimized 3D printed poly lactic acid scaffold for bone tissue engineering application. **Ceramics International**, v. 46, n. 3, p. 3443–3455, 2020.

MUELLER, A. A. et al. Missing facial parts computed by a morphable model and transferred directly to a polyamide laser-sintered prosthesis: an innovation study. **British Journal of Oral and Maxillofacial Surgery**, v. 49, n. 8, p. e67–e71, 2011.

NGO, T. D. et al. Additive manufacturing (3D printing): a review of materials, methods, applications and challenges. **Composites Part B: Engineering**, v. 143, p. 172–196, 2018.

NIAZA, K. V et al. 3D-printed scaffolds based on PLA/HA nanocomposites for trabecular bone reconstruction. **Journal of Physics: Conference Series**, v. 741, n. 1, p. 012068, 2016.

O'BRIEN, F. J. Biomaterials & scaffolds for tissue engineering. **Materials Today**, v. 14, n. 3, p. 88–95, 2011.

PATNAIK, S.; PANDA, A. K.; KUMAR, S. Thermal degradation of corn starch based biodegradable plastic plates and determination of kinetic parameters by isoconversional methods using thermogravimetric analyzer. **Journal of the Energy Institute**, v. 93, n. 4, p. 1449-1459, 2020.

PAWAR, R. P. et al. Biomedical applications of poly(lactic acid). **Recent Patents on Regenerative Medicine**, v. 4, n. 1, p. 40–51, 2014.

PEREGO, G.; CELLA, G. D.; BASTIOLI, C. Effect of molecular weight and crystallinity on poly(lactic acid) mechanical properties. **Journal of Applied Polymer Science**, v. 59, n. 1, p. 37-43, 1996.

PICKETT, J. E.; GIBSON, D. A.; GARDNER, M. M. Effects of irradiation conditions on the weathering of engineering thermoplastics. **Polymer Degradation and Stability**, v. 93, n. 8, p. 1597–1606, 2008.

PICKETT, J. E.; COYLE, D. J. Hydrolysis kinetics of condensation polymers under humidity aging conditions. **Polymer Degradation and Stability**, v. 98, n. 7, p. 1311–1320, 2013.

PICKETT, J. E. Weathering of plastics, in: **Handbook of Environmental Degradation Of Materials**, Schenectady: Elsevier Inc., New York, p. 163–184, 2018.

PICKETT, J. E. et al. Accelerated weathering parameters for some aromatic engineering thermoplastics. **Polymer degradation and stability**, v. 166, p. 135-144, 2019.

PICKETT, J. E. Introduction to polymer weathering, stabilization, and testing, in: **Service Life Prediction of Polymers and Coatings**, Schenectady: William Andrew Publishing, New York, p. 1–18, 2020.

PILLA, S. et al. Polylactide-pine wood flour composites. **Polymer Engineering & Science**, v. 48, n. 3, p. 578-587, 2008.

POSPÍŠIL, J. et al. Factors affecting accelerated testing of polymer photostability. **Polymer Degradation and Stability**, v. 91, n. 3, p. 417–422, 2006.

PRAPRUDDIVONGS, C.; SOMBATSOMPOP, N. Roles and evidence of wood flour as an antibacterial promoter for triclosan-filled poly(lactic acid). **Composites Part B: Engineering**, v. 43, n. 7, p. 2730–2737, 2012.

PUTNAM, A. J.; MOONEY, D. J. Tissue engineering using synthetic extrcellular matrices. **Nature Medicine**, v. 2, n. 7, p. 824–826, 1996.

RASSELET, D. et al. Oxidative degradation of polylactide (PLA) and its effects on physical and mechanical properties. **European Polymer Journal**, v. 50, n. 1, p. 109–116, 2014.

REN, T. et al. The bone formation in vitro and mandibular defect repair using PLGA porous scaffolds. **Journal of Biomedical Materials Research - Part A**, v. 74, n. 4, p. 562–569, 2005.

Resolução de Diretoria Colegiada – RDC/ANVISA nº 56, de 6 de abril de 2001. http://antigo.anvisa.gov.br/legislacao#/ (accessed 08 March 2022).

ROETHER, J. A. et al. Development and in vitro characterisation of novel bioresorbable and bioactive composite materials based on polylactide foams and bioglasss for tissue engineering applications. **Biomaterials**, v. 23, n. 18, p. 3871–3878, 2002.

ROSENZWEIG, D. H. et al. 3D-Printed ABS and PLA scaffolds for cartilage and nucleus pulposus tissue regeneration. **International Journal of Molecular Sciences**, p. 15118–15135, 2015.

SAIJO, H. et al. Maxillofacial reconstruction using custom-made artificial bones fabricated by inkjet printing technology. **Journal of Artificial Organs**, v. 12, n. 3, p. 200–205, 2009.

SALGADO, A. J.; COUTINHO, O. P.; REIS, R. L. Bone tissue engineering: State of the art and future trends. **Macromolecular Bioscience**, v. 4, n. 8, p. 743–765, 2004.

SAHMANI, S. et al. Calcium phosphate-PLA scaffolds fabricated by fused deposition modeling technique for bone tissue applications: fabrication, characterization and simulation. **Ceramics International**, v. 46, n. 2, p. 2447-2456, 2020.

SÁNDOR, G. K. et al. Adipose stem cell tissue-engineered construct used to treat large anterior mandibular defect: a case report and review of the clinical application of good manufacturing practice-level adipose stem cells for bone regeneration. **Journal of Oral and Maxillofacial Surgery**, v. 71, n. 5, p. 938–950, 2013.

SANTONJA-BLASCO, L.; RIBES-GREUS, A.; ALAMO, R. G. Comparative thermal, biological and photodegradation kinetics of polylactide and effect on crystallization rates. **Polymer Degradation and Stability**, v. 98, n. 3, p. 771–784, 2013.

SANTOS, R. M. et al. Outdoor and accelerated weathering of acrylonitrile-butadiene-styrene: a correlation study. **Polymer Degradation and Stability**, v. 98, n. 10, p. 2111–2115, 2013.

SAVIOLI LOPES, M.; JARDINI, A. L.; MACIEL FILHO, R. Poly(lactic acid) production for tissue engineering applications. **Procedia Engineering**, v. 42, p. 1402–1413, 2012.

SAWPAN, M. A. et al. Effect of accelerated weathering on physico-mechanical properties of polylactide bio-composites. **Journal of Polymers and the Environment**, v. 27, n. 5, p. 942–955, 2019.

SCHOFER, M. D. et al. Influence of poly(l-lactic acid) nanofibers and bmp-2 – containing poly(l-lactic acid) nanofibers on growth and osteogenic differentiation of human mesenchymal stem cells. **The Scientific World Journal**, v. 8, p. 1269–1279, 2008.

SHARIF, F. et al. Bioresorbable antibacterial PCL-PLA-nHA composite membranes for oral and maxillofacial defects. **Polymer Composites**, v. 40, n. 4, p. 1564–1575, 2019.

SHARMA, S. K.; MUDHOO, A. **A handbook of applied biopolymer technology: synthesis, degradation and applications**. Royal society of chemistry, London, 2011.

SHIM, I. K. et al. Novel three-dimensional scaffolds of poly(L -lactic acid) microfibers using electrospinning and mechanical expansion: fabrication and bone regeneration. **Journal of Biomedical Materials Research B: Applied Biomaterials**, p. 150–160, 2010.

SIAKENG, R. et al. Accelerated weathering and soil burial effect on biodegradability, colour and textureof coir/pineapple leaf fibres/PLA biocomposites. **Polymers**, v. 12, n. 2, 2020.

SILVESTRINI, R. **Síntese e caracterização de poli(ácido lático) (PLA) via micro-ondas**. Master's thesis – Universidade Federal do Rio Grande do Sul. Porto Alegre, p. 94. 2020.

SINGHVI, M. S.; ZINJARDE, S. S.; GOKHALE, D. V. Polylactic acid: synthesis and biomedical applications. **Journal of Applied Microbiology**, v. 127, n. 6, p. 1612–1626, 2019.

STARES, S. L. **Usinagem de parafusos implantáveis de P(L/DL)LA autorreforçados**, PhD thesis, Universidade Federal de Santa Catarina, 2010.

THOMAS M. SCHMITT. Methods for polymer molecular weight measurement, in: G. G. Sward (Ed.) **Paint and coating testing manual**, ASTM International, West Conshohocken, 2012, pp. 908–913.

TRISI, P. et al. Implant micromotion is related to peak insertion torque and bone density. **Clinical Oral Implants Research**, v. 20, n. 5, p. 467–471, 2009.

TSUJI, H.; KIDOKORO, Y.; MOCHIZUKI, M. Enzymatic degradation of poly(l-lactic acid) fibers: effects of small drawing hideto. **Journal of Applied Polymer Science**, v. 103, p. 2064–2071, 2007.

ULERY, B. D.; NAIR, L. S.; LAURENCIN, C. T. Biomedical applications of biodegradable polymers. **Journal of Polymer Science Part B: Polymer Physics**, p. 832–864, 2011.

VAEZI, M.; YANG, S. Extrusion-based additive manufacturing of PEEK for biomedical applications. **Virtual and Physical Prototyping**, v. 10, n. 3, p. 123–135, 2015.

VARSAVAS, S. D.; KAYNAK, C. Weathering degradation performance of PLA and its glass fiber reinforced composite. **Materials Today Communications**, v. 15, p. 344–353, 2017.

VERRASTRO NETO, A. et al. The impact of different torques for the insertion of immediately loaded implants on the peri-implant levels of angiogenesis- and bone-related markers. **International Journal of Oral and Maxillofacial Surgery**, v. 47, n. 5, p. 651–657, 2018.

VISSCHER, D. O. et al. Cartilage tissue engineering: preventing tissue scaffold contraction using a 3D-printed polymeric cage. **Tissue Engineering - Part C: Methods**, v. 22, n. 6, p. 573–584, 2016.

WACHSEN, O.; PLATKOWSKI, K.; REICHERT, K. H. Thermal degradation of poly-l -lactide -studies on kinetics, modelling and melt stabilisation. **Polymer Degradation and Stability**, v. 57, n. 1, p. 87–94, 1997.

WANG, J. et al. The odontogenic differentiation of human dental pulp stem cells on nanofibrous poly(l-lactic acid) scaffolds in vitro and in vivo. **Acta Biomaterialia**, v. 6, n. 10, p. 3856–3863, 2010.

WANG, X. et al. 3D printing of polymer matrix composites: a review and prospective. **Composites Part B: Engineering**, v. 110, p. 442–458, 2017.

WANG, J. et al. Surface entrapment of chitosan on 3D printed polylactic acid scaffold and its biomimetic growth of hydroxyapatite. **Composite Interfaces**, v. 26, n. 5, p. 465–478, 2018.

WANG, W. et al. Photo-oxidative resistance and adjustable degradation of poly-lactic acid (PLA) obtained by biomass addition and interfacial construction. **Polymer Degradation and Stability**, v. 194, p. 109762, 2021.

WEIR, N. A. et al. Degradation of poly-L-lactide. Part 2: Increased temperature accelerated degradation. **Proceedings of the Institution of Mechanical Engineers, Part H: Journal of Engineering in Medicine**, v. 218, n. 5, p. 321–330, 2004.

WEST, C. et al. Effects of gamma irradiation upon the mechanical and chemical properties of 3D-printed samples of poly lactic acid. **Journal of Manufacturing Science and Engineering**, v. 141, n. 4, 2019.

WHITE, J. R.; TURNBULL, A. Weathering of polymers: mechanisms of degradation and stabilization, testing strategies and modelling. **Journal of Materials Science**, v. 29, n. 3, p. 584–613, 1994.

XU, H. et al. Rapid prototyped PGA/PLA scaffolds in the reconstruction of mandibular condyle bone defects. **International Journal of Medical Robotics and Computer Assisted Surgery**, v. 6, n. 1, p. 66-72, 2010.

YANG, F. et al. Fabrication of nano-structured porous PLLA scaffold intended for nerve tissue engineering. **Biomaterials**, v. 25, n. 10, p. 1891–1900, 2004.

YANG, F. et al. Electrospinning of nano/micro scale poly(l-lactic acid) aligned fibers and their potential in neural tissue engineering. **Biomaterials**, v. 26, n. 15, p. 2603–2610, 2005.

YANG, X.; DING, X. Prediction of outdoor weathering performance of polypropylene filaments by accelerated weathering tests. **Geotextiles and Geomembranes**, v. 24, n. 2, p. 103–109, 2006.

YANG, Y. et al. Additive manufacturing of bone scaffolds. **International Journal of Bioprinting**, v. 5, n. 1, p. 1–25, 2019.

YATIGALA, N. S.; BAJWA, D. S.; BAJWA, S. G. Compatibilization improves performance of biodegradable biopolymer composites without affecting UV weathering characteristics. **Journal of Polymers and the Environment**, v. 26, n. 11, p. 4188–4200, 2018.

YEN, H. J. et al. Evaluation of chondrocyte growth in the highly porous scaffolds made by fused deposition manufacturing (FDM) filled with type II collagen. **Biomedical Microdevices**, v. 11, n. 3, p. 615–624, 2009.

YEW, G. H. et al. Natural weathering of poly(lactic acid): effects of rice starch and epoxidized natural rubber. **Journal of Elastomers and Plastics**, v. 41, n. 4, p. 369–382, 2009.

YUAN, X.; MAK, A. F. T.; YAO, K. Comparative observation of accelerated degradation of poly(L-lactic acid) fibres in phosphate buffered saline and a dilute alkaline solution. **Polymer Degradation and Stability**, v. 75, n. 1, p. 45–53, 2002.

ZAIDI, L. et al. Effect of natural weather on the structure and properties of polylactide/Cloisite 30B nanocomposites. **Polymer Degradation and Stability**, v. 95, n. 9, p. 1751–1758, 2010.

APPENDIX A - 3D Printing Parameters

Table 17 - Simplify 3D software parameters used to 3D print the PLA scaffolds.

(continue)

EXTRUSER		
Overview		
Noozle Diameter		0.30 mm
Extrusion Multiplier		1,00
Extrusion Width		Automatic
Ooze Control		
Retraction Distance		3,00 mm
Extra Restart Distance		0.00 mm
Retraction Vertical Lift		0.00 mm
Retraction Speed		60.00 mm/s
LAYER		
Layer Configurations		
Primary Layer Height		0.10 mm
Top Solid Layers		0
Bottom Solid Layers		0
Outline/Perimeter Shells		1
Outline Direction		From the inside out
First Layer Configurations		
First Layer Heigth		100%
First Layer Width		110%
Firt Layer Speed		20%
Start Points		Optimize start points for faster printing
ADDITION		
Skirt/Brim		
Skirt Layers		2
Skirt Offset from Part		0.00 mm
Skirt Outlines		6
INFILL		
General		
Internal Fill Pattern		Rectilinear
External Fill Pattern		Concentric
Interior Fill Percentage	(Porous Outer Part) (Solid Inner Part)	20% 100%
Outline Overlap		50%
Infill Extrusion Width		80%
Minimum Infill Length		0,00 mm
Print Sparse Infill Every		1
Internal Infill Angle Offsets		45 °/-45 °
External Infill Angle Offsets		45 °/-45 °

Table 17 - Simplify 3D software parameters used to 3D print the M20_45 specimens.

(conclusion)

TEMPERATURE	
Overview	
Temperature Controller Type	Extruder
Wait for temperature controller to stabilize before beginning build	Yes
Per Layer Temperature Setpoints	
Layer 1	205 °C
Layer 2	200 °C
COOLING	
Per Layer Fan Speed	
Layer 1	0%
Layer 2	100%
Speed Overrides	
Adjust printing speed for layers below	15.00 seconds
Allow speed reductions down to	20%
Fan Overrides	
Increase fan speed for layers below	8.00 seconds
Maximum cooling fan speed	100%

Source: Author.

APPENDIX B – T-H-R Test Report

INSTITUTO SENAI DE TECNOLOGIA CERÂMICA

Relatório de Ensaio Nº: 32680.2021.B- V.0

01. Dados Contratação:

Solicitante:

Razão Social:	Dachamir Hotza/CNPq
Endereço:	Universidade Federal de Santa Catarina - Depto. Eng. Química UFSC Trindade - Florionópolis/SC **CEP**: 88040900
Proposta Comercial:	1126.2021.V0
Contato:	Dachamir Hotza **E-mail:** dhotza@gmail.com

02. Dados da Amostra fornecida pelo Cliente:

Identificação da Amostra:	6 cilindros		
Informações Adicionais:	PRL: Dachamir Hotza		
Matriz e Origem Amostra:	Polímero-CRIC - Polímero		
Data de Coleta:	04/05/2021 07:11:00	**Data de Recebimento:**	04/05/2021 08:15:00
Data de Início dos Ensaios:	11/05/2021 11:13:17	**Data Conclusão dos Ensaios:**	18/06/2021 11:31:02
Lote: ND	**Quantidade por Amostras:**		5peças

03. Resultados:

Ensaio		Un
Determinação da resistência ao intemperismo acelerado UV-A e UV-B/ Ensaio baseado na norma NBR 9512:1986 e ASTM G154-9 - Data Conclusão: 18/06/2021		
	Resultado	
Avaliação 1- Ciclos	2	
Avaliação 1- Observação	Sem alterações.	-
Avaliação 2- Ciclos	8	
Avaliação 2- Observação	Sem alterações.	-
Avaliação 3- Ciclos	14	
Avaliação 3- Observação	Amarelamento.	-
Avaliação 4- Ciclos	20	
Avaliação 4- Observação	Amarelamento.	-
Avaliação 5- Ciclos	28	
Avaliação 5- Observação	Amarelamento.	-

Local da Realização dos Ensaios: Instalação permanente do LDCM

1. Cláusula de Responsabilidade

".

Os resultados tem significação restrita, aplicando-se tão somente à amostra ensaiada. / Não se admite qualquer responsabilidade referente à exatidão da amostragem e identificação da amostra a menos que esta tenha sido efetuada mediante supervisão do LDCM. Salvo menção expressa, as amostras foram selecionadas pelo solicitante /A reprodução deste relatório só será autorizada na forma de uma reprodução integral.

.. O LDCM não se torna responsável pelo uso que o solicitante, outra pessoa ou entidade venham a dar aos dados ou indicações contidos no presente relatório, em prejuízo ou benefício das marcas comerciais que o solicitante tenha podido citar como identificação das amostras submetidas ao estudo. / O cliente possui um prazo máximo de 45 dias, a partir da data de emissão do relatório, para contestar informações contidas neste. Somente será aceita a contestação de resultados se a quantidade da amostra entregue respeitar a quantidade mínima para cada ensaio. Após este período,caso a empresa não retirar a amostra será descartada pelo LDCM. Na declaração de conformidade não é considerada a incerteza de medição.

APPENDIX C – DSC Curves

Figure 29 - DSC curves obtained for samples subjected to accelerated weathering under 35 °C (first batch).

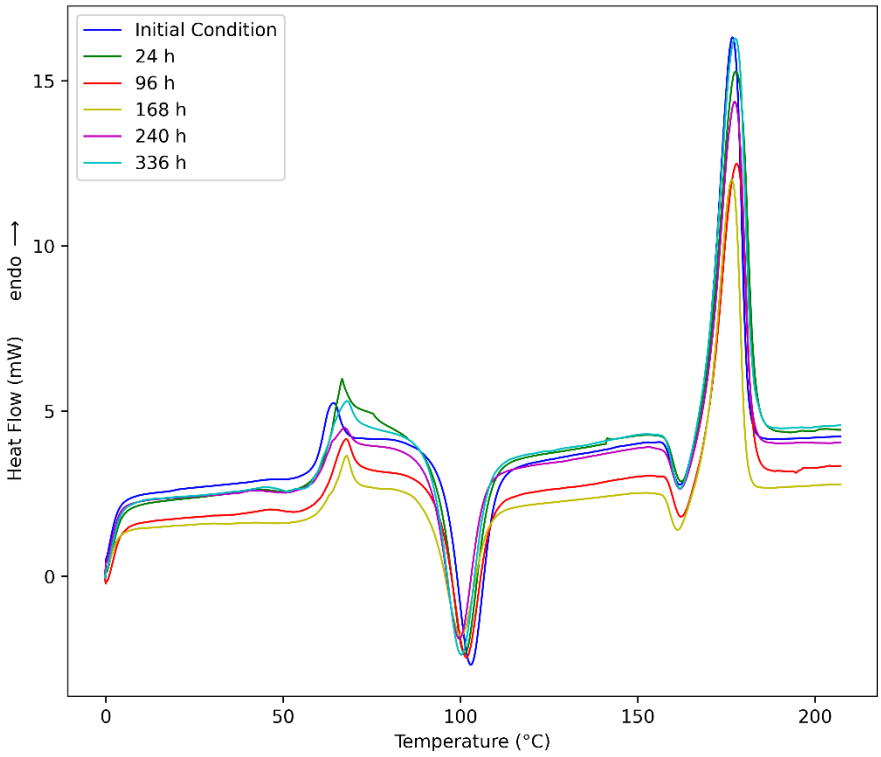

Source: Author.

Figure 30 - DSC curves obtained for samples subjected to accelerated weathering under 35 °C (second batch).

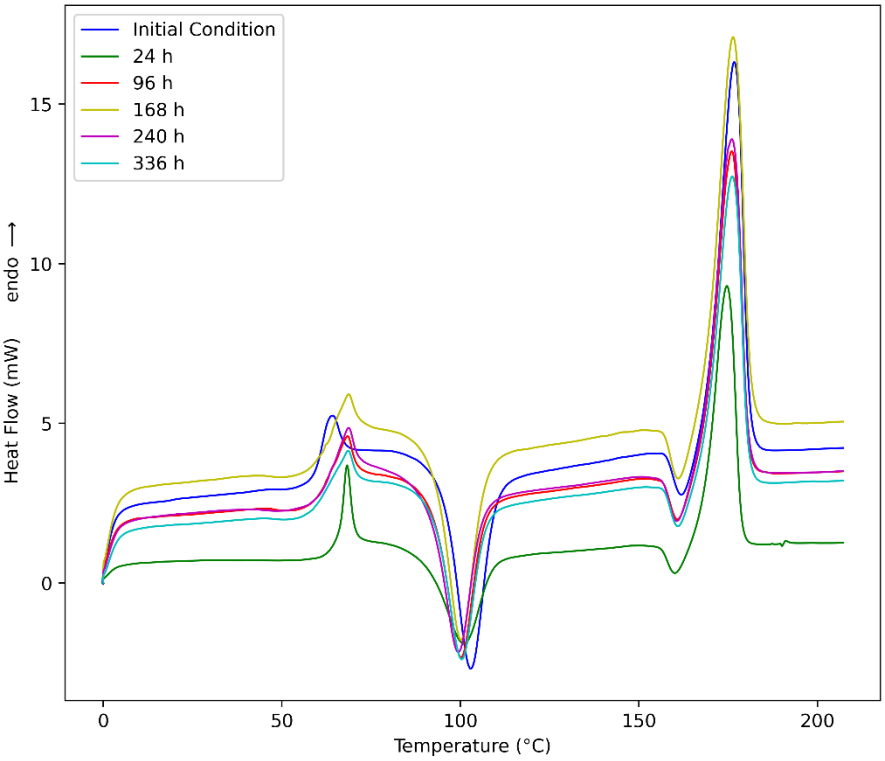

Source: Author.

Figure 31 - DSC curves obtained for samples subjected to accelerated weathering under 45 °C (first batch).

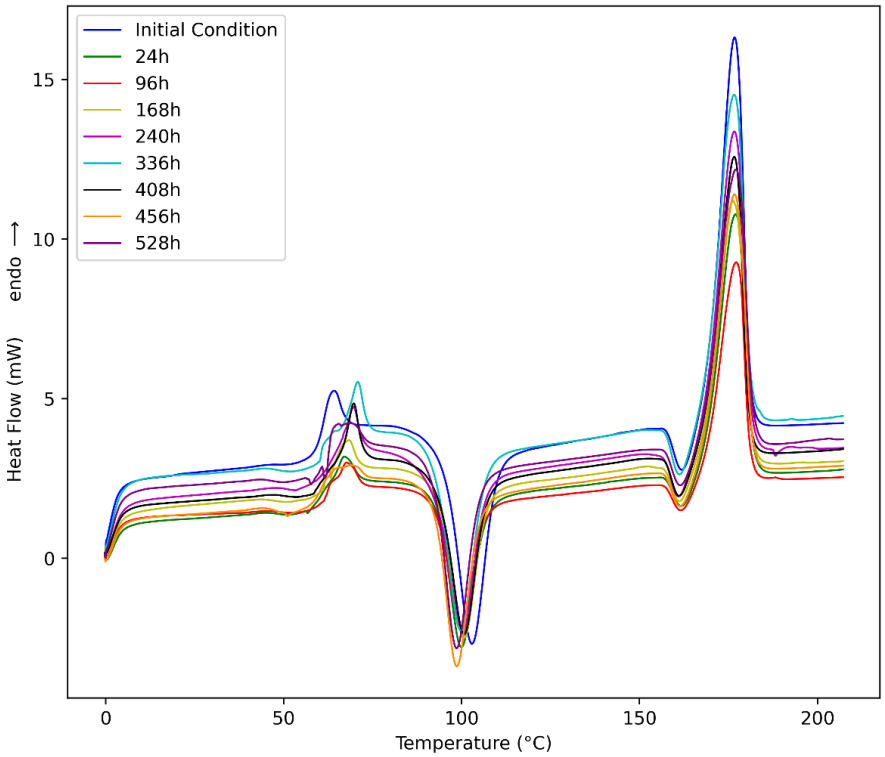

Source: Author.

Figure 32 - DSC curves obtained for samples subjected to accelerated weathering under 45 °C (second batch).

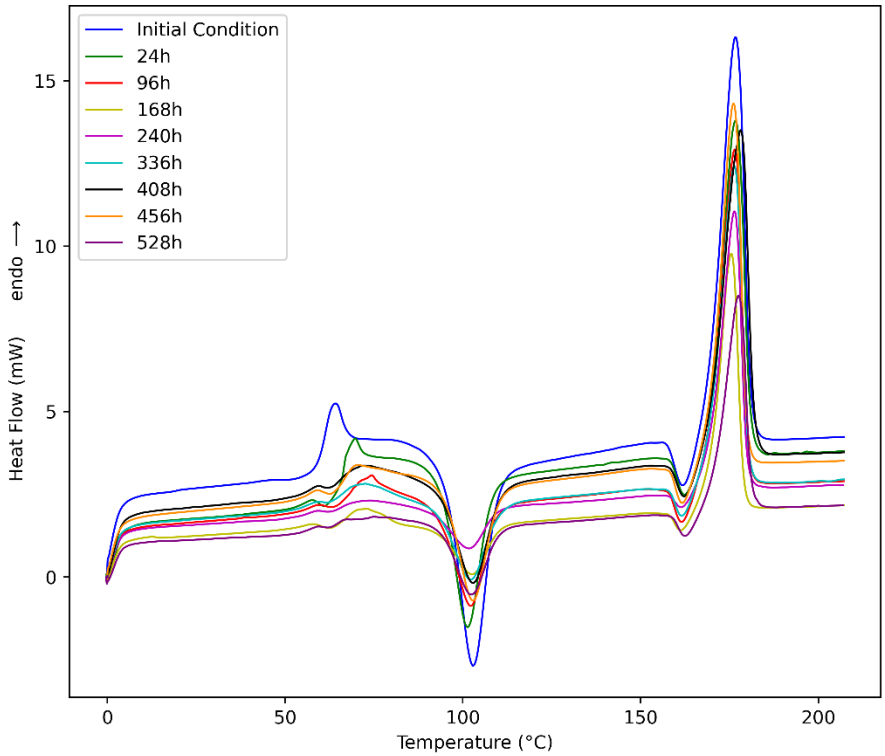

Source: Author.

Figure 33 - DSC curves obtained for samples subjected to accelerated weathering under temperature, radiation, and humidity control (second batch).

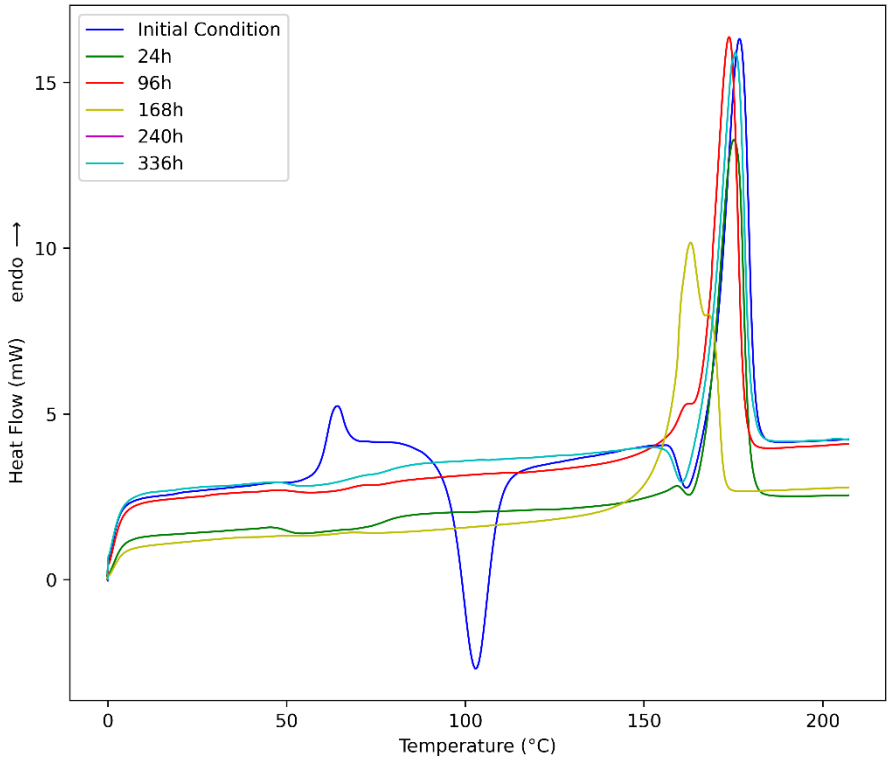

Source: Author.